Disentangling the Roles of Form and Motion in Fish Swimming Performance

Disentangling the Roles of Form and Motion in Fish Swimming Performance

A dissertation presented

by

Kara Lauren Feilich

to

The Department of Organismic and Evolutionary Biology

in partial fulfillment of the requirements

for the degree of

Doctor of Philosophy

in the subject of

Biology

Harvard University

Cambridge, Massachusetts

May 2017

Dissertation Advisor: Professor George Lauder Kara Lauren Feilich

Disentangling the Roles of Form and Motion in Fish Swimming Performance

Abstract

A central theme of comparative biomechanics is linking patterns of variation in morphology with variation in locomotor performance. This presents a unique challenge in fishes, given their extraordinary morphological diversity and their complex fluid-structure interactions. This challenge is compounded by the fact that fishes with varying anatomy also use different kinematics, making it difficult to disentangle the effects of morphology and kinematics on performance. My dissertation used interdisciplinary methods to study evolutionary variation in body shape with respect to its consequences for swimming performance.

In Chapter 1, I used bio-inspired mechanical models of caudal fins to study the effects of two evolutionary trends in fish morphology, forked tails and tapered caudal peduncles, on swimming performance. I demonstrated that shape and stiffness interact, making prediction of performance from shape alone questionable; and that correlated variation across body parts may be necessary to reap the benefits of any one body part's specialized morphology. This suggested that if there were locomotor adaptations in fish morphology, they should occur as correlated suites of morphological change.

In Chapter 2, following the hypothesis that locomotor specialization should occur as correlated morphological changes, I studied body and fin shape evolution in the cichlid fishes. I demonstrated that the body and fins show correlated evolution corresponding to purported ecomorphological specializations. However, morphological evolution suggesting locomotor adaptation is not itself proof of adaptive differences in locomotor performance.

Without being able to account for other traits contributing to swimming performance, it is impossible to ascribe performance differences to morphology alone. In Chapter 3, I developed a method for measuring steady swimming kinematics and performance that allows comparison across species, separating form from kinematics. I used this method to demonstrate the confounding effects of kinematics and morphology in three species of cichlid that are considered ecomorphological specialists. Finally, in Chapter 4, I tested several means of comparing unsteady kinematics and performance across species. Combined, these studies highlight the multivariate nature of morphological evolution, the need to incorporate both morphology and kinematics when determining their effects on performance, and provide a means of disentangling kinematics from morphology for statistical and phylogenetic comparison.

Table of Contents

Abstract iii
List of Figures ix
List of Tables xi
Acknowledgements xii

Introduction: Untangling knots: the challenges of comparative evolutionary biomechanics (especially in fishes) 1

Chapter 1: Passive mechanical models of fish caudal fins: effects of shape and stiffness on self-propulsion 9
1.1 Summary 9
1.2 Background 10
1.3 Materials and Methods 13
1.3.1 Foil design and experimental setup 14
1.3.2 Force analysis 18
1.3.3 Statistics 19
1.3.4 Particle image velocimetry 20
1.3.5 Midline kinematics 20
1.4 Results 20
1.4.1 Force and swimming speed 20
1.4.2 Midline kinematics 22
1.4.3 Flow visualization 27
1.5 Discussion 27
1.5.1 Propulsion of differently-shaped flexible foils 27
1.5.2 Hydrodynamics of differently-shaped foils 34
1.5.3 Implications for fish tail shape function 36
1.6 References 37

Chapter 2: Correlated evolution of body and fin morphology in the cichlid fishes 44
2.1 Summary 44
2.2 Background 45
2.3 Methods 50
2.3.1 Morphological data collection 50
2.3.2 Phylogenetic data and clade assignment 53

Table of Contents (Continued)

2.3.3 Morphological variation of single structures……... 55
2.3.4 Analyses of morphological disparity……... 56
2.3.5 Phylogenetic signal and convergence in cichlid ……. 56
morphology
2.3.6 Analysis of morphological covariation and co-evolution… 57
among structures
2.3.7 Allometric trends……..... 57
2.4 Results ……... 58
2.4.1 Morphological variation of single structures…….. 58
2.4.2 Phylogenetic signal in cichlid morphology……. 65
2.4.3 Disparity through time……. 66
2.4.4 Covariation of fins and body shape……. 66
2.5 Discussion…… 69
2.5.1 Body and fin shape variation encompasses specialist forms 78
2.5.2 Features associated with locomotor specializations exhibit. 80
correlated evolution
2.5.3 Cichlid morphology is dictated by neither ancestry nor …. 82
convergence
2.5.4 Diversification of locomotor structures coincides with ….. 83
adaptive radiation and speciation
2.5.5 Functional implications of correlated evolution ……. 84
2.6 Data archiving……. 86
2.7 References…….. 87

Chapter 3: Swimming with multiple propulsors: measurement and comparison 98
of swimming gaits in three species of neotropical cichlids
3.1 Summary……..... 98
3.2 Background……. 99
3.3 Materials and Methods…… 102
3.3.1 Fish care and maintenance……...…… 102
3.3.2 Steady swimming performance trials and analysis ……. 103
3.3.3 Kinematic data collection and analysis……... 104
3.3.4 Parameterization of gait as a trajectory through propulsive 106
space
3.3.5 Note on body size and scaling……..... 109

Table of Contents (Continued)

3.4 Results……. 109
3.4.1 Differences in kinematic strategy……. 109
3.4.2 Differences in morphology do not necessarily impose ….. 114
differences in performance
3.4.3 High variation in use of the non-primary propulsor …… 117
3.5 Discussion……... 119
3.5.1 Context for comparison of propulsive gaits……. 119
3.5.2 Quantifying kinematic strategy provides a means of …….. 122
isolating and comparing gaits
3.5.3 Potential for many-to-one mapping of morphology and …. 123
kinematics on performance
3.5.4 Choices and refinement of the gait trajectory approach ….. 123
3.5.5 Future directions for the study of swimming gaits …….. 125
3.6 References…… 126

Chapter 4: Measuring kinematics and performance during acceleration in swimming fishes 131
4.1 Summary……. 131
4.2 Background……. 132
4.3 Materials and Methods……..... 134
4.3.1 Animal care and maintenance…….. 134
4.3.2 Swimming trials and behavior categorization ……..… 134
4.3.3 Measurement of kinematics and fin beat parameters …….. 137
4.3.4 Statistical analysis of kinematic parameters…..... 139
4.3.5 Sinusoidal regression as estimate of steadiness…….. ……. 140
4.3.6 Cross-correlation of Fourier transforms to compare across and within behaviors 141
4.4 Results……. 142
4.4.1 General observations of acceleratory kinematics……..… 142
4.4.2 Period and amplitude variation with maximum ……... 146
instantaneous speed and acceleration
4.4.3 Correlation with best-fit sine waves as indicator of ……. 147
steadiness
4.4.4 Fourier transform shape is not a good indicator of behavior 147
4.5 Discussion …….. 153
4.6 References …… 157

Table of Contents (Continued)

Appendix to Chapter 2 160
Chapter 2 Supplemental Tables …… 161
Chapter 2 Supplemental Figures ……... 182

Appendix to Chapter 3 197
Chapter 3 Supplemental Table …….. 198

Appendix to Chapter 4 199
Chapter 4 Supplemental Tables ……. 200

List of Figures

Chapter 1

1.1 Foil shapes and descriptive shape metrics
1.2 Representative force, torque and calculated data from two foils
1.3 Swimming performance metrics for self-propelling foils
1.4 Midline envelopes showing lateral excursion of foil motion
1.5 Flow visualization around self-propelling flexible white foils
1.6 Flow visualization around self-propelling stiff coral foils

Chapter 2

2.1 Body landmarks and fin lengths used in morphometric analyses
2.2 Morphospace plots showing principal component scores from size-corrected traits of anatomical structures
2.3 Cichlid disparity through time for each anatomical structure
2.4 Partial least squares canonical variates displaying covariation of body shapes and median fin shapes
2.5 Schematic depiction of partial least squares canonical variate loadings of covarying features
2.6 Partial least squares canonical variates displaying covariation of independent contrasts of body shapes and median fin shapes

Chapter 3

3.1 Lateral profiles and representative pectoral and caudal fin beats
3.2 Hypothetical “gait trajectories” and 2-D projections of three potential swimming “types”
3.3 Pectoral and caudal fin beat frequencies, amplitudes, and “effort” as a function of steady swimming speed
3.4 Representative midline kinematics of each species at a range of speeds
3.5 Mean Reynolds number and Strouhal number as a function of steady swimming speed

List of Figures (Continued)

3.6 Pectoral-caudal gait transition speed and maximum prolonged swimming speed

3.7 Median species gait trajectories and gait space occupation

3.8 Mean gait trajectories and gait space occupation for individual fishes

Chapter 4

4.1 Schematic diagram showing multiple kinematic pathways to accelerate to the same final speed

4.2 Caudal fin beat kinematics for steady swimming, linear accelerations, and burst accelerations

4.3 Fin beat parameters and body and tail tip accelerations during three swimming behaviors

4.4 Detrended tail tip motion during three swimming behaviors and their best fit sine waves

4.5 Detrended tail tip motion during three swimming behaviors and the fast Fourier transforms of those traces

4.6 Maximum normalized pairwise cross-correlations between Fourier transforms of bass tail beat motions, and the speed differences between trials

4.7 Maximum normalized pairwise cross-correlations between Fourier transforms of trout tail beat motions, and the speed differences between trials

List of Tables

Chapter 1

1.1 Foil name abbreviations, shapes, flexural stiffnesses, and color code

1.2 Summary of two-way ANOVA on aligned ranks for four variables

Chapter 2

2.1 Hypotheses describing evolutionary covariation

2.2 Loadings of morphological traits on principal components

2.3 Loadings of morphological traits on phylogenetically-corrected principal components

2.4 Loadings of morphological traits on partial least squares canonical variates

Chapter 3

3.1 Linear mixed effects models of variation in fin beat frequency, amplitude, and "effort" with respect to speed and species

Chapter 4

4.1 Correlation coefficients comparing each trial to its best-fit sine wave

Acknowledgements

There are far too many people for me to acknowledge in just a few pages—each of whom has contributed to this dissertation in some form or another. But I do need to write something.

First, none of this would have ever been possible without the staunch, unflinching support of my mother, Daryl Altman, and my brother, Ethan Feilich. My mother has always been my best role model, my harshest critic, and my best friend. She is the inspiration for all of my virtues. There is no better human on this planet. My brother always has unwavering faith in me, while also encouraging me to always do better. I hope someday to be as clever as he, and as kind. And though I only met him in my 2nd year of this thing called graduate school, Ryan Feather has been a constant companion since—keeping me fed, strong, motivated, and loved.

I would like to acknowledge the invaluable support of my advisor, Professor George Lauder. George has generously given of his time, patience, resources, ideas and enthusiasm (mostly patience), while letting me pursue projects that might have seemed untenable at first glance. I have had unprecedented academic freedom in the Lauder Lab, and I wonder how I will fare without it. But George is more than just an academic advisor, he is a fount of knowledge with respect to the history and execution of research in our field. There are few things I would rather hear than "You should really know about him/her/it/this/that." And there are few people who are such perceptive guides with respect to maintaining quality and depth of research. I would do well to be a scientist and historian of his depth and caliber.

Andrew Biewener and Jonathan Losos both provided helpful guidance as members of my dissertation committee, and I consider it one of the great failings of my graduate career that I did not take greater advantage of their counsel.

Perhaps no two people at Harvard deserve as much credit for supporting my research as Karsten Hartel and Andrew Williston. Karsten has in turn been patient teacher, sage advisor, mover of heavy objects, source of brilliant ideas and hidden knowledge, networker supreme, caring listener, scientific father figure: he is a jack of all trades and master of all trades. I am beyond fortunate to have spent so many hours in the fish collection with him in my attempts to glean all he has to offer. Andy is a scholar, gentleman, mover of heavy objects, sounding board second to none, and I hope he will agree with me when I say he is a dear, dear friend. In all my excitement with respect to finishing this crazy journey, I must also admit that leaving these two is a bittersweet sensation.

Maggie Arethusa Bean Starvish deserves equal thanks and praise. She has been confidante, friend, voice of reason, and the glue that held my lab life together. She is one very special lady. My labmates, first Nicole Danos, Erin Blevins, and Jeanette Lim, then Kelsey Lucas and Dylan Wainwright have all been dear as siblings to me, and keep me sharp. My padawan learner, Alexander Weickhardt, and my most trusted R2-D2 Brianna Laing—you too are my brother and sister. You have learned so much, but not as much as you have taught me.

The many friends and colleagues in Organismic and Evolutionary Biology, the MCZ, and the Ernst Mayr Library at Harvard have kept me afloat and engaged through the most difficult periods of my graduate career. To my cohort, I owe my sanity. I am eternally indebted to Ambika Kamath, Alexandra Brown, Katie Boronow, Peter Wilton, Brent Hawkins, and Joel Nitta, each of whom have been more important to me than they could possibly imagine (from the lab, to the ER). Mary Sears, Ronnie Broadfoot, Jose Rosado, Breda Zimkus, Paul Dwyer, Irv Dumay, Chris Preheim, Alex Hernandez, Yesenia Quezada, Mona Alexis, and all the others who

have helped me and supported me along the way—you will never know how much it meant to me.

Dave Ellerby, my friend and mentor, should get a novel in these acknowledgements, though I can only afford a few sentences. I aspire to his eye for experimental rigor, his kindness, and his general knowledge of everything. I know that I can always count on him for advice and friendship – and he'd better know that, because he's never getting rid of me.

Finally, I owe thanks to all the people I haven't mentioned, or worse, have forgotten. The coffee shop baristas, the tea tenders, the bartenders, the old friends and the new, the kind faces and uplifting words of all of you have been channeled in to this text. I have a personal rule: if I see someone enough that it's awkward not to greet them, I must introduce myself. And you all have proven the rule's worth over and over. I appreciate you all so very much.

Page intentionally left blank

Introduction

Untangling knots: the challenges of comparative evolutionary biomechanics (especially in fishes)

Kara L. Feilich

The naïve student of evolutionary biomechanics may maintain the belief that her field is possible—that the questions we ask can be answered. She may learn that those questions might be answered, eventually—but the answers lie at the center of a tremendous, encrusted Gordian knot. The knot is composed of the many tangled facets of an organism that contribute to biomechanics. One strand is the pure morphology of an organism: the anatomical pieces within which life is maintained. Another is the organism's physiology, the mechanisms and functions maintaining that life. Of course, these strands are intimately entwined with one another: the anatomical structure facilitates the physiological process, and vice versa. Then, there is the behavior of the organism, a finicky thread demonstrating that just because an organism can, morphologically and physiologically, do something, does not mean it actually does such a thing, or that the thing is of any importance to the organism (Husak, 2006). Ecology, development, each additional trait of an organism is a fiber interwoven with the others. When comparing organisms, one must also deal with the additional tangles presented by these many threads' evolutionary heritage, balls of string hanging off the knot, with themselves only partially understood until the advent of the time machine. And the whole mess of matted fibers, is encircled by the rough crust that is composed of the researcher's entrenched biases and assumptions, and historical biases and assumptions as well. How then, is the student of biomechanics to link any one trait to a specific consequence? While this is probably a challenge

of all science—linking cause and effects in the face of confounding variables—it seems particularly acute in evolutionary biology.

Perhaps the only method we have is to try and account for the variation represented by the different strands that make up the knot—to try to tease the many variables apart, tracing and unraveling each strand as much as possible. In this context, fish swimming biomechanics is, and has been, one particularly intricate tangle. Swimming kinematics, morphology, and physiology are inextricably linked. Determining how the interactions of these traits impact hydrodynamic performance is limited by the status of the field of fluid mechanics and its computational power: even a completely simulated hydrodynamic model of a single fish, doing a single behavior, can take months with present technology—these modeling approaches are themselves active areas of research (e.g. Soiropoulos and Yang, 2014). Information about how fish swim in the field is scarce; and the most cited reference (Webb, 1991) for "routine swimming" was a study done under fairly constrictive laboratory conditions in a single species, so the relative importance of observed laboratory trends is difficult to estimate. Even the lines of action of fish myotomal muscle are complicated to interpret due to their anatomical complexity (Gemballa and Röder, 2004, Muller and van Leeuwen, 2006, Shadwick and Gemballa, 2006). Thus, each strand incorporated into the metaphorical knot is itself an untidy composite fiber. I am by no means the first to observe these challenges (for instance, see Lauder, 2011)—and in many respects they are a welcome challenge for ambitious researchers.

Another challenge, which while not inherent to fish biomechanics, cannot be ignored, is the tendency for hypotheses about the interrelationship between traits and swimming performance to be adopted in the absence of sufficient experimental data. The series of studies by Paul Webb in the 1980's that serve as the ideological foundation for this dissertation provide

one such set of hypotheses. Chief among these studies are "Locomotor Patterns in the Evolution of Actinopterygian Fishes" (Webb, 1982), and "Body Form, Locomotion, and Foraging in Aquatic Vertebrates" (Webb, 1984). These were landmark studies (combined, they have been cited over 1000 times), building on and integrating the earlier observations of pre-eminent ichthyologists like P. Humphrey Greenwood and Donn Rosen with the fundamental biomechanical requirements of fish swimming. These studies provided a framework for understanding how commonly observed patterns of convergent evolution that could not be directly tested may relate to hydrodynamic thrust generation. Webb was forthright in the assumptions he was making while putting together these hypotheses, and acknowledged that "These functional hypotheses will evolve as data accumulate, and also as the phylogenetic reference framework evolves" (1982). He also recognized that the knowledge of fish biomechanics at the time he was writing was insufficient to test some of the hypotheses he proposed:

> *"…the limited meager knowledge on fish locomotion mechanisms must be recognized. To a large extent research has concentrated on body/caudal fin locomotion, particularly steady (constant speed) swimming. Many fish rarely swim. Fish rarely swim steadily. They frequently use non-caudal fins. Indeed, research may have concentrated on biologically and behaviorally less important swimming modes! In spite of the inevitable constraints, a general, and necessarily preliminary, analysis of locomotor patterns in actinopterygian phylogeny seems possible."* (Webb, 1982)

Webb's framework was a necessary step in understanding the evolution of locomotor morphology in fishes. It provides testable hypotheses for morphology-function relationships.

Some of these hypotheses are considered more thoroughly within this dissertation, and as such, they are discussed briefly below. However, despite Webb's own caveats, his hypotheses have been used again and again as direct support for adaptive function of observed morphological changes. At best, this is merely lazy, and Webb's hypotheses will ultimately hold for these cases. At worst, the assumption of a given relationship will mask interesting diversity, and perpetuate an oversimplified understanding of swimming morphology and biomechanics.

My goal in this dissertation was to continue the work of fish biomechanists past and present, including Paul Webb, in teasing apart intertwined traits. Thereby, I hoped to help us begin to understand how morphology and kinematics have, independently and in tandem, evolved to facilitate swimming performance in all its forms.

Chapter 1 was an attempt to simplify the question of how morphology affects performance by removing all biological confounding variables using a simple physical model. The goal was to address a long held hypothesis, supported by convergent morphological evolution and experimental fluid dynamics, and incorporated into Webb's framework: that a narrow caudal peduncle and a semi-lunate tail would increase swimming economy by increasing thrust and reducing drag (Webb, 1982, Webb, 1984, Lighthill, 1969). Perhaps unsurprisingly, this approach proved both fruitful and frustrating—even in a simple plastic model, the relationship between any performance metric and shape is complicated. However, this study gave rise to the suggestion that only having a semi-lunate tail might not be enough to reap the benefits of a semi-lunate tail. Rather, the body needs to have a trailing edge that promotes flow separation upstream of the leading edge of the semi-lunate tail to reap a hydrodynamic advantage—and even then, it may only be possible with favorable kinematic phasing of body and tail undulation.

Chapter 2 was inspired both by Webb's framework, and by the interesting observation in Chapter 1 that multiple morphological traits may need to evolve in tandem for an adaptive benefit to be accrued as the result of any single trait. In a now famous figure, Webb outlined hypothesized patterns of morphological evolution in association with locomotor and foraging specialization (Webb 1984). He categorized these specializations as "body-caudal fin periodic propulsion" (cruisers) with narrow caudal peduncles and lunate tails, "body caudal fin transient propulsion" (accelerators) with large body depth posteriorly and large area posterior fins, and "median and paired fin propulsion" (maneuverers) with deep laterally compressed bodies and extended median fins (Webb, 1984). I used cichlid fishes as a model adaptive radiation of fishes, to see if these features—including the understudied median fins—evolved together as hypothesized, or were more modular in their patterns of evolution.

Chapter 3 followed on the tails of Chapter 2: after having learned that fish do show patterns of morphological evolution in keeping with Webb's hypotheses, I wanted to see if fishes with the given morphologies reap the associated hypothesized hydrodynamic benefits of their morphology. This is impossible without also accounting for differences in motion patterns, which confound the effects of morphology along with other variables. To mitigate this confounding factor, I devised a means of comparing steady swimming kinematics within and across taxa. In Chapter 3, I used this method to look at the steady swimming kinematics and performance of three putative locomotor-morphology specialists—only one of which was supposed to be a steady swimming specialist.

Finally, in Chapter 4, I began to address the lack of studies and methods for the comparison of unsteady swimming movements—another necessary precursor to understanding how morphology and kinematics interact to produce performance.

In sum, I hope that this thesis sheds light on how multiple traits can interact with one another to affect fish swimming hydrodynamics, and propose new methods by which we can continue untangling the Gordian knot of evolutionary swimming biomechanics.

References

Gemballa, S. and K. Röder. (2004). From head to tail: the myoseptal system in basal actinopterygians. *J. Morphol.* 259: 155-171.

Husak, J. F. (2006). Does survival depend on how fast you can run or how fast you do run? *Funct. Ecol.* 20: 1080-1086.

Lauder, G. V. (2011). Swimming hydrodynamics: ten questions and the technical approaches needed to resolve them. *Exp. Fluids.* 51: 23-35.

Lighthill, M. J. (1969). Hydromechanics of aquatic animal propulsion. *Ann. Rev. Fluid Mech.* 1: 413-446.

Müller, U. K. and J. L. van Leeuwen. (2006). Undulatory fish swimming: from muscles to flow. *Fish and Fisheries*. 7: 84-103.

Shadwick, R. E. and S. Gemballa. (2006). Structure, kinematics, and muscle dynamics in undulatory swimming. In Fish Biomechanics (ed. R.E. Shadwick and G.V. Lauder) San Diego, CA: Academic Press. pp. 241-280.

Sotiropoulos, F. and X. Yang. (2014). Immersed boundary methods for simulating fluid-structure interactions. *Prog. Aerosp. Sci.* 65: 1-21.

Webb, P. W. (1982). Locomotor patterns in the evolution of actinopterygiian fishes. *Amer. Zool.* 22: 329-342.

Webb, P. W. (1984). Body form, locomotion and foraging in aquatic vertebrates. *Amer. Zool.* 24: 107-120.

Webb, P. W. (1991). Composition and mechanics of routine swimming of rainbow trout, *Oncorhynchus mykiss*. *Can. J. Fish. Aquat. Sci.* 48: 583-590.

Page intentionally left blank

Chapter 1

Passive mechanical models of fish caudal fins: effects of shape and stiffness on self-propulsion

Kara L. Feilich and George V. Lauder

1.1 Summary

Fishes are found in a great variety of body forms with tail shapes that vary from forked tuna-like tails to the square-shaped tails found in some deep-bodied species. Hydrodynamic theory suggests that a fish's body and tail shape affects undulatory swimming performance. For example, a narrow caudal peduncle is believed to reduce drag, and a tuna-like tail to increase thrust. Despite the prevalence of these assertions, there is no experimental verification of the hydrodynamic mechanisms that may confer advantages on specific forms. Here, we use a mechanically-actuated flapping foil model to study how two aspects of shape, caudal peduncle depth and presence or absence of a forked caudal fin, may affect different aspects of swimming performance. Four different foil shapes were each made of plastics of three different flexural stiffnesses, permitting us to study how shape might interact with stiffness to produce swimming performance. For each foil, we measured the self-propelling swimming speed. In addition, we measured the forces, torques, cost of transport and power coefficient of each foil swimming at its self-propelling speed. There was no single 'optimal' foil exhibiting the highest performance in all metrics, and for almost all measures of swimming performance, foil shape and flexural stiffness interacted in complicated ways. Particle image velocimetry of several foils suggested that stiffness might affect the relative phasing of the body trailing edge and the caudal fin leading edge, changing the flow incident to the tail, and affecting hydrodynamics of the entire foil. The results of this study of a simplified model of fish body and tail morphology suggest that

considerable caution should be used when inferring a swimming performance advantage from body and tail shape alone.

1.2 Background

Fishes are remarkably versatile swimmers, exhibiting high performance in many different aspects of aquatic locomotion. Some species can migrate long distances, crossing oceans with limited fuel reserves, while others use rapid acceleration to catch prey. Still other species are able to maneuver through spatially complex habitats such as mangroves or coral reefs. Given this remarkable diversity of swimming behavior, it is hardly surprising that fish morphology is also highly varied. Body and tail shape are thought to be among the chief determinants of swimming performance, and particular shapes are thought to be advantageous for different swimming behaviors. Yet, surprisingly, controlled experimental investigations of the effects of body and tail shape on swimming performance are scarce.

Convergence of many distantly-related fishes on a small set of distinct body shapes raises the question of whether those shapes are advantageous for specific aspects of swimming performance—either by having the lowest cost of transport (CoT), the highest self-propelling speed, or the best maneuverability. For instance, several species of pelagic, highly-active cruising fishes have converged on a body plan with a narrow caudal peduncle (the region just in front of the tail where the body narrows) and a forked or semi-lunate tail. This suggests that such a body shape provides enhanced swimming economy, either by increasing thrust or reducing drag (Webb, 1984, Webb, 1988, Wolfgang *et al.,* 1999, Blake *et al.,* 2009).

The proximate physical mechanisms by which body shape might confer a hydrodynamic advantage, however, remain uncertain. There are many covarying features of biological

propulsors, such as their differing evolutionary history and physiology, that make it difficult to determine the specific effect of shape (as an isolated single factor) on performance using studies of living biological systems. Simple mechanical models, while not a replacement for direct study of biological phenomena, facilitate the reduction of such sources of unexplained variance, thereby allowing the researcher to draw more direct inferences about the effects of the variable in question on specific parameters of performance.

Several hydrodynamic theories suggest mechanisms by which narrow caudal peduncles and sweptback tails could enhance swimming performance. Most of these are motivated by slender-body theory (Lighthill, 1975), which implies that undulating bodies exhibit an inherent tradeoff between thrust and drag: bodies and tails with large surface area have a greater ability to generate thrust, but in doing so, the large surface area incurs an energetic cost due to increased drag. Fusiform bodies reduce this drag cost, but stouter fishes typically have more muscle and surface area available for thrust production (Webb, 1984). These theories remain limited by the extent of our knowledge of the hydrodynamics of bodies of varying stiffness, activation, and kinematics. Basic knowledge of these body-fluid interactions continues to grow, and computational fluid dynamic studies are beginning to fill this gap in knowledge (see, for example, Borazjani and Daghooghi, 2013). While promising, these simulations must be tested and replicated in the real world (e.g. Borazjani *et al*., 2012).

Tail structure and kinematics may also mitigate a fusiform body's theoretical low thrust production. Fish with fusiform bodies have long, narrow peduncles to separate the tail from the body. This narrowing means that, if all else were equal, a fusiform body could not shed as much energy into the wake as a stout body. However, the separation between the tail and body allows the tail to oscillate without resulting in energetically costly inertial recoil that would arise from

high amplitude side-to-side oscillation of the body (Lighthill, 1975, Lindsey, 1978, Magnuson, 1978, Webb, 1992, Wolfgang *et al*., 1999). A semi-lunate or forked tail may allow a fusiform body to produce high thrust via the generation of leading edge suction (Chopra and Kambe, 1977, Magnuson, 1978, Karpouzian *et al*., 1990). This mechanism has not yet been observed in live fishes, but is predicted by computational models of caudal fin kinematics (Borazjani and Daghooghi, 2013) where a leading edge vortex (LEV) on the fish tail has been proposed to increase thrust.

Differences in fish body and tail shape also appear to be coupled with differences in body stiffness (Webb, 1984). Thunniform and carangiform swimmers with their deep bodies, narrow caudal peduncles and semi-lunate tails appear to have stiffer bodies and tails than fishes with more generalized body shapes such as trout or bluegill sunfish (Webb, 1984). The co-occurrence of particular shapes with particular stiffnesses will complicate attempts to determine experimentally in live fishes how shape and stiffness may interact during locomotion.

Recently, controlled studies using simple mechanical and robotic 'flapping foil' models have provided for the removal of these confounding factors, allowing the study of how fundamental physical traits affect swimming performance. The non-linear effects of traits such as stiffness and length on swimming of flexible foils or strip-like panels have been measured, as have resonant phenomena resulting from the foil-fluid interaction, and the effect of near-wall swimming and center of mass oscillations (Lauder *et al*., 2011, Lauder *et al.*, 2012, Alben *et al*., 2012, Dewey *et al*., 2013, Wen and Lauder, 2013, Shelton *et al*., 2014, Quinn *et al*., 2014a, Quinn *et al*., 2014b).

These flapping-foil models may appear somewhat distant from the biological systems they attempt to emulate, but the ease of their control and manipulation makes it possible to

address comparative and complex biological questions with targeted experiments (Lauder *et al*., 2012, Shelton *et al*., 2014). We use this framework here to focus on the specific question of how fish-like peduncle and tail shape may affect swimming performance in a simplified system. While the results of studies using this model system may not be directly applicable to biological fish swimming, they can shed light on causal hydrodynamic phenomena that would make particular shapes effective, suggesting further avenues for investigation in live fish systems. Using flexible flapping foils designed to span a range of observed fish peduncle and tail shapes and stiffnesses, and using foil materials that match the range of known fish body stiffnesses, we measured how differences in body and caudal fin shape affect swimming speed, hydrodynamics, and CoT. Using a mechanical controller, we were able to precisely control the leading edge motion of these flexible foil shapes, and to quantify the self-propelled swimming speeds of each shape and stiffness.

Following the hypotheses outlined by Webb and others (Lighthill, 1975, Lindsey, 1978, Magnuson, 1978, Webb, 1984, Borazjani and Sotiropoulos, 2010), we hypothesized that foils with narrow caudal peduncles would be the most economical swimmers, while foils with deep peduncles might produce more thrust at greater energetic cost. In addition, we suspected that the presence of a forked tail in conjunction with a narrow peduncle might further increase thrust, without adding an offsetting economic cost. Stiffness was expected to interact with these effects by modulating the timing of interactions between the body trailing edge and the tail leading edge, and we expected that an intermediate stiffness would provide the most effective phasing of the body and tail and hence enhance thrust.

1.3 Materials and Methods

1.3.1 *Foil design and experimental setup*

To model the effects of caudal peduncle depth and tail shape on swimming performance, we created four foil shapes each with either a narrow or a deep caudal peduncle, and a forked or unforked tail shape (Figure 1.1). Foils were laser cut from three thicknesses/stiffnesses of plastic shim stock, and for ease of identification we refer to these by the color of the shim stock used as in our previous paper (Shelton *et al.,* 2014). Foil identification conventions and the flexural stiffness ranges of each foil are given in Table 1.1. The flexural stiffness of the foils used here encompasses a wide range of the stiffnesses observed in real fishes (Lauder *et al*., 2012, Shelton *et al*., 2014). Long *et al*. (2002) measured the stiffness of hagfish (*Myxine glutinosa*) bodies at a value of 3×10^{-4} N m^2. McHenry *et al*. (1995) derived flexural stiffness values for sunfish bodies of $\sim 1 \times 10^{-3}$ N m^2 near the head to 1×10^{-6} N m^2 near the tail. Hereafter, specific foils are named by combining the first letter of the color of the material with the number of the foil shape as in table 1.1, e.g. C1 is the relatively inflexible coral-colored foil with a narrow peduncle and forked tail (Figure 1.1, Table 1.1).

Foil body aspect ratio was calculated as follows:

$$AR = \frac{l^2}{A}, \quad (1.1)$$

where l is foil body length (18.5 cm), and A is the foil area.

We used a Riemann sum to approximate the second moment of area for each foil shape, as a shape metric, to describe the distribution of area along the foil. Briefly, each foil shape was divided into 37–0.5 cm wide trapezoidal segments from the anterior edge to the end of the foil (18.5 cm from the leading edge). For each foil segment, j, the average height was calculated. Each segment was then assumed to be a rectangle having width of 0.5 cm, and height equal to

the average segment height. Using this approach, the shape descriptor second moment of area of the foil with respect to the leading edge axis (S) was approximated as follows:

$$S = \int r^2 \, \mathrm{d}A \approx \sum_{j=1}^{37} A_j r_j^2, \quad (1.2)$$

where r_j is the distance from the centroid of foil segment j to the leading edge.

Foil flexural stiffness was calculated for the deepest and the narrowest point of the 'body' portion of the foil, the leading edge and the peduncle, respectively. Young's modulus (E) values for each of the three foil materials, white, yellow, and coral, were available from collaborators' earlier work (Quinn, personal communication; Quinn *et al*. 2014a, 2014b). The second moment of area of the foil about the axis of foil bending (I) was calculated at each of the two locations as follows:

$$I = \frac{b^3 h}{12}, \quad (1.3)$$

for a rectangular cross-section with neutral axis vertical through the centroid, where b is the foil thickness and h is the height of the foil at the location of interest. Note that this is an entirely separate calculation from that of S, which was used to describe the foil shape over the long axis. Flexural stiffness (EI) was calculated the product of E and I.

Foils were moved using a computer-controlled mechanical actuator designed to flap flexible foils in oncoming flow. This device is the same one used in our earlier research on aquatic propulsion (see Lauder *et al*., 2011, Lauder *et al.*, 2012, Quinn *et al*., 2014a, Quinn *et al*., 2014b, Wen *et al*., 2013, Wen *et al.*, 2014). Each foil was clamped by a round shaft fitted with an ATI-Nano17 six-axis force–torque transducer (ATI Industrial Automation, Apex, NC, USA) at the leading edge, and attached to a carriage placed on a recirculating swimming flume. A custom LabVIEW program (National Instruments Corp., Austin, TX, USA) controlled a heave motor on

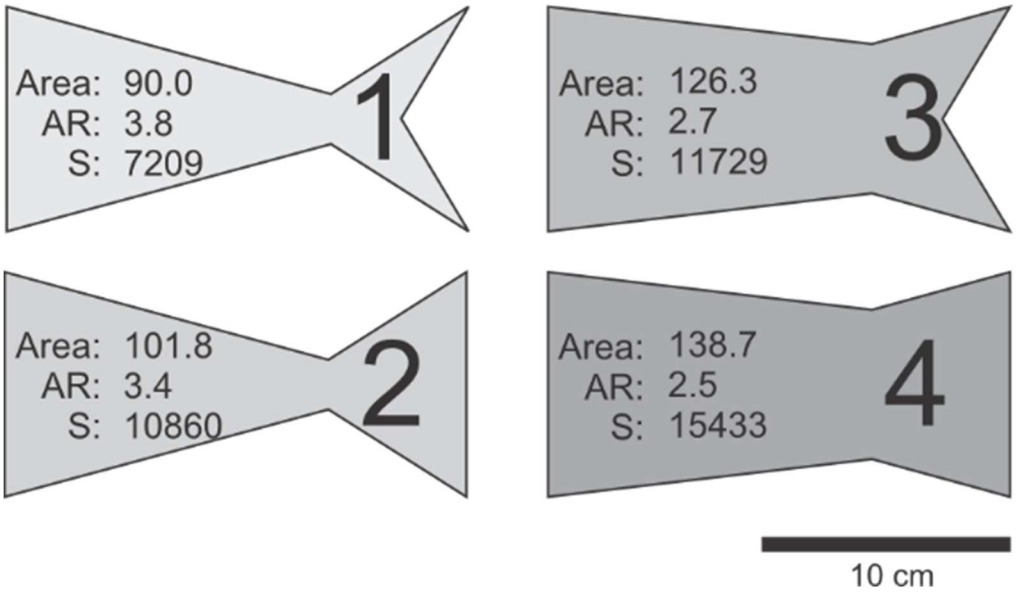

Figure 1.1. Foil shapes and descriptive shape metrics. Units are as follows: area (cm^2), aspect ratio (AR, unitless), shape-descriptor second moment of area (S, cm^4). Identifying shape number is in large print on the foil 'tail'. Also see Table 1.1 for details of foil properties, and for color codes that identify the material stiffnesses studied.

Table 1.1. Foil name abbreviations, shapes, flexural stiffness ranges, and color code used in this study. See Figure 1.1 for images of foil shapes. The name abbreviations indicate foil color and foil shape. W indicates the white foil color, Y yellow, and C coral.

Foil	Shape	Min EI (Pa m4)	Max EI (Pa m4)	Mass (g)	Color
W1	1	$7.0*10^{-5}$	$2.9*10^{-4}$	2.26	
W2	2	$7.0*10^{-5}$	$3.1*10^{-4}$	2.56	
W3	3	$2.0*10^{-4}$	$3.0*10^{-4}$	3.19	
W4	4	$1.9*10^{-4}$	$3.1*10^{-4}$	3.52	
Y1	1	$5.0*10^{-4}$	$2.1*10^{-3}$	5.72	
Y2	2	$5.0*10^{-4}$	$2.2*10^{-3}$	6.6	
Y3	3	$1.4*10^{-3}$	$2.2*10^{-3}$	8.02	
Y4	4	$1.4*10^{-3}$	$2.2*10^{-3}$	8.89	
C1	1	$1.5*10^{-3}$	$6.3*10^{-3}$	8.32	
C2	2	$1.5*10^{-3}$	$6.6*10^{-3}$	9.35	
C3	3	$4.3*10^{-3}$	$6.5*10^{-3}$	11.75	
C4	4	$4.3*10^{-3}$	$6.6*10^{-3}$	12.79	

the carriage, moving the shaft with ±1 cm sinusoidal heave at 2 Hz and 0° pitch. These parameters approximate the kinematics of the posterior body region of swimming fishes (Lauder and Madden, 2006, Shelton *et al*., 2014).

A second custom LabVIEW program monitored fore-aft forces as the foil was flapping. Flow speed was changed manually until the observed fore-aft forces were within 0.005 N of 0.000 N. The flow speed at which this occurred was recorded. This procedure was repeated seven times, the highest and lowest recorded speeds were removed, and the self-propelling speed was calculated as the mean average of the remaining five speeds recorded for each foil.

1.3.2 *Force analysis*

Ten flapping trials for each foil were performed at that foil's self-propelling speed. For each trial, heave position, forces and torques were recorded continuously for ten seconds (e.g. Figure 1.2). Fore-aft forces were filtered in IgorPro (Wavemetrics, Inc., Portland, OR, USA) using a custom narrow band-pass to remove 2 Hz noise that resulted from the imposed heave motion. The force in the fore-aft direction (F_x) was expected to have a dominant 4 Hz signal (i.e. twice the heave frequency) based on our previous work. All force and torque traces were smoothed for ease of analysis.

A custom IgorPro program was written to calculate derived measures of performance from the original three-force axes (F_x, F_y, F_z), self-propulsion speed (U_{eq}), and foil heave position (Y_{pos}). Foil power curves were calculated by multiplying the values of the instantaneous heave velocity and the force applied in the direction of the heave axis (F_y), as follows:

$$P(t) = \frac{\mathrm{d}Y_{pos}}{\mathrm{d}t} F_y. \quad (1.4)$$

The net work done on the foil by the motor was calculated as the integral of the power curve,

(1.5) $W_{net} = \int P(t)\,\mathrm{d}t$.

The work per heave cycle (hereafter, 'work per cycle') was calculated by dividing the net work done over a 10 s trial by the number of cycles in that time period (20 cycles). The foil power coefficient was calculated following Read *et al*. (2003), where ρ is the fluid density, c is the mean chord, and s is the mean span of the foil.

(1.6) $C_p = \frac{2\overline{P}}{\rho U_{eq}^3 cs}$.

CoT was calculated in two ways. First, CoT was calculated as the net work done over the course of each 10 s trial divided by the total distance traveled (U_{eq} * 10 s). Then, mass-specific CoT was calculated by dividing the first measurement by the foil mass. Torque oscillation of the foil about the rod (T_z) was calculated as the average ($T_{max} - T_{min}$) for 20 heave cycles. This torque can be interpreted as the tendency for body and tail oscillation to cause a yawing moment at the anterior end of the foil.

1.3.3 *Statistics*

The Shapiro-Wilk W test for normality and Levene's test for homogeneity of variance were conducted in JMP Pro 9 (SAS Institute Inc., Cary, NC, USA). All metrics were heteroscedastic with non-normal distributions, so all data were transformed using an aligned rank transform in ARTool v. 1.5.1 (Wobbrock *et al.,* 2011). Comparisons among foil shapes and stiffnesses were then conducted using two-way ANOVAs in JMP Pro 9, following the procedure detailed in Wobbrock *et al*. (2011) (Table 1.1). Significant differences were determined

following a false detection rate correction, to reduce the chance of type I error from multiple testing, with a maximum allowable false detection rate of 5% (see Benjamini and Hochberg, 1995).

1.3.4 *Particle image velocimetry (PIV)*

While flapping at the self-propelling speed, flow around foils was filmed in ventral view, via a 45° mirror, with a high speed camera (Photron PCI-1024; each frame with 1 megapixel resolution) at a frame rate of 1000 Hz. Near neutrally buoyant particles were illuminated using a Coherent 10 Watt laser, and analyzed using DaVis v. 7.2.2 (LaVision GmbH, Goettingen, GER) PIV software. The start of each flapping cycle was defined as when the leading edge was at its right-most lateral excursion. Still frames were taken when a visible trailing edge vortex was formed off the trailing edge of the foil 'body', and when that vortex had moved down the foil far enough to interact with flow at the 'tail' leading edge. For opaque flapping foils, the shadow of the foil blocked visualization of flow on the right side of the foil. For ease of interpretation, these unusable shadow areas were masked using CorelDRAW X5 (Corel Corp., Ottawa, CAN).

1.3.5 *Midline kinematics*

Midline envelopes were digitized from high-speed videos by tracing the foil midline every 0.125 s from the start of one flapping cycle to the start of the subsequent cycle, for a total of eight traces, using a custom MATLAB program (The MathWorks, Inc., Natick, MA, USA).

1.4 Results

1.4.1 *Force and swimming speed*

Swimming foils exhibited a sinusoidal thrust profile, with two thrust peaks for every foil oscillation cycle (Figure 1.2). With every thrust peak, the foil power curve dips slightly negative, showing that for a brief period, the undulating foil is actually doing work on the rod, instead of the rod and motor working on the foil. Foils are self-propelling, and hence F_x averages to zero over a flapping cycle (Figure 1.2).

There were significant interactions between shape and stiffness for every swimming performance metric measured except for the self-propelled swimming speed, U_{eq} (Figure 1.3, Table 1.2) for which the interaction term was not significant. Self-propelled swimming speed varied significantly with both foil shape and stiffness, with the yellow intermediate-stiffness foil in the Y4 (deep peduncle) shape exhibiting the fastest swimming speed overall. The stiffest (coral) foil material with the C3 and C4 shapes showed the slowest swimming speeds. For two of the three materials tested, white and coral, U_{eq} did not change substantially with shape (Figure 1.3). For the medium-stiffness, yellow foils, it appeared that U_{eq} is highest in the foils with deep peduncles, and higher still in the deep peduncle foil with an unforked tail (Figure 1.3).

For all foils, the energy cost per heave cycle depended on foil material more than foil shape. The stiffest foils (coral) had higher energetic costs per heave cycle than the yellow foils, and the flexible white foils had the lowest costs per heave cycle. The CoT, however, exhibited opposite trends depending on whether or not mass was incorporated in to the calculation (Figure 1.3; Table 1.2). Coral foils exhibited the lowest mass-specific CoT, and the white foils had the highest mass-specific CoT, while the opposite was true when mass was not accounted for (Figure 1.3; Table 1.2). This discrepancy is the result of less-flexible coral foils being much heavier than the white flexible foils, while the yellow foils were of an intermediate mass.

The most flexible flapping foils tended to have similar power coefficients across all shapes. The power coefficients of the medium-stiffness yellow foils tended to be lower in shapes with greater surface area. The stiffest, coral foils, however, tended to have higher power coefficients with higher surface area.

Torque also varied with foil stiffness more than foil shape (Figure 1.3). The coral foils all had similar, high torques, and the white foils had similar low torques. An interesting exception to this trend is foil Y4, the medium stiffness foil with a deep peduncle and an unforked tail. Y4 exhibited the highest torques of any foil, as well the highest U_{eq}.

There was considerable variance observed in the work, power, and CoT of some foils, particularly among the yellow and coral foils (Figure 1.3). The force measurements used in the derivation of these values were very sensitive to small changes in the initial conditions, and the observed scatter may result from even minor variation in the forces measured from trial to trial. We have reported the raw data for these measures in order to accurately convey this scatter.

1.4.2 *Midline kinematics*

Foil kinematics vary considerably with both foil shape and foil material (Figure 1.4). Material stiffness (Table 1.1) governed the number of wavelengths on each foil, with the white foils exhibiting approximately 1.5 wavelengths, while the other materials only supported about 0.5 wavelengths. Shape, too, had an effect on midline kinematics, by modulating the lateral excursion of any particular point along the foil. For instance, foils with narrow peduncles tended to exhibit greater lateral excursion of the peduncle notch than foils with deep peduncles (Figure 1.4). Interestingly, while shape did affect lateral excursion, it did not appear to change the position of nodes and antinodes along the body.

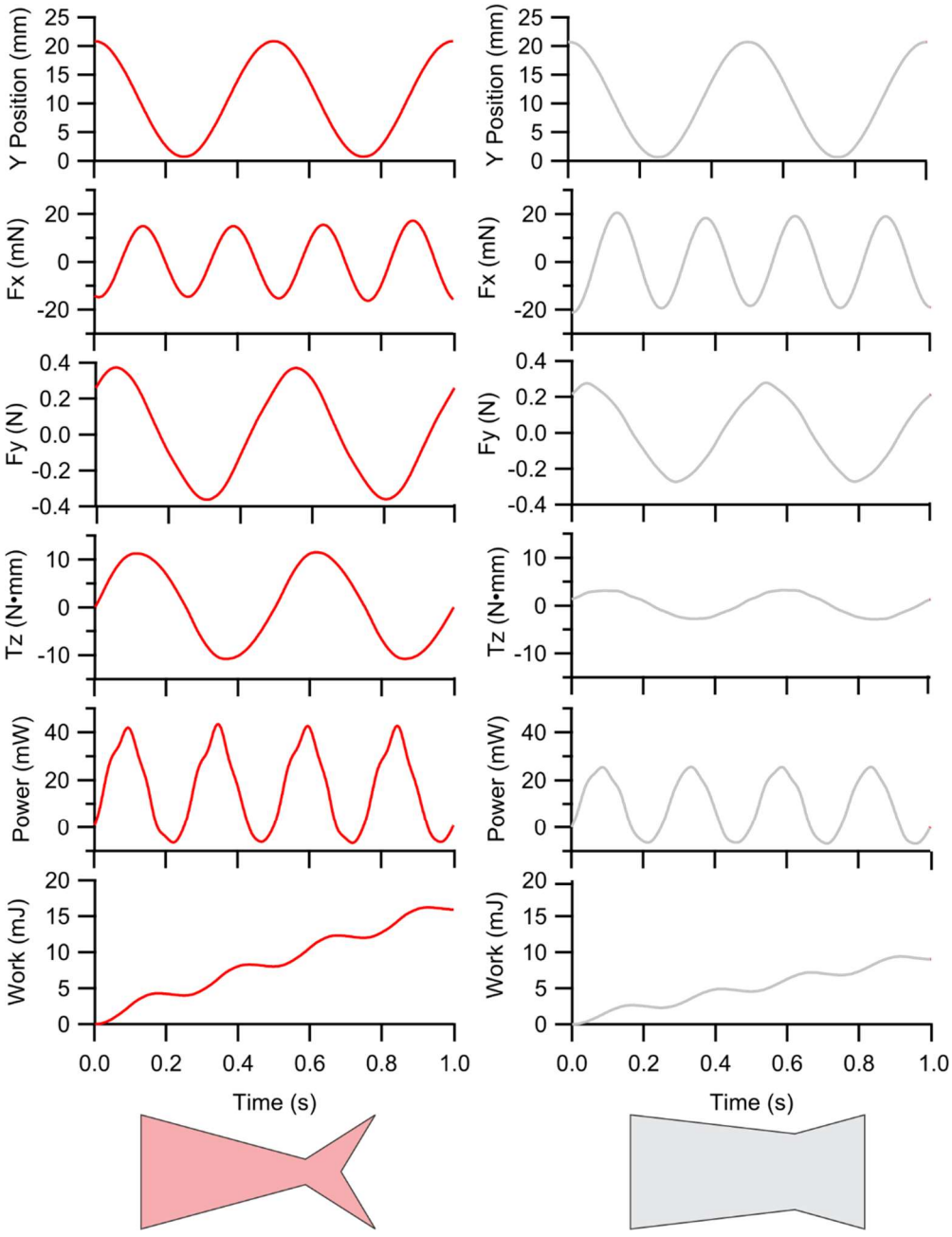

Figure 1.2. Representative force, torque, and calculated data from foils C1 (left) and W4 (right) when each is swimming at its self-propelled speed.

Note that the swimming foils are self-propelling, and so the F_x curves average to zero over a cycle.

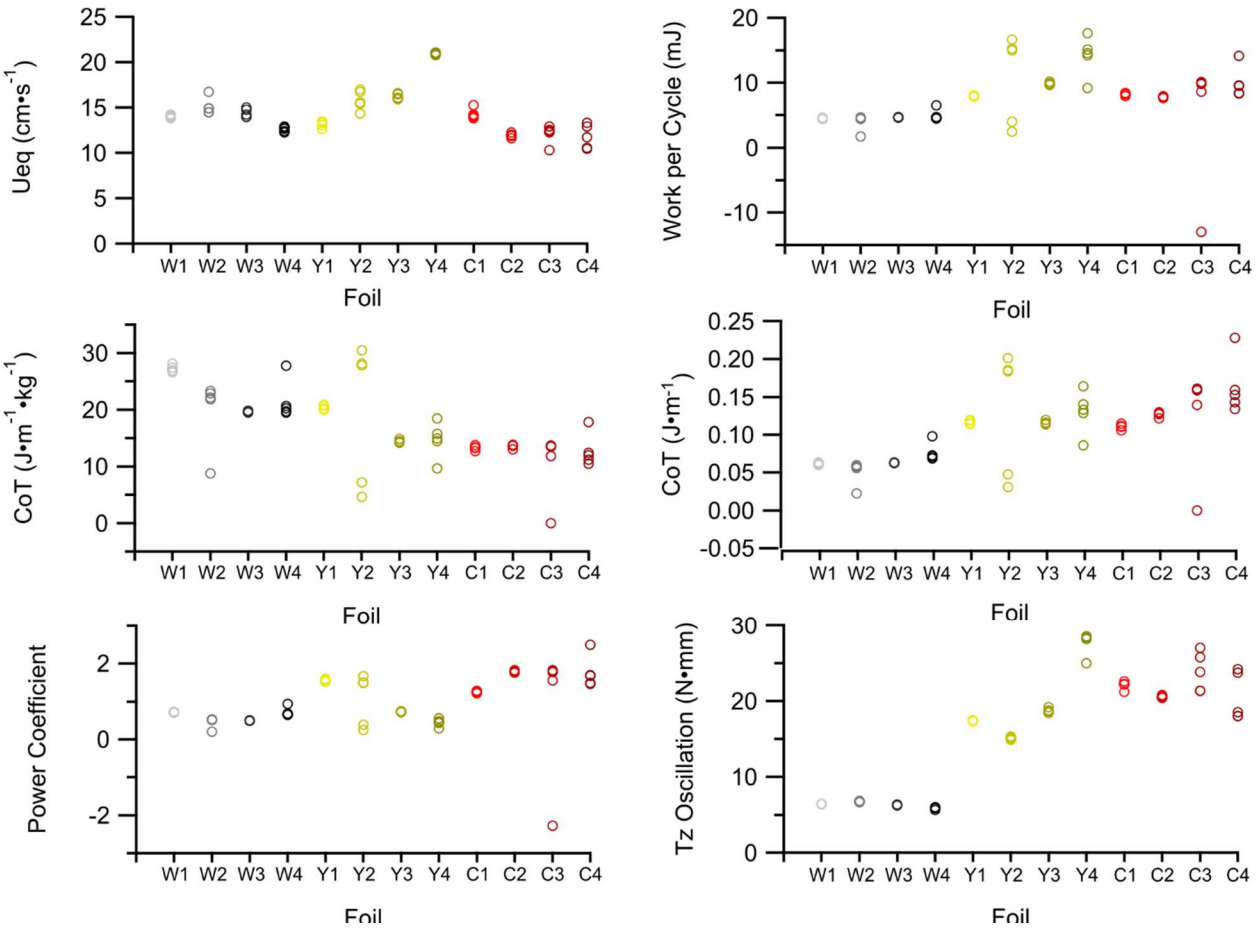

Figure 1.3. Swimming performance metrics for self-propelling foils. Raw data from each of the five trials per foil are shown. Points are translucent to show any overlap. Statistical analyses of these data are presented in Table 1.2.

Table 1.2. Summary of two-way ANOVA on aligned ranks for four variables.

Variables	**Source of Variation**	***df***	**F-ratio**	**Prob.**
Ueq	Shape	3	35.60	<0.0001*
	Stiffness	2	12.78	0.0007*
	Shape x Stiffness	6	0.02	0.8989
Mass-specific CoT	Shape	3	4.22	0.01[a]
	Stiffness	2	31.07	<0.0001[a]
	Shape x Stiffness	6	4.49	0.0011[a]
Power coefficient	Shape	3	5.03	0.0041[a]
	Stiffness	2	43.88	<0.0001[a]
	Shape x Stiffness	6	11.52	<0.0001[a]
Tz Oscillation	Shape	3	14.23	<0.0001[a]
	Stiffness	2	81.25	<0.0001[a]
	Shape x Stiffness	6	47.87	<0.0001[a]

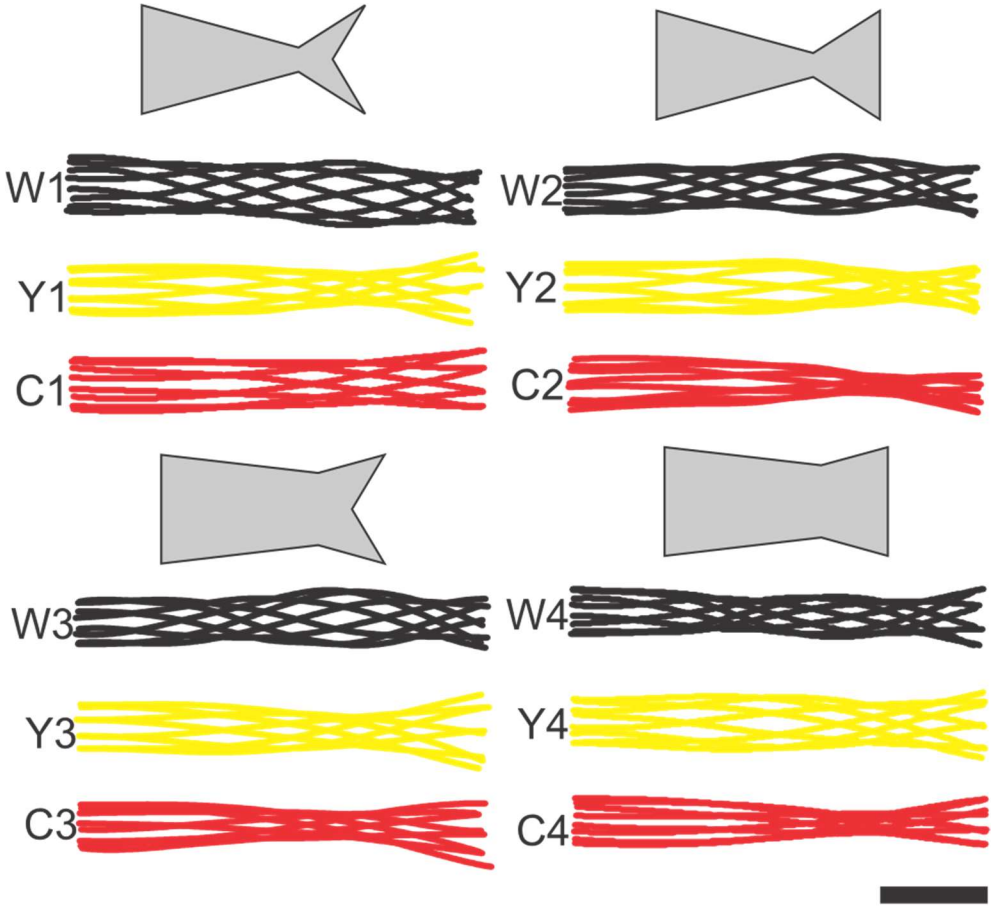

Figure 1.4. Midline envelopes showing the lateral (side-to-side) excursion of foil motion along the length for self-propelling foils of different shapes and stiffnesses. Scale bar represents 5 cm for all foil shapes.

1.4.3 *Flow visualization*

PIV revealed that flow patterns at the peduncle notch of each foil varied considerably, while midline flow patterns were far more consistent across stiffnesses and shapes (Figures 1.5 and 1.6). Of particular interest were flow patterns around the caudal peduncle (through the peduncle notch), where flow off the trailing edge of the upstream 'body' segment of the foil appeared to greatly modify the flow incident on the tail leading edge. For foils with narrow peduncles, in the plane of the peduncle notch, there was obvious flow through the gap between the body and the tail. This flow was not observed in the plane of the foil midline. Depending on the foil's shape and stiffness, flow through the peduncle notch could either increase the tail's effective angle of attack, or result in almost no flow immediately anterior to the tail (Figures 1.5 and 1.6).

Phase differences between the body trailing edge and the tail leading edge were observed, and likely were caused by the interaction of tail shape and stiffness. These phase differences produced interesting changes in the flow incident on the tail as well—dictating whether or not flow off the body trailing edge would interact with the tail, or merely pass the tail by (Figures 1.5 and 1.6). We noted the presence of a leading edge vortex (LEV) on the tail leading edge of foil C1, a foil of the stiffest material with both a narrow peduncle and a tail fork, which appears to be a product of such a fluid-structure interaction (hollow arrow, Figure 1.6). A bound LEV was not observed on any other foil.

1.5 Discussion

1.5.1 *Propulsion of differently-shaped flexible foils*

Fish tail fin shape and its impact on locomotor function has been the subject of research

Figure 1.5. Flow visualization around self-propelling flexible white foils, W1 (top panel) and W4 (bottom panel). The top row in each panel shows flow at the foil midline, the bottom row shows flow at the middle of the caudal 'notch'. Time is given as percent completion of one flap cycle, where 0% is at the lowest heave point. Times were chosen to show the appearance of a vortex at the trailing edge of the body (column 1), and the point at which that vortex reaches the fore-aft position of the tail leading edge (column 2). Vortices from the body trailing edge are indicated with white arrows. Scale bars represent 5 cm. Vorticity (blue, clockwise rotation; red, counterclockwise rotation) is also shown on each image.

Figure 1.5 (Continued)

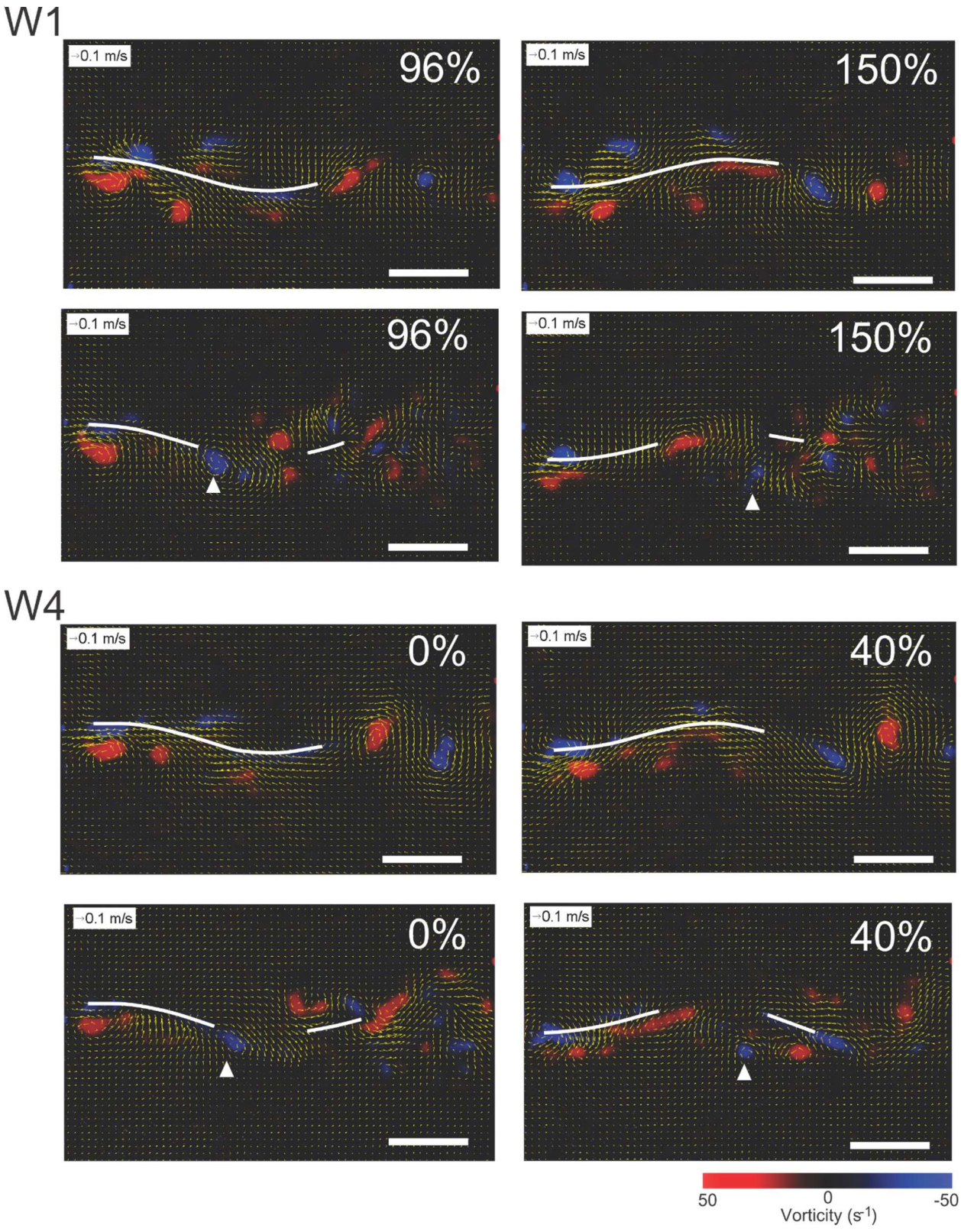

Figure 1.6. Flow visualization around self-propelling stiff coral foils, C1 (top panel) and C4 (bottom panel). The top row in each panel shows flow at the foil midline, the bottom row shows flow at the middle of the caudal 'notch'. Time is given as percent completion of one flap cycle, where 0% is at the lowest heave point. Times were chosen to show the appearance of a vortex at the trailing edge of the body (column 1), and the point at which that vortex reaches the fore-aft position of the tail leading edge (column 2). Vortices from the body trailing edge are indicated with white arrows. Scale bars represent 5 cm. Vorticity (blue, clockwise rotation; red, counterclockwise rotation) is also shown on each image.

Figure 1.6 (Continued)

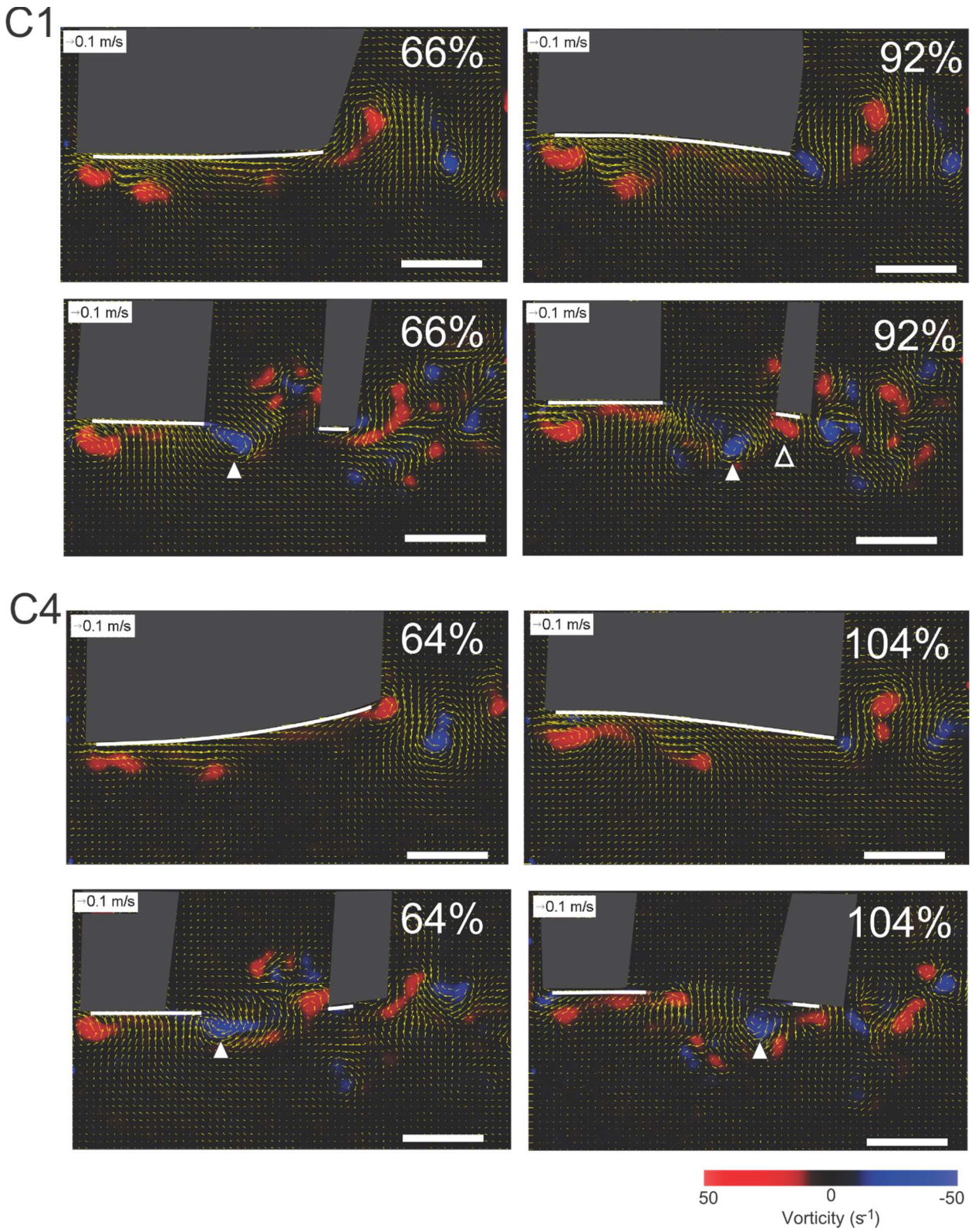

for more than a century (*e.g.* Ryder, 1886, Breder, 1926, Affleck, 1950, Webb, 1978). From observations of the evolutionary transition from heterocercal to homocercal tails and their potential for lift generation by the tail (Ryder, 1886, Grove and Newell, 1936) to early mechanical studies of tail function (Grove and Newell, 1936, Affleck, 1950), it was clear that tail shape has the potential to impact swimming performance. Using mechanical models to isolate the effects of particular shapes was an important first step, and the paper by Affleck (1950) is a classic in this regard. Although these early studies used stiff plates, and were largely qualitative, they proved that shape can exert a large influence on the forces experienced by a fish during undulatory swimming. A later study performed a more direct manipulation of fish tails—determining how partial amputation of the tail affected swimming performance (Webb, 1973a). These manipulations, however, appeared to have little effect on the swimming performance of trout with altered tails. More recent studies (*e.g.* Plaut, 2000, Blake *et al.,* 2009, Law and Blake, 1996, Webb and Fairchild, 2001) have used natural variation in fish body and tail shapes and a comparative approach to investigate the effect of changes in fish morphology on locomotor performance.

Lauder *et al*. (2012) summarized previous results obtained using the flapping foil apparatus used in this study, and showed differences in swimming performance between flexible foil models with different trailing-edge shapes. Their study, which employed several differently shaped foils, including a simple model of a homocercal (symmetrical tail) and another with a shark-like (asymmetrical) tail, demonstrated that 3D flow over the entire tail was more complicated than the section of flow observed in the plane of the foil midline. They also demonstrated that even simple changes in trailing edge shape could effect large changes in the forces produced by the foil (Lauder *et al.,* 2012). Subsequent work using this same flapping foil

mechanism attempted to determine how length or stiffness alone affect swimming performance (Shelton *et al.,* 2014). Data from Alben *et al*. (2012) suggest that specific combinations of foil length and stiffness can exhibit multiple performance optima. However, those experiments were conducted on rectangular foils, and did not include shape manipulations. One additional area to consider in flexible foil propulsion is the oscillation that would naturally occur in the center of mass if the foils were truly unconstrained to move freely in a fluid environment. Under the current experimental constraints, foils cannot oscillate in the upstream–downstream (x) direction as the heave motor constrains the leading edge to lateral motion only.

In this study as in the other papers cited above, the swimming flexible foils do not exhibit unconstrained center of mass motion as observed in freely swimming fishes (Xiong and Lauder, 2014), and thus will show momentary small imbalances in the forces during propulsion. Wen and Lauder (2013) addressed this constraint by allowing controlled x-direction motion and varying the extent of this movement to determine the effect on thrust forces of center of mass motion. They found that reductions in the magnitude of thrust force oscillation could be achieved by allowing the swimming foils to oscillate axially during propulsion. This study is a continuation of this overall body of work on flexible panel propulsion, and we use controlled manipulations of a simple experimental model to remove confounding factors and ask a specific question: how might two aspects of shape, namely, the narrow caudal peduncle and the forked tail so often associated with economical cruising, affect swimming performance. The long-held hypothesis, largely based on hydrodynamic principle instead of experimental data, was that both narrow peduncle and a forked tail would reduce swimming CoT. In particular, we expected the combination of narrow peduncle and forked tail to maintain high speed at a lower energetic cost (Brill, 1996).

The results, however, do not agree with this simple assertion. The effects of both tail shape and tail stiffness interacted, such that it was difficult to predict any general performance difference between a deep peduncle and a narrow one, and between forked and unforked tails (Figure 1.3, Table 1.2). Even stiffness alone seemed to generate unexpected changes in foil swimming performance. Within any of the three given stiffnesses/materials, the effects of shape on performance were irregular. Z-torques increased as material flexural stiffness increased—the coral foils had the highest torques, and the white foils had the lowest (Figure 1.3, Table 1.2).

In sum, our results suggest that both shape and stiffness are important in determining the propulsive performance of undulating foils and that complex interactions between these two parameters occur.

1.5.2 *Hydrodynamics of differently-shaped foils*

PIV of the different foils complemented the performance measures in that flow, too, behaved in a complex manner depending on shape and stiffness. In particular, flow off the midline axis was highly variable, and provided new information about how the foil interacted with the surrounding fluid that is not captured in the plane of the midline. The off-midline flow was complex, especially in the region between the body and the tail parts of the foil due to the sharp edges encountered by the flow. This suggests that three-dimensional flow surrounding the tail is dependent on shape—especially that of the peduncle —and that studying midline flow alone fails to uncover much of the variation in the hydrodynamics of different shapes. This reinforces the views of Tytell *et al*. (2008), and more recent studies taking advantage of volumetric PIV (Flammang *et al*., 2011) and computational fluid dynamic modelling (Borazjani and Daghooghi, 2013): fishes and other flapping bodies with irregular shapes do not operate in

flatland. Their moving, three-dimensional shapes influence hydrodynamic flow patterns significantly.

One way that shape and stiffness may be working in tandem to modulate performance is by altering kinematics, specifically, by modulating the phase relationship of the body and the tail (Lighthill, 1970; Figures 1.5 and 1.6). The presence of a body trailing edge and a tail leading edge, which varies with shape (Figure 1.1), allows flow from the body to interact with or even dictate the flow incident on the tail. Body and tail flow interaction appears to be modulated by foil kinematics. For instance, with foil C1, the kinematics were such that the vorticity off the trailing edge of the body interacts with the leading edge of the tail, changing the tail's effective angle of attack (Figure 1.6). In other foils, such as foil W4, the leading edge of the tail was nowhere near the vorticity shed by the body when that vorticity passed the tail (Figure 1.5). Shape and stiffness thus interact to produce varying kinematics. The kinematics may be what ultimately drives swimming performance in these foils by altering the phasing of flows in the gap between the body and tail regions of the foils (also see Drucker and Lauder, 2001, Akhtar *et al.*, 2007 and Standen and Lauder, 2007 for discussion of flow interactions among fins in fishes). Indeed, the optimal kinematics (see Eloy, 2013) for a given body shape vary considerably—even within the limitations of elongated-body theory. Taken as a whole, these results suggest that body-tail phase relationships may be a useful potential determinant of swimming performance.

The presence of a LEV on foil C1 is intriguing, given that leading edge vorticity is suspected to play a role in the presumed benefits of forked and semi-lunate tails (Chopra and Kambe, 1977, Karpouzian *et al.,* 1990, Borazjani and Daghooghi, 2013). This vortex appears to be the product of the effective angle of attack created by the interaction of vorticity off the body and on the tail, forming a weak, but discernable rearward jet (Figure 1.6). A LEV on the foil tail

surface may enhance propulsion via leading edge suction in the same manner suggested by Borazjani and Daghooghi (2013) in their computational fluid dynamic study of fish tail function. We note that foil C1 had a higher U_{eq} than the other foil shapes of the same material (Figure 1.3). The placement of the bound LEV on foil C1 suggests that it would produce suction to pull the tail forwards and augment thrust. If that is the case, it suggests a narrow, stiff peduncle might be required for LEV thrust enhancement: the narrow peduncle to ensure a distinct body trailing edge and tail leading edge, and the stiffness to create the proper phase relationship between body and tail during undulatory propulsion. Whether this mechanism plays a role in fish swimming has yet to be determined for live fish, but remains a tantalizing possibility.

1.5.3 *Implications for fish tail shape function*

The foils used in this study are simplified models of actual fish tails, and yet, even their performance appears to be dictated by a complex interaction of shape and stiffness. It was difficult to determine any predictive relationship between shape and performance, and there was no single shape or stiffness with the best performance for all performance metrics. The flow pattern produced by a given tail shape was governed by the interaction of the body and tail flows, suggesting that tail shapes cannot be studied in isolation of the body. Because the flow incident on the tail is in large part determined by the movement of the body in front of it, an isolated tail foil, without a body component, may not accurately model tail hydrodynamics in the freely-swimming fishes.

The foils used in this study are not intended to exactly replicate fish motion, but rather to investigate the complexity of shape as factor affecting undulatory locomotor dynamics, and suggest future avenues of research in biological systems of undulatory propulsion. The changes

produced by varying shape of the foils—including the interaction of flow between anterior and posterior regions of the foils—suggest the possibility of similar interactions having a role in fish locomotion. A few notable studies have observed interactions among median fins in live fish similar to those of the foils in the present study (Drucker and Lauder, 2001, Standen and Lauder, 2007, Tytell *et al*., 2008). Future research in biological systems may reveal the importance of such shape-based hydrodynamic interactions in fish swimming.

The complexity of this study's findings also demonstrate that even one shape can behave differently depending on the kinematics with which it's moved, how the body in front of the tail is shaped and moves, and the body and tail's material properties. Many of the foils in this study contradicted the simplistic hypotheses about function. For example, the forked tail with the narrow peduncle region (the most 'tuna-like' tail) did not display the highest U_{eq} or the lowest energetic cost at all stiffnesses (Figure 1.3). All of this is not to say that existing hypotheses about how fish body and tail shape affect swimming performance are wrong. Rather, it suggests that extrapolating any performance advantage from morphology alone is a risky venture. The assumptions behind the claims of adaptive morphology may be correct, but until the implied mechanistic links between morphology and performance are proven, they remain assumptions. Morphology and performance often have complicated interrelationships. Until there are data demonstrating that a morphological feature directly affects a specific metric of swimming performance, equating morphological differences with performance differences is premature.

1.6 References

Affleck, R. J. (1950). Some points in the function, development, and evolution of the tail in fishes. *Proc. Zool. Soc. Lond*. 120: 349-368.

Akhtar, I., R. Mittal, G. V. Lauder, and E. Drucker. (2007). Hydrodynamics of a biologically inspired tandem flapping foil configuration. *Theor. Comput. Fluid Dyn*. 21: 155-170.

Alben, S., C. Witt, T. V. Baker, E. J. Anderson and G. V. Lauder. (2012). Dynamics of freely swimming flexible foils. *Phys. Fluids.* 24: 051901.

Benjamini, Y. and Y. Hochberg. (1995). Controlling the false discovery rate: a practical and powerful approach to multiple testing. *J. R. Stat. Soc. Series B* 57: 289-300.

Blake, R. W., J. Li and K. H. S. Chan. (2009). Swimming in four goldfish *Carassius auratus* morphotypes: understanding functional design and performance employing artificially selected forms. *J. Fish Biol*. 75: 591-617.

Borazjani, I. and M. Daghoogi. (2013). The fish tail motion forms an attached leading edge vortex. *Proc. R. Soc. Lond. B*. 280: 20122071.

Borazjani, I. and F. Sotiropoulos. (2010). On the role of form and kinematics on the hydrodynamics of self-propelled body/caudal fin swimming. *J. Exp. Biol*. 213: 89-107.

Borazjani, I., F. Sotiropoulos, E. D. Tytell, and G. V. Lauder. (2012). Hydrodynamics of the bluegill sunfish C-start escape response: three-dimensional simulations and comparison with experimental data. *J. Exp. Biol.* 215: 671-684.

Breder, C. M. (1926). The locomotion of fishes. *Zoologica*. 4: 159-297.

Brill, R. W. (1996). Selective advantages conferred by the high performance physiology of tunas, billfishes, and dolphin fish. *Comp. Biochem. Physiol.* 113A: 3-15.

Chopra, M. G. and T. Kambe. (1977). Hydromechanics of lunate-tail swimming propulsion. Part 2. *J. Fluid Mech.* 79: 49-69.

Dewey, P. A., B. M. Boschitsch, K. W. Moored, H. A. Stone and A. J. Smits. (2013). Scaling laws for the thrust production of flexible pitching panels. *J. Fluid Mech.* 732: 29-46.

Eloy, C. (2013). On the best design for undulatory swimming. *J. Fluid Mech.* 717: 48-89.

Flammang, B. E., G. V. Lauder, D. R. Troolin, and T. E. Strand. (2011). Volumetric imaging of fish locomotion *Biol. Lett.* 7: 695-698.

Grove, A. J. and G. E. Newell. (1936). A mechanical investigation into the effectual action of the caudal fin of some aquatic chordates. *Ann. Mag. Nat. Hist.* 17: 280-290.

Karpouzian, G., G. Spedding and H. K. Cheng. (1990). Lunate-tail swimming propulsion. Part 2. Performance analysis. *J. Fluid Mech.* 210: 329-351.

Lauder, G. V. and P. G. A. Madden. (2006). Learning from fish: kinematics and experimental hydrodynamics for roboticists. *Int. J. Autom. Comput.* 4: 325-335.

Lauder, G. V., B. Flammang and S. Alben. (2012). Passive robotic models of propulsion by the bodies and caudal fins of fish. *Integr. Comp. Biol.* 52: 576-587.

Lauder, G. V., J. Lim, R. Shelton, C. Witt, E. Anderson and J. L. Tangorra. (2011). Robotic models for studying undulatory locomotion in fishes. *Mar. Technol. Soc. J.* 45: 45-55.

Law, T. C. and R. W. Blake. (1996). Comparison of the fast-start performances of closely related, morphologically distinct three-spine sticklebacks *(Gasterosteus sp.)*. *J. Exp. Biol.* 199: 2595-2604.

Lighthill, M. J. (1970). Aquatic animal propulsion of high hydrodynamical efficiency. *J. Fluid Mech.* 44: 265-301.

Lighthill, M. J. (1975) Mathematical Biofluiddynamics. Philadelphia: SIAM.

Lindsey, C. C. (1978). Form, function, and locomotory habits in fish. In Fish Physiology, Vol. 7. Locomotion (ed. W. S. Hoar and D. J. Randall), pp. 1-100. New York: Academic Press.

Long, J., M. Koob-Emunds, B. Sinwell and T. J. Koob. (2002). The notochord of hagfish *Myxine glutinosa*: visco-elastic properties and mechanical functions during steady swimming. *J. Exp. Biol.* 205: 3819-3831.

Magnuson, J. J. (1978). Locomotion by scombrid fishes: hydromechanics, morphology, and behavior. In Fish Physiology, Vol. 7. Locomotion (ed. W. S. Hoar and D. J. Randall), pp. 239-313. New York: Academic Press.

McHenry, M. J., C. A. Pell and J. A. Long. (1995). Mechanical control of swimming speed: stiffness and axial wave form in undulating fish models. *J. Exp. Biol*. 198: 2293-2305.

Plaut, I. (2000). Effects of fin size on swimming performance, swimming behavior and routine activity of zebrafish *Danio rerio*. *J. Exp. Biol*. 203: 813-820.

Quinn, D. B., G. V. Lauder and A. J. Smits. (2014a). Flexible propulsors in ground effect. *Bioinsp. Biomimet.* 9: 1-9.

Quinn, D. B., G. V. Lauder and A. J. Smits. (2014b). Scaling the propulsive performance of heaving flexible panels. *J. Fluid Mech.* 738: 250-267.

Read, D. A., F. S. Hover and M. S. Triantafyllou. (2003). Forces on oscillating foils for propulsion and maneuvering. *J. Fluid. Struct.* 17: 163-183.

Ryder, J. A. (1886). On the origin of heterocercy and the evolution of the fins and fin rays of fishes. *Rep. U.S. Comm. Fish and Fisheries.* 12: 981-1107.

Shelton, R., P. Thornycroft and G. V. Lauder. (2014) Undulatory locomotion of flexible foils as biomimetics models for understanding fish propulsion. *J. Exp. Biol.* 217: 2110-2120.

Standen, E. M. and G. V. Lauder. (2007). Hydrodynamic function of dorsal and anal fins in brook trout (*Salvelinus fontinalis*). *J. Exp. Biol*. 210: 325-339.

Tytell, E. D., E. M. Standen, and G. V. Lauder. (2008). Escaping Flatland: three-dimensional kinematics and hydrodynamics of median fins in fishes. *J. Exp. Biol.* 211: 187-195.

Webb, P. W. (1973a). Effects of partial caudal-fin amputation on the kinematics and metabolic rate of underyearling sockeye salmon (*Onchorhynchus nerka*) at steady swimming speeds *J. Exp. Biol.* 59: 565-582.

Webb, P. W. (1978). Fast-start performance and body form in seven species of teleost fish. *J. Exp. Biol*. 74: 211-226.

Webb, P. W. (1984) Body form, locomotion and foraging in aquatic vertebrates. *Amer. Zool.* 24: 107-120.

Webb, P. W. (1988). Simple physical principles and vertebrate aquatic locomotion. *Amer. Zool.* 28: 709-725.

Webb, P. W. (1992). Is the high cost of body/caudal fin undulatory swimming due to increased friction drag or inertial recoil? *J. Exp. Biol.* 162: 157-166.

Webb, P. W. and A. G. Fairchild. (2001). Performance and maneuverability of three species of teleostean fishes. *Can. J. Zool.* 79: 1866-1877.

Wen, L. and G. V. Lauder. (2013). Understanding undulatory locomotion in fishes using an inertia-compensated flapping foil robotic device. *Bioinsp. Biomimet.* 8: 046013.

Wen, L., J. C. Weaver and G. V. Lauder. (2014). Biomimetic shark skin: design, fabrication, and hydrodynamic function. *J. Exp. Biol.* 217: 1656-1666.

Wobbrock, J. O., L. Findlater, D. Gergle and J. J. Higgins. (2011). The aligned rank transform for nonparametric factorial analyses using only ANOVA procedures. In Proceedings of the ACM conference on human factors in computing systems (CHI '11). Vancouver, British Columbia (May 7-12, 2011)., pp. 143-146. New York: ACM Press.

Wolfgang, M. J., J. M. Anderson, M. A. Grosenbaugh, D. K. Yue and M. S. Triantafyllou. (1999). Near-body flow dynamics in swimming fish. *J. Exp. Biol.* 202: 2303-2327.

Xiong, G. and G. V. Lauder. (2014). Center of mass motion in swimming fish: effects of speed and locomotor mode during undulatory propulsion. *Zoology*. 117: 269-281.

Page intentionally left blank

Chapter 2

Correlated evolution of body and fin morphology in the cichlid fishes

Kara L. Feilich

2.1 Summary

Body and fin shapes are chief determinants of swimming performance in fishes. Different configurations of body and fin shapes can suit different locomotor specializations. The success of any configuration is dependent upon the hydrodynamic interactions between body and fins. Despite the importance of body–fin interactions for swimming, there are few data indicating whether body and fin configurations evolve in concert, or whether these structures vary independently. The cichlid fishes are a diverse family whose well-studied phylogenetic relationships make them ideal for the study of macroevolution of ecomorphology. This study measured body, and caudal and median fin morphology from radiographs of 131 cichlid genera, using morphometrics and phylogenetic comparative methods to determine whether these traits exhibit correlated evolution. Partial least squares canonical analysis revealed that body, caudal fin, dorsal fin, and anal fin shapes all exhibited strong correlated evolution consistent with locomotor ecomorphology. Major patterns included the evolution of deep body profiles with long fins, suggestive of maneuvering specialization; and the evolution of narrow, elongate caudal peduncles with concave tails, a combination that characterizes economical cruisers. These results demonstrate that body shape evolution does not occur independently of other traits, but among a suite of other morphological changes that augment locomotor specialization.

2.2 Background

The explosive speciation and diversification of cichlid fishes has made the group an ideal model system for the study of evolution and adaptation. In addition to taxonomically diverse clades endemic to the African rift lakes, the family also includes morphologically and behaviorally diverse fishes from South America, West Africa, and the Indian subcontinent (Liem, 1973, Genner *et al.,* 2007). In the context of extensive and robust phylogenetic hypotheses of cichlid interrelationships (Salzburger *et al.,* 2005, Genner *et al.,* 2007, Friedman *et al.,* 2013, McMahan *et al.,* 2013; Schwarzer *et al.,* 2015, and others), comparative biologists focusing on this lineage are afforded the opportunity to study the process and mechanisms that underpin adaptive radiation, and the evolution of morphological systems that are implicated in the group's adaptive success. Several studies have focused on the explosive cichlid radiation to study the process of morphological evolution (Liem, 1973, Kocher *et al*., 1993, Winemiller, *et al.* 1995, Albertson *et al.,* 2003, Clabaut *et al.,* 2007, Young *et al.,* 2009), with some recent studies exploring the evolution of functionally related structures (Rüber and Adams, 2001, Muschick *et al.,* 2012, Kusche *et al.,* 2014, Astudillo-Clavijo *et al.,* 2015).

Although many morphological studies focus on body shape in isolation, there is a large body of work showing that fin morphology may be just as important as body shape. Fin shape and configuration vary widely, and serve multiple functions during swimming, including thrust production, stabilization, and maneuvering (Webb, 1982, Webb, 1984, Weihs, 1989; Lauder *et al.*, 2002, Lauder and Drucker, 2004). The role of pectoral fin shape and kinematics in swimming performance has been discussed for several labriform taxa (Walker and Westneat, 2002, Thorsen and Westneat, 2005), and median fin variation has been discussed with respect to balistiform locomotion (Wright, 2000, Blake *et al.,* 2009, Dornberg *et al.,* 2011). Biomechanists have long

considered caudal fin shape in its relation to swimming performance, particularly in the context of swimming economy (e.g., Affleck, 1950, Borazjani and Daghoogi, 2013). Species descriptions and the taxonomic literature refer often to meristic counts of fin elements in the median fins, but rarely consider the shapes of fins in explicitly functional contexts. In one study, Dornberg et al. (2011) examined the correlations between fin and body shapes within triggerfishes (family Balistidae). However, given the unique mode of locomotion in this group—"balistiform" swimming, in which dorsal and anal fins are the main propulsors—it is unlikely that the patterns they uncovered apply generally to non-balistid fishes. The functional roles of different fin shapes have been considered in several earlier studies including those using physical (Affleck, 1950, Lauder *et al.,* 2012, Feilich and Lauder, 2015), theoretical (Lighthill, 1970), and computational models (Borazjani and Daghoogi, 2013).

To exclude midline fins from the morphometrics literature belies their importance for locomotion. In some fishes, such as bluegill (*Lepomis macrochirus*), the dorsal fin alone may account for more than 10% of total thrust production during steady swimming, and over a third of the lateral forces during turning (Drucker and Lauder, 2001). Caudal peduncle and caudal fin morphology have been discussed in the biomechanics literature as having the potential to reduce drag, increase thrust, and interact with the median fins during locomotion, but this has not been explored in an explicitly phylogenetic context (Weihs, 1989, Triantafyllou *et al.,* 2000). Recent biomechanics research provides increasing evidence that fin–fin and fin–body interactions may be very important in terms of their ability to explain the effect of potential morphological adaptations on locomotor performance (Akhtar *et al.,* 2007, Tytell *et al.,* 2008, Feilich and Lauder, 2015).

Given the importance of the fins and body operating in tandem to facilitate swimming and feeding, the question arises as to whether fin and body shape evolution are tightly correlated, or whether body and fins largely evolve independently of one another. This study leverages the diversity of cichlid body and fin morphology and the strong history of cichlid evolutionary morphology to investigate how fins and body shape co-vary and evolve within the lineage. To answer this question, I take a comparative morphometric approach, examining the variety of cichlid shapes, and any patterns of correlated evolution among fins and body.

Previous studies of cichlid body shape evolution have demonstrated consistent patterns in variation among several cichlid clades. The major axis of cichlid body–shape diversity, as in many other fishes, appears to be body elongation (Clabaut *et al.,* 2007, Friedman, 2010; Muschick *et al.,* 2012, Claverie and Wainwright, 2014, Astudillo-Clavijo *et al.,* 2015). Elongation is largely associated with increases in vertebral count, vertebral length, and/or with elongation of the "snout" (Ward and Mehta, 2010). Most cichlid morphospaces, and many morphospaces for other fish taxa, also suggest that variation in isolated regions of the body (e.g., caudal peduncle depth and length, head length) contribute significantly to overall morphological disparity (Clabaut *et al*., 2007, Claverie and Wainwright, 2014, Montaña *et al*., 2014).

Studies of both feeding morphology and body shape, among cichlids and ecologically similar species, provide strong evidence of an ecomorphological link between both body shape and pharyngeal jaw morphology with trophic niche (Winemiller *et al.,* 1995, Rüber and Adams, 2001, Clabaut *et al.,* 2007, Muschick *et al.,* 2012, López-Fernández *et al.,* 2012). For example, piscivores tend to have long shallow heads, and large anterior bodies (Clabaut *et al.,* 2007, López-Fernández *et al.,* 2012). This pattern in trophic ecomorphology has also been described in

other fishes, including temperate sunfishes (Ehlinger and Wilson, 1988), arctic char (Snorrason *et al.,* 1994), and sea breams (Antonucci *et al.,* 2009).

Within cichlids, some clades exhibit more body shape variation than others. Studies of all African cichlids show that while the species richness of the haplochromine radiation is astounding, within-group morphological variation of the haplochromines is lower than that of the paraphyletic Tanganyikan and West African non-haplochromine cichlids (Chakrabarty, 2005). In the neotropical cichlids, the geophagines have the highest within group body shape variation (Arbour and López-Fernández, 2014). To date, no studies have compared the morphological variation across both African and Neotropical cichlid clades.

This study makes use of the vast morphological diversity of cichlids and builds on earlier morphometric studies of fish evolution to fill the gap in the literature as to body and median fin covariation. I measured body and fin morphology in 131 cichlid genera, and used two separate phylogenetic hypotheses of cichlid evolution to assess the extent to which morphological evolution of individual structures and correlated evolution among structures occurred. I hypothesized that if body and fin shape were constrained according to existing hypotheses of locomotor specialization, extremes in body and fin shape would co-occur in patterns consistent with those hypotheses (Table 2.1). Specifically, a set of predictions were made derived from the oft-applied (though less-oft-tested) hypotheses proposed by Webb (1984), with two different null predictions, explained in Table 2.1.

Table 2.1. Framework and rationale for hypotheses describing evolutionary covariation.

	Hypothesis	Prediction	Rationale
Null hypotheses	Null 1: Complete modularity	No morphological covariation between any two-structure pairing.	In a rapidly evolving clade, it is possible that all structures are effectively evolving independently and/or that there is no selection for correlated evolution of structures.
	Null 2: Complete covariation	All structures exhibit perfectly correlated evolution, with similar patterns of disparity through time.	If the body and fins are actually a single unit, and the distinction among them is merely a useful tool for descriptive anatomy, and/or if selection for correlated evolution is very strong (i.e., only very few combinations of traits satisfy the organism's functional needs), then one would expect all structures to evolve together.
Functional linkage hypotheses	Link 1: Body-caudal fin	Body shape and caudal fin shape exhibit correlated evolution, with similar patterns of disparity through time.	Species specializing in steady swimming economy are expected to have both a fusiform "tuna-like"shape, and forked or lunate tails to reduce drag and increase thrust during body–caudal fin swimming (Lighthill, 1970, Webb,1984, Weihs, 1989, Feilich and Lauder, 2015). If swimming economy is a major selective pressure, one may expect to see correlated evolution of these two propulsive structures.
	Link 2: Dorsal fin- anal fin	Dorsal fin shape and anal fin shape exhibit correlated evolution, with similar patterns of disparity through time.	There are both functional and developmental linkages between the dorsal and anal fin. The dorsal and anal fin form symmetrically about the longitudinal axis of the fish, suggesting that they are a developmental module (Mabee et al., 2002). Their function in stabilizing roll and maneuver may be enhanced by symmetric structure as well.
	Link 3: Body - caudal fin Body - dorsal fin Caudal fin - dorsal fin	Body, caudal fin, and dorsal fin will all exhibit correlated evolution with similar patterns of disparity through time.	See body–caudal fin module hypothesis, and the dorsal fin may play a role in wake recapture and drag reduction by interacting with flow shed by the body and orienting it relative to the leading edge of the tail to increase thrust (Tytell *et al.,* 2008, Borazjani and Daghoogi, 2013, Feilich and Lauder, 2015).
	Link 4: Body - dorsal fin Body - anal fin Dorsal fin – anal fin	Body, dorsal fin, and anal fin will all exhibit correlated evolution with similar patterns of disparity through time.	See dorsal fin–anal fin module, and a deep-bodied, round lateral profile are thought to permit greater turning moments in maneuvering specialists (Webb, 1984).

Null hypothesis 1 is the prediction expected given complete modularity of body and fins, with changes in one structure occurring independently of changes in any other structure, with low integration across structures. Null hypothesis 2 is the opposite prediction, that all structures exhibit perfect covariation and correlated evolution, with high integration across all structures. These null hypotheses were unlikely to explain cichlid morphology, but provided a basis for comparison to check for other patterns in morphological evolution. The alternative hypotheses describe patterns of correlated evolution that one may expect given selection for locomotion-related configurations. These hypotheses predict patterns of linkage between structures that interact during undulatory swimming, described in Table 2.1. Correlated evolution between the structures in the alternative hypotheses would reflect evolution toward an expected locomotor specialist phenotype.

2.3 Methods

2.3.1 *Morphological data collection*

Morphological diversity in cichlids is generally believed to be highest at the intergeneric level, with only minor differences in morphology within genera (Stauffer *et al.,* 1997, Albertson *et al*., 1999, López-Fernández *et al*. 2012); so sampling efforts focused on measuring as many different genera as possible. One hundred and thirty-one cichlid museum specimens were obtained from the MCZ or AMNH (Supp. Table S2.1), and a specimen radiograph of *Retroculus* was obtained from the NMNH Ichthyology collection database. All specimens were adults in good condition, and if any structure was damaged, it was excluded from the analysis of that structure. It was assumed that differences in morphology due to initial method of preservation (formalin or ethanol fixation) or specimen age would be minimal compared to variation from

differences in species morphology (Lai, 1963). For those species known to exhibit sexual dimorphism, specimens that were either female or indistinguishable from female were used. Specimens were imaged using a Kevex PXS10-16W x-ray source (Thermo Electron Corp., Scotts Valley, CA), and a PaxScan 4030R digital imaging subsystem (Varian Medical Systems, Salt Lake City, UT). These radiographs were used to obtain data for subsequent analysis.

Twenty-seven geometric morphometric (GM) landmarks (Figure 2.1, in red; Supp. Table S2.2), were used to describe lateral body shape. These landmarks were chosen to be easily recognizable anatomical features that provide coverage over the body while also being informative with respect to the anatomical source of shape variation. Homology constraints on landmark choice were relaxed in order to include information on the position of the soft and spiny portions of the dorsal and anal fins on the body. The landmarks for the insertions of these fins represent the first (anterior-most) spine and ray, middle spine and ray, and last (posterior-most) spine and ray. For specimens with even numbers of spines and/or rays, the "middle" spine/ray was chosen as follows: if there were 10 spines, the middle spine was the fifth spine. Landmarks were recorded from the radiographs using TPSDig2 (Rohlf, 2013). These landmarks were then processed using generalized Procrustes analysis in MorphoJ (Klingenberg, 2011) to isolate the variation in shape from that of body size. The resulting generalized Procrustes coordinates were exported from MorphoJ and used as inputs for further morphometric analyses. Centroid size for each specimen was also obtained from MorphoJ, and used in subsequent analyses of allometry.

Fin shape changes with behavior, and the fins are rarely extended after specimen fixation. Given this source of variation, anal, dorsal, and caudal fin shapes were parameterized according

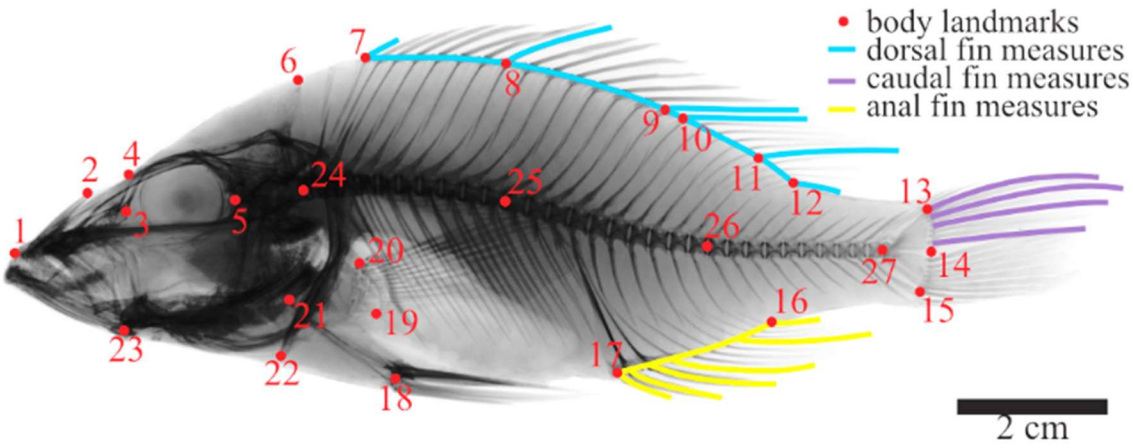

Figure 2.1. Body landmarks and fin lengths used in morphometric analyses, shown on a representative specimen (MCZ49441 *Stigmatochromis woodi*). To analyze shape independently of size, generalized Procrustes coordinates were used to compare body shape, fin base lengths were expressed as the ratio of fin base length to total length, and fin element lengths were expressed as the residual of fin element length on centroid size.

to the length of the fin (for the dorsal and anal fins) and its associated skeletal elements—either fin spines or fin rays (Figure 2.1). The lengths of the dorsal and anal fin elements were recorded using ImageJ version 1.48 (Schneider *et al.* 2012) for each of the first, middle, and last spines and rays, as determined for the geometric landmarks, by manually fitting a spline to each fin element. Dorsal and anal fin length was measured as the length of the body curvature at the fin insertion. Cichlid caudal fins are generally homocercal, and caudal fin ray counts are very highly conserved. All of the specimens in this study possessed eight costal fin rays in the dorsal half of the caudal fin. Therefore, to parameterize shape of the caudal fin, the lengths of caudal fin rays 1, 3, 5, and 8, as counted from the dorsal caudal fin margin, were measured (Figure 2.1).

Procrustes transformation of GM landmarks accounted for differences in the body size of specimens, but linear fin measurements initially do not account for body size. To account for size variation in fin length and fin element length in an attempt to isolate differences in shape, linear measurements were scaled in one of two ways. Dorsal and anal fin base lengths (along the body margin) were divided by body length, and the resulting ratio was used for subsequent analysis. To account for overall body size in the fin element lengths, the length of each fin element for each specimen was linearly regressed on specimen centroid size in R, and the residual of each specimen from these regressions was used as a size-normalized input for subsequent analyses (Supp. Figure S2.3).

2.3.2 *Phylogenetic data and clade assignment*

There is controversy over the timescale of cichlid evolution, and even with similar topologies, comparative analyses can be very sensitive to the differences in branch length of a phylogeny. Estimates for the date of the Pseudocrenilabrinae–Cichlinae divergence, and the

diversification of African cichlids vary in the recent literature by more than 40 million years (Genner *et al.,* 2007, Friedman *et al.,* 2013, McMahan *et al.,* 2013). To account for both possible timelines of cichlid evolution, all phylogenetic comparative methods in this study were performed twice: each time using a different tree. One tree, Friedman *et al.* (2013), proposes a short-branch-length timeline for cichlid evolution. The second tree, McMahan *et al.* (2013), proposes a long-branch-length timeline. The two phylogenies were both pruned using *ape* (Paradis *et al.,* 2004) to include only those taxa for which I had morphological data. The pruned trees contained 52 and 50 species, respectively, retaining approximately half of the taxa of the original trees, and those taxa were evenly distributed over the original trees. Twenty-eight species were common to both pruned phylogenies, and for these species, the same morphological data were used for each analysis. However, the sister nodes including these species largely differed between the two pruned phylogenies.

In order to facilitate visualization of phylogenetic patterns in morphology in non-phylogenetic analyses, each specimen was assigned to a larger clade. Usually, the assignment was the cichlid tribe to which the specimen belonged (Supp. Figures S2.1, S2.2). For neo-tropical species, tribe assignments were generally determined according to McMahan *et al.* (2013), and consistent across the recent literature (Supp. Figure S2.2, Supp. Table S2.1). The state of African cichlid tribes, however, is in flux, and tribe assignments in the literature are inconsistent. Therefore, specimens from Africa were only grouped by tribe for noncontroversial tribes. For controversial groups, monophyletic clades from Friedman *et al*. (2013) were assigned numbers (Supp. Figures S2.1, S2.2; Supp. Table S2.1), and specimens were assigned to one of the numbered clades. Clade assignments were determined from Friedman *et al.* (2013) for species represented in that phylogeny. For all other African species, a broad literature search was

used to find phylogenies placing the taxa within a broader tree, and each taxon was assigned to the group of its nearest neighbor represented in the referenced phylogenies (see Supp. Table S2.1 and associated references for phylogenies used).

2.3.3 *Morphological variation of single structures*

To determine the amount and nature of the variation of particular structures, separate principal components analyses (PCA) were conducted for body shape, caudal fin shape, dorsal fin shape, and anal fin shape. For body shape, general Procrustes coordinates were used as the input for PCA, and for the median fins, the normalized base and fin element lengths were used. When the measurements used in PCA are of different scales, or the variance of individual variables differs greatly, PCA using the covariance matrix may lose much of its meaning (Joliffe, 2002). Therefore, to mitigate the effects of using different measurements, all PCAs were conducted using correlation matrices. Only species for which the body and fins were intact in good condition were included in those analyses: if a specimen had a damaged caudal fin, it was not included in the caudal fin PCA (see Supp. Table S2.1 for which specimens were included in each analysis). PCAs were conducted using R base statistics. The number of PCs used to describe each structure was determined by including n PCs such that for the variance explained by PC n, $\text{var}(n) > \text{var}(n + 1) \times 2$. In some cases (dorsal fin and anal fin), only one PC met this condition, but a second PC was included for the purpose of two-dimensional data visualization. Procrustes coordinates were projected into tangent space for visual analysis.

Phylogenetic PCAs were conducted using *phytools* on both phylogenies to account for phylogenetic patterns in morphology from common ancestry, using the subsets of morphological data represented on the phylogenies (Revell, 2009, Revell, 2012).

2.3.4 *Analyses of disparity*

Disparity through time (DTT) plots (Harmon *et al*., 2003) were generated using the R package *geiger* (Harmon *et al*., 2008) from the size-normalized data for each structure, using the tree data from the Friedman and the McMahan trees. Only those taxa that were included in either phylogeny were incorporated into this analysis.

2.3.5 *Phylogenetic signal and convergence in cichlid morphology*

To determine whether there was significant phylogenetic signal in the variation of structures, K_{mult}, a multitrait measure of phylogenetic signal, was calculated for each of the four structures over both reference phylogenies following the procedure of Adams (2014) using *geomorph* (Adams and Otarola-Castillo, 2013). To visually assess the extent of phylogenetic signal in cichlid morphology, phylomorphospace plots were produced from the original PCA for each phylogeny-specific dataset using *phytools* (Revell, 2012).

To determine focal groups that may have been subject to convergent evolution, SURFACE analyses using the R package *surface* (Ingram and Mahler, 2013) were conducted on each set of phylogenetic PC scores for the first PCs of each structure. SURFACE uses Ornstein-Uhlenbeck stabilizing selection models and stepwise Akaike Information Criterion to locate regime shifts on a tree and identify whether those shifts are towards convergent regimes (Ingram and Mahler, 2013). This allows one to look for convergent regimes that best explain a given set of trait data, with no need for *a priori* information about focal groups. Following SURFACE analysis, groups identified as convergent by surface were used as input focal groups in the R

package *windex* (Arbuckle and Minter, 2015), to measure the strength of the convergence using the Wheatsheaf index (Arbuckle *et al.,* 2014).

2.3.6 *Analysis of morphological covariation and coevolution among structures*

The principal goal of this study was to look for patterns of co-occurrence and co-evolution of particular body and fin shapes. To these ends, multiple two-block partial least-squares canonical analyses (PLS-CA) were used, treating the morphological data from each individual structure (i.e., body shape or fin shape) as a block of data. PLS-CA uses an iterative algorithm to find pairs of canonical variates (CVs), where each CV is associated with one of the two blocks of data. Each CV is selected to explain its associated data block well, and to have a high correlation with the other CV (Tenenhaus, 1998). A useful feature of PLS-CA is that the data blocks provided as inputs are treated symmetrically, without implying the predictor and response relationships typical of regression-based analyses. PLS-CA is analogous to PCA in that the first pair of canonical variates explains the most covariation in the multiblock dataset. PLS-CAs were performed using the R package *plsdepot* (Sanchez, 2012), which implements PLS-CA as defined in Tenenhaus (1998).

PLS-CAs were performed on the normalized trait data for all measured specimens for each two-structure pairing. Separate PLS-CAs were performed on phylogenetic independent contrasts (PICs) of the trait data for each phylogeny specific dataset. PICs were calculated using *ape* (Paradis *et al.,* 2004). See Supp. Table S2.1 for which specimens were included in each analysis.

2.3.7 *Allometric trends*

While all traits in this study were size-corrected, this does not preclude the possibility of allometric trends in morphology: it is still possible for shape variation to correlate with size. In order to identify size-linked variation in shape, linear regressions of principal component scores and centroid size were calculated (Supp. Table S2.3, Supp. Figure S2.3). To assess the existence of allometric trends visually, centroid size was plotted on top of each structure's morphospace, which allowed for a visual assessment of the extent to which areas of morphospace were restricted to particular body size fishes (Supp. Figure S2.4).

2.4 Results

2.4.1 *Morphological variation of single structures*

In cichlid fishes, the major axis of body shape variation was one of body depth (Figure 2.2; PC1; Supp. Tables S2.2, S2.3). This PC explained more than 33% of the variation in cichlid body shape, with shapes ranging from deep-bodied species to those with slender lateral profiles. Notably, the GM landmarks that captured body length information did not load heavily on PC1 (Tables 2.2, 2.3). PC2 only explained ~15% of body shape variation, and appeared to show body "truncation," distinguishing those body profiles with long heads and peduncles from those with minimal peduncle length (Tables 2.2, 2.3; Figure 2.2). The clustering of taxonomic groups in body morphospace suggests that some of this shape variation may be attributable to phylogenetic constraint, but see the section below on analyses of phylogenetic signal, as well as Supp. Figures S2.5 and S2.6.

Over 95% of the variation in caudal fin shape was described by two PCs (Tables 2.2, 2.3; Figure 2.2). PC1, which explained 65% of the variance in caudal fin shape, described the length of caudal fin rays relative to size (Tables 2.2, 2.3; Figure 2.2). Individuals scoring highly on this

PC had all four measured caudal fin rays shorter than would be predicted for their size. PC2 for caudal fin shape explained over 30% of variation in the caudal fin, and described fin concavity: specimens scoring highly on PC2 had long first and third caudal fin rays, and shorter fifth and eighth caudal fin rays (Figure 2.2; Tables 2.2, 2.3). In general, this described a trend of increasing "forked appearance" of the tail along PC2.

Dorsal fin shape was best described by a single PC that explained 45% of the observed shape variation (Tables 2.2, 2.3). This PC described lengthening of the central structures of the dorsal fin—as is evidenced by the high loadings of the last dorsal fin spine, first dorsal fin ray, and middle dorsal fin ray relative to the other marginal fin elements (Figure 2.2; Tables 2.2, 2.3). Dorsal fin PC2 described the tendency for fishes with longer dorsal fin bases to have short anterior fin spines, and a short posterior fin ray with respect to other fishes of their size; but PC2 only explained 19% of the variation in dorsal fin shape (Tables 2.2, 2.3).

Anal fin shape was similarly well described by a single PC, explaining 52% of that fin's observed variation (Tables 2.2, 2.3). As for the dorsal fin, anal fin PC1 described a correlated change in length across all of the fin elements measured, with highly negative loadings for the last anal fin spine, first anal fin ray, and middle anal fin ray (Figure 2.2; Tables 2.2, 2.3). This similarity in loadings likely reflected the dorsoventral symmetry of median fins.

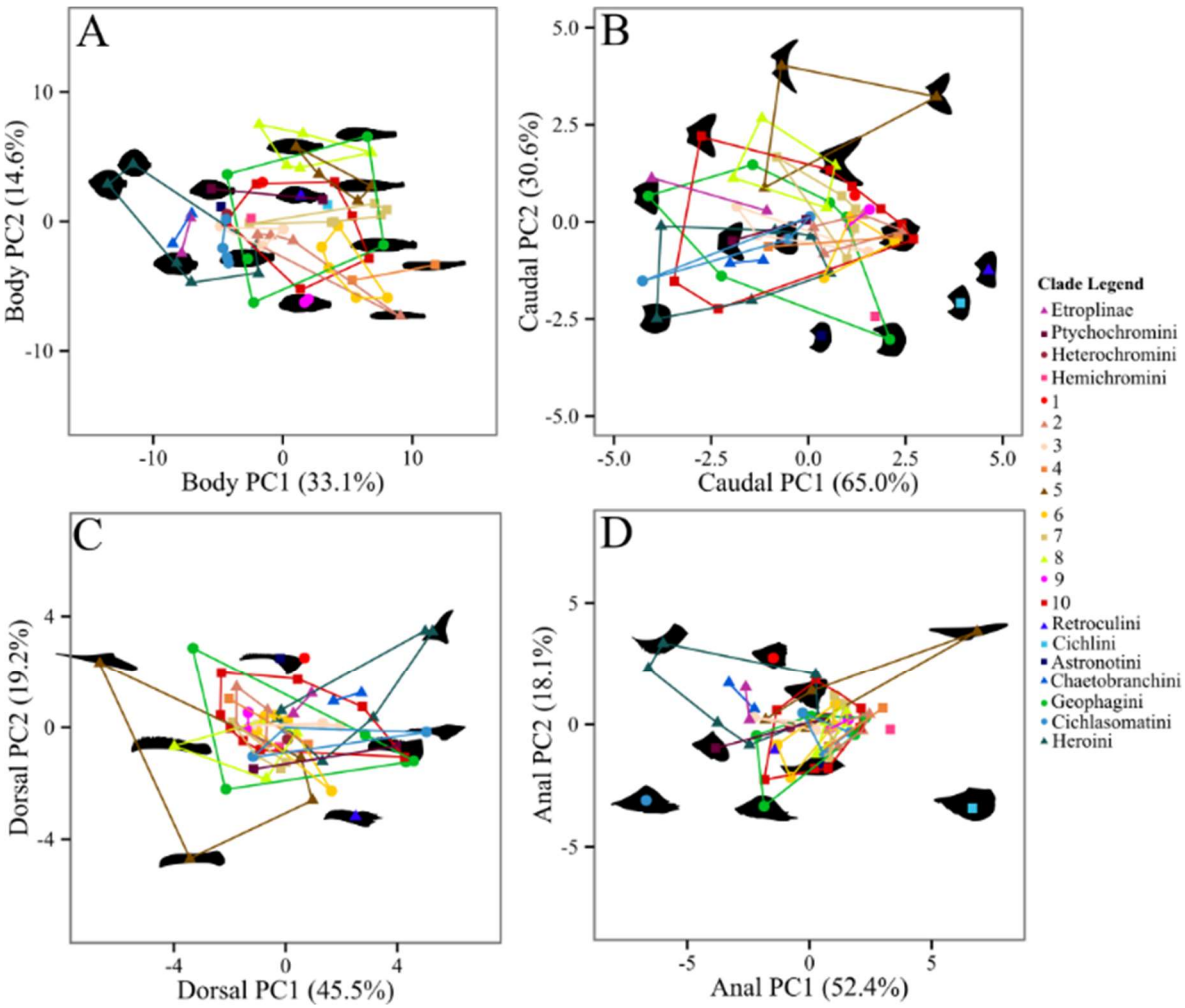

Figure 2.2. Morphospace plots showing principal component scores from size corrected traits of anatomical structures. (A) Body shape, from 26 morphological landmarks. (B) Caudal fin shape, from 4 lengths. (C) Dorsal fin shape, from 7 lengths. (D) Anal fin shape, from 7 lengths. Variance explained by each principal component is included in parentheses next to the appropriate axis label. Species silhouettes are shown centered about their corresponding point in each graph, to aid visual interpretation. Explanation of legend is given in the text and illustrated in Supp. Figures S2.1 and S2.2. Polygons are drawn by connecting the most extreme members of each clade.

Table 2.2 Loadings of morphological traits on principal components. For body shape, only the 10 variables with the highest magnitude loadings were included. For body shape variables, the number indicates the coordinate, and the letter (x or y) indicates the relevant component of the coordinate (see Figure 2.1 for coordinate labels). Full listings of variable loadings can be reproduced using data available in the Dryad package (Feilich, 2016).

Table 2.2 (Continued)

Body Shape			
Variable	PC1 (33.1%)	Variable	PC2 (14.6%)
8y	0.23	10x	-0.34
7y	0.23	9x	-0.34
22y	-0.22	11x	-0.30
18y	-0.22	8x	-0.27
6y	0.22	6x	0.22
9y	0.22	14x	0.21
17y	-0.21	13x	0.21
10y	0.21	7x	0.21
11y	0.21	5x	0.21
21y	-0.20	24x	0.21

Caudal Fin		
Variable	PC1 (65.0%)	PC2 (30.6%)
Fin ray 1 (CFR1)	-0.47	0.56
Fin ray 3 (CFR3)	-0.55	0.36
Fin ray 5 (CFR5)	-0.56	-0.35
Fin ray 8 (CFR8)	-0.41	-0.66

Dorsal Fin		
Variable	PC1 (45.5%)	PC2 (19.2%)
Base length (Dbase)	0.18	0.44
Fin spine 1 (DFS1)	0.01	-0.67
Fin spine mid (DFSmid)	0.40	-0.33
Fin spine last (DFSlast)	0.52	0.10
Fin ray 1 (DFR1)	0.51	0.18
Fin ray mid (DFRmid)	0.49	0.02
Fin ray last (DFRlast)	0.21	-0.44

Anal Fin		
Variable	PC1 (52.4%)	PC2 (18.1%)
Base length (Abase)	-0.30	0.29
Fin spine 1 (AFS1)	-0.33	-0.20
Fin spine mid (AFSmid)	-0.46	0.09
Fin spine last (AFSlast)	-0.50	0.18
Fin ray 1 (AFR1)	-0.46	0.09
Fin ray mid (AFRmid)	-0.35	-0.45
Fin ray last (AFRlast)	-0.05	-0.79

Table 2.3 Loadings of morphological traits on phylogenetically-corrected principal components. For body shape, only the 10 variables with the highest magnitude loadings were included. For body shape variables, the number indicates the coordinate, and the letter (x or y) indicates the relevant component of the coordinate (see Figure 2.1 for coordinate labels). Full listings of variable loadings can be reproduced using data available in the Dryad package (Feilich, 2016).

Table 2.3 (Continued)

Body Shape							
Friedman et al 2013				McMahan et al 2013			
Variable	phylPC1 (34.9%)	Variable	phylPC2 (18.1%)	Variable	phylPC1 (33.8%)	Variable	phylPC2 (25.7%)
7y	0.93	10x	-0.96	8y	-0.96	13x	-0.93
8y	0.92	9x	-0.96	9y	-0.95	10x	0.92
18y	-0.92	11x	-0.77	17y	0.94	9x	0.91
6y	0.90	8x	-0.70	10y	-0.94	14x	-0.91
22y	-0.87	14x	0.57	18y	0.91	27x	-0.87
17y	-0.86	13x	0.54	7y	-0.90	15x	-0.86
27x	-0.83	15x	0.51	22y	0.89	8x	0.85
19y	-0.81	27x	0.49	6y	-0.82	11x	0.80
16y	-0.82	10y	0.47	11y	-0.79	13y	0.74
9y	0.81	9y	0.45	24x	-0.78	4x	-0.60

Caudal Fin				
Tree	Friedman et al 2013		McMahan et al 2013	
Variable	phylPC1 (60.5%)	phylPC2 (33.6%)	phylPC1 (68.9%)	phylPC2 (26.8%)
Fin ray 1 (CFR1)	-0.57	0.77	-0.79	0.59
Fin ray 3 (CFR3)	-0.80	0.52	-0.92	0.30
Fin ray 5 (CFR5)	-0.91	-0.34	-0.91	-0.32
Fin ray 8 (CFR8)	-0.79	-0.58	-0.79	-0.68

Dorsal Fin				
Tree	Friedman et al 2013		McMahan et al 2013	
Variable	phylPC1 (73.3%)	phylPC2 (9.9%)	phylPC1 (73.7%)	phylPC2 (13.0%)
Base length (Dbase)	0.18	0.03	0.35	-0.34
Fin spine 1 (DFS1)	-0.10	-0.01	0.09	0.18
Fin spine mid (DFSmid)	0.57	-0.03	0.56	0.06
Fin spine last (DFSlast)	0.83	-0.45	0.86	-0.42
Fin ray 1 (DFR1)	0.87	-0.44	0.90	-0.36
Fin ray mid (DFRmid)	0.98	0.18	0.94	0.34
Fin ray last (DFRlast)	0.41	0.62	0.16	0.58

Anal Fin				
Tree	Friedman et al 2013		McMahan et al 2013	
Variable	phylPC1 (61.3%)	phylPC2 (26.0%)	phylPC1 (73.0%)	phylPC2 (16.2%)
Base length (Abase)	0.32	-0.03	-0.40	0.32
Fin spine 1 (AFS1)	0.60	-0.22	-0.63	-0.16
Fin spine mid (AFSmid)	0.71	-0.36	-0.80	0.17
Fin spine last (AFSlast)	0.82	-0.51	-0.90	0.34
Fin ray 1 (AFR1)	0.78	-0.57	-0.90	0.35
Fin ray mid (AFRmid)	0.85	0.53	-0.87	-0.48
Fin ray last (AFRlast)	0.20	0.44	-0.32	-0.65

There were no obvious allometric trends in the shape of individual morphological structures (Supp. Table S2.3, Supp. Figure S2.4). In general, larger cichlids occupied a greater proportion of the fin morphospace than smaller cichlids, but smaller cichlids occupied a greater proportion of body morphospace (Supp. Figure S2.4). This may be an artefact of the relative number of small cichlid species to large-bodied species in the cichlids as a group, and/or in the study sample.

2.4.2 *Phylogenetic signal in cichlid morphology*

As has been found previously (Clabaut *et al*., 2007, Muschick *et al.,* 2012), there is less phylogenetic signal in cichlid morphology than is predicted under a Brownian model of trait evolution, though this deviation from the BM model was only significant in two out of eight cases. Across the Friedman tree dataset, K_{mult} ranged from 0.303 (for dorsal fin shape) to 0.367 (for body shape), which, while much lower than the expected $K_{mult} = 1$ for a BM model, was never significant at the $p < 0.05$ level following false detection rate correction (Benjamini and Hochberg, 1995). For the McMahan tree dataset, K_{mult} ranged from 0.547 (for anal fin shape) to 0.741 (for caudal fin shape). These values were significant for anal fin and dorsal fin shape following false detection rate correction, indicating that the dorsal and the anal fins were more different among related species than expected under a BM model. This is consistent with the repeated findings that trait evolution in cichlids, be that trait diet, body shape, or pharyngeal jaw shape, is by and large independent of species' ancestral history (Clabaut *et al.,* 2007, Muschick *et al*., 2012). This was visually confirmed by the phylomorphospace plots generated from each of the two cichlid phylogenies (Supp. Figures S2.5, S2.6). There were some taxa identified as having convergent morphology according to the SURFACE algorithm, but analyses of these

focal groups in *windex* revealed no statistically significant convergence beyond that which may be expected randomly given the cichlid phylogenetic topology (Supp. Figures S2.7-S2.10).

2.4.3 *Disparity through time*

Increases in disparity, particularly in body shape and median fin shape, paralleled increases in taxonomic diversity through time (Figure 2.3, Supp. Figure S2.11; Friedman *et al.,* 2013, McMahan *et al.,* 2013). Peaks in body and median fin disparity above that predicted by a null model of morphological evolution occur at the same time as the Cichlinae–Pseudocrenilabrinae split (as estimated by the tree from which the DTT plot was produced, ~45 myr for analyses using the Friedman *et al.* 2013 data, and ~72 myr for analyses using the McMahan *et al.* 2013 data), and later peaks at about the same time as the haplochromine radiation (< 1 myr from the Friedman *et al.* 2013 data, no haplochromines were included in the McMahan *et al*. 2013 data).

2.4.4 *Covariation of fins and body shape*

Body and fin morphology in cichlids is characterized by tight covariation of structures (Figures 2.4 and 2.6, Supp. Figure S2.12; Table 2.4, Supp. Tables S2.4-S2.5). The major axes of body and fin covariation as determined by PLS-CA depict linked variation that combines the major axes of variation found in the single-structure PCAs. Deep body profiles and fin length elongation (relative to body size) were always represented as the first CV pair in all of the PLS-CAs of body and fin shape (Figure 2.5; Table 2.4, Supp. Tables S2.4, S2.5). The first CVs of all

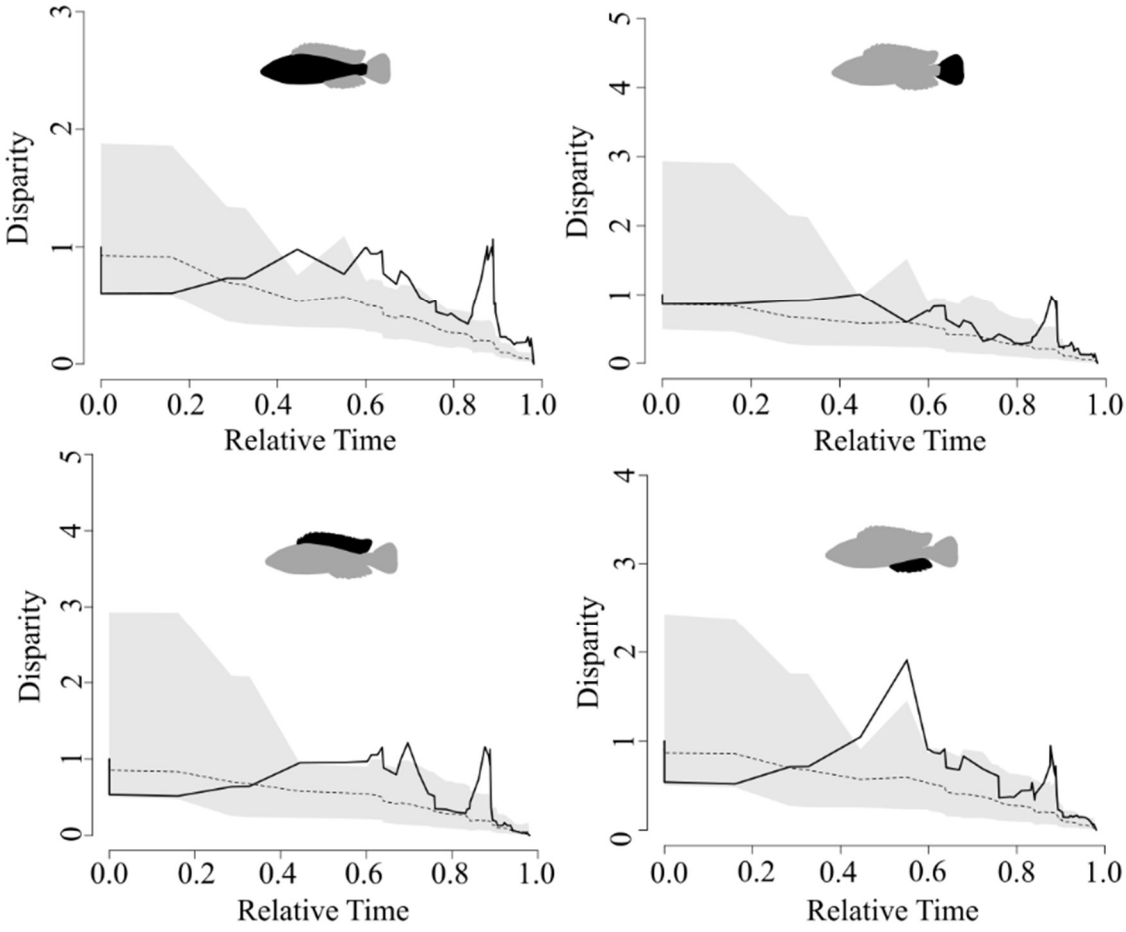

Figure 2.3. Cichlid disparity through time (black line) for each anatomical structure calculated from the Friedman tree dataset with 95% confidence intervals following the method of Slater *et al.* 2013. Each structure is indicated in black on a silhouette. Mean expected disparity under the BM model is shown as the dotted line. Peaks above the gray confidence interval show higher disparity than expected under a BM model of trait evolution. Relative time is calculated from the tree length of the pruned subtrees specific to each morphological structure.

fin–fin analyses also reflected covariation of fin element length: fin element lengths are directly correlated—if one fin is long relative to body size, all of the fins tend to be long relative to body size (Figure 2.5, Table 2.4, Supp. Tables S2.4, S2.5). In general these analyses reflect strong covariation of gross morphology, where deep-bodied fishes have long fin elements, and elongate/narrow-bodied fishes have short fin elements relative to body centroid size, with correlation coefficients between the first pairs of body–fin CVs ranging from r = 0.48 to r = 0.72 (Figure 2.5, Table 2.4, Supp. Tables S2.4, S2.5). The strongest pattern of correlated evolution was that represented by the first pair of CVs describing the dorsal and anal fin (r = 0.88, r = 0.84, r = 0.88 in the non-phylogenetic analysis, Friedman tree analysis, and McMahan tree analysis, respectively): as the dorsal fin elements elongated, so did the anal fin elements (Figures 2.4, 2.5; Tables 2.4, S2.4, S2.5).

Although the second pairs of CVs describe slightly weaker correlations (Figure 2.4; Table 2.4, Supp. Tables S2.4, S2.5), they also suggest strong and functionally relevant patterns of shape covariation (Figure 2.5). Unlike the first CV pairs, the second pairs also often describe changes in fin shape beyond that of lengthening or shortening of all fin elements together. In other words, for the second CV pairs, the shape changes represented result in differences in the fin margin profile, not merely fin length (Figure 2.5). Notable patterns of covariation among the second CV pairs included lengthening and narrowing of the caudal peduncle with the evolution of a more forked caudal fin (Body–Caudal Fin CV2, r = 0.52, r = 0.57, r = 0.52 in the non-phylogenetic analysis, Friedman tree analysis, and McMahan tree analysis, respectively; Figures 2.4, 2.5), and the shortening of dorsal and anal fin terminal fin elements as the fin bases lengthened (Dorsal–Anal Fin CV2, r = 0.64; Figures 2.4, 2.5).

As with evolutionary patterns of single structure variation, the correlated evolutionary changes in each two-structure pairing mirrored the patterns observed in the analyses that did not explicitly include phylogenetic information (Supp. Tables S2.4, S2.5). PLS-CAs of PICs of body and fin measures revealed that the evolution of deeper body profiles in cichlids co-occurred with the evolution of longer fins relative to body size; and the evolution of shallower body profiles was accompanied by the evolution of shorter fins (Supp. Tables S2.4, S2.5). In addition, the evolution of narrow, elongate caudal peduncles corresponded with the evolution of a shorter dorsal fin base, and the evolution of a more concave, forked tail (Supp. Tables S2.4, S2.5).

2.5 Discussion

An underlying assumption of fish swimming biomechanics is the existence of trade-offs in locomotor performance, resulting in selection for specialist forms that excel in certain aspects of locomotor performance to the exclusion of others. There are forms associated with economical cruising, with maximizing burst acceleration, and with execution of tight maneuvers. No single form is considered optimal for all aspects of swimming performance. The proposed prevalence of specialist forms raises the hypothesis that functional structures of locomotor morphology, the fins and the body, should vary between specialized forms. Either these structures should exhibit correlated evolution toward configurations beneficial for locomotor specialization, or retain generalist morphology with no one feature overspecialized compared to others.

Body shape disparity among the cichlid fishes has been studied extensively, repeatedly demonstrating common axes of diversification across many lineages, including the tropheines

Figure 2.4. Partial least-squares canonical variates displaying covariation of body shape and median fin shapes across cichlid species without controlling for phylogenetic information. Polygons are drawn using line segments connecting the most extreme members of each clade, with monotypic clades represented by single points. Point color and shapes and polygon color indicate clade assignment following the key in Figure 2.2, and Supp. Figures S2.1, and S2.2. All of the two-structure comparisons show tight correlation between the first pair of canonical variates (described in Figure 2.5 column A and Table 2.4).

Figure 2.4 (Continued)

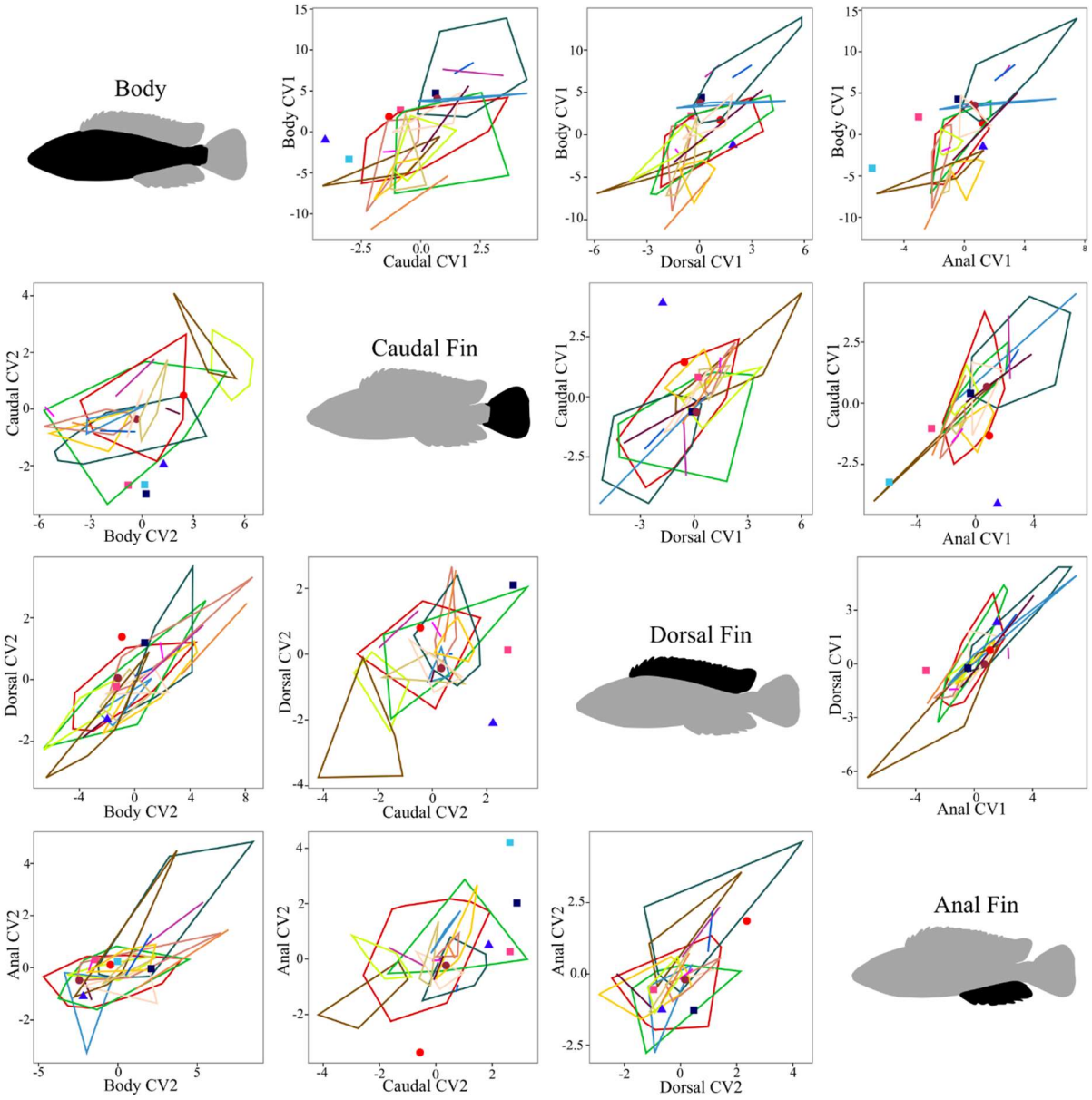

Figure 2.5. Schematic depiction of partial least-squares canonical variate loadings of covarying features on a representative haplochromine cichlid (MCZ131287 *Neochromis greenwoodi*). First canonical variate pairs exhibited the strongest covariation, while only some of the second canonical variate pairs were significant. Arrows indicate the direction of the loadings: solid arrows indicate spatial movement of geometric landmarks, and dashed arrows indicate lengthening or shortening of fin elements. Arrow thickness indicates the strength of the loading: thin arrows indicate a loading of magnitude greater than 0.2 but less than 0.5, and thick arrows indicate a loading of 0.5 or greater. The strongest relationships were between body depth and fin length. The first pairs of canonical variates (left column) show that as body depth increases, all three median fins get longer, and that all median fins tend to lengthen together.

Figure 2.5 (Continued)

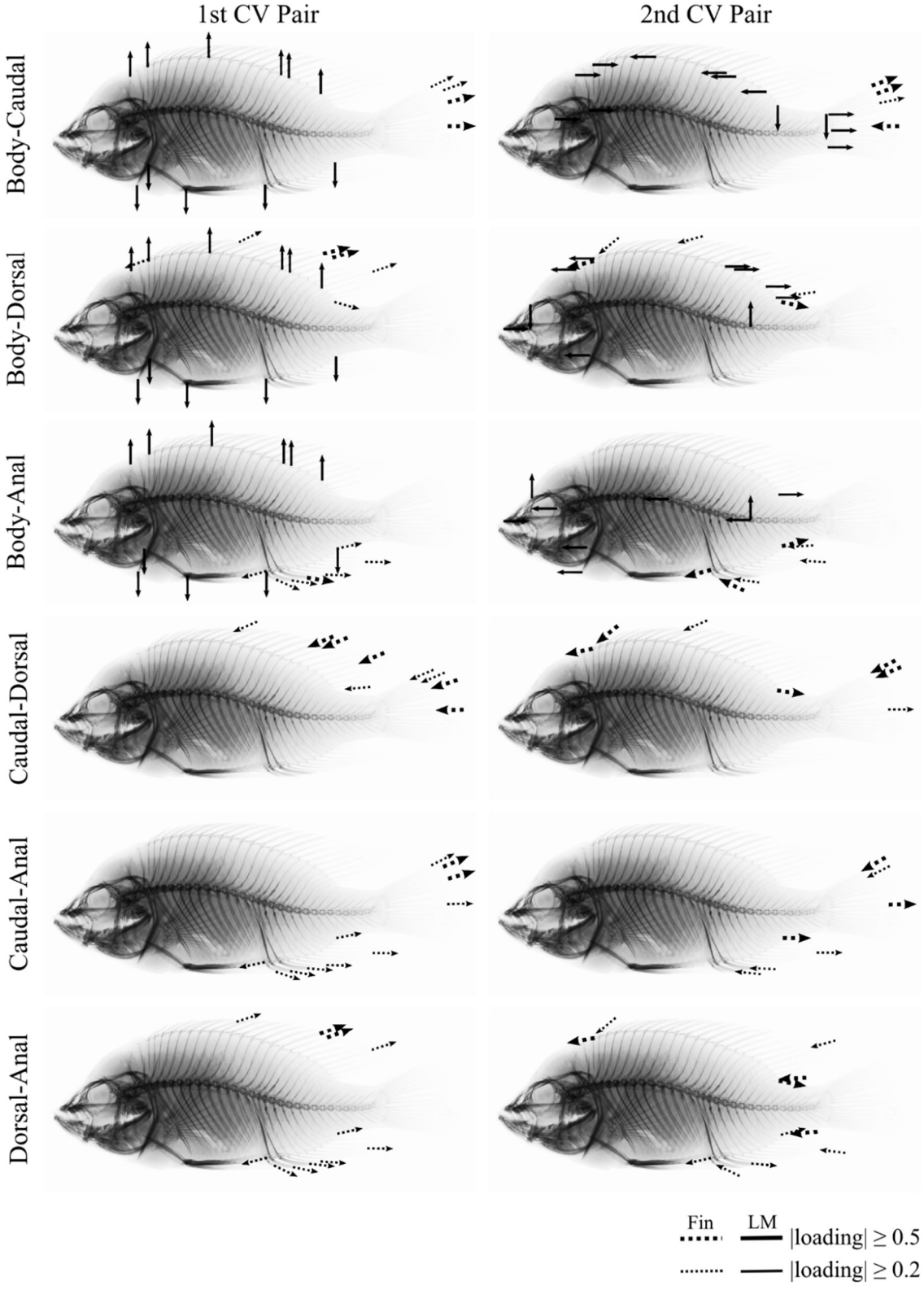

Table 2.4 Partial least squares canonical variate variable loadings. Loadings are followed by the amount of variance in each variable explained by the canonical variate (for second canonical variate pairs, this is reported as the cumulative variation explained by CV pairs 1 and 2, less the variation explained by CV pair 1). For PLS including body shape data, only the 10 body shape variables with the greatest magnitude loadings are reported. Correlation coefficients relating each pair of PLS canonical variates are reported in parentheses.

Table 2.4 (Continued)

Body-Caudal PLS							
First CV Pair (r = 0.61)				Second CV Pair (r = 0.52)			
Variable	CV1 Body Loading	Variable	CV1 Caudal Loading	Variable	CV2 Body Loading	Variable	CV2 Caudal Loading
8y	0.23 (92%)	CFR1	0.39 (36%)	10x	-0.35 (84%)	CFR1	0.68 (60%)
7y	0.23 (90%)	CFR3	0.50 (61%)	9x	-0.35 (83%)	CFR3	0.51 (34%)
22y	-0.22 (88%)	CFR5	0.61 (92%)	11x	-0.31 (67%)	CFR5	-0.16 (3%)
18y	-0.22 (86%)	CFR8	0.51 (64%)	8x	-0.28 (53%)	CFR8	-0.50 (32%)
9y	0.22 (86%)			6x	0.25 (43%)		
17y	-0.22 (85%)			13x	0.24 (39%)		
10y	0.22 (83%)			14x	0.24 (39%)		
6y	0.22 (83%)			5x	0.23 (37%)		
11y	0.22 (82%)			24x	0.23 (36%)		
21y	-0.21(77%)			15x	0.22 (35%)		
Body-Dorsal PLS							
First CV Pair (r = 0.71)				Second CV Pair (r = 0.79)			
Variable	CV1 Body Loading	Variable	CV1 Dorsal Loading	Variable	CV2 Body Loading	Variable	CV2 Dorsal Loading
8y	0.23 (94%)	Dlength	0.21 (14%)	11x	0.31 (63%)	Dlength	0.84 (76%)
7y	0.23 (91%)	DFS1	-0.02 (0%)	12x	0.25 (42%)	DFS1	-0.36 (14%)
18y	-0.23 (86%)	DFSmid	0.38 (44%)	26y	0.25 (41%)	DFSmid	-0.33 (12%)
17y	-0.23 (86%)	DFSlast	0.54 (88%)	4y	-0.24 (37%)	DFSlast	-0.06 (0%)
9y	0.22 (85%)	DFR1	0.53 (88%)	9x	0.24 (36%)	DFR1	-0.01 (0%)
22y	-0.22 (85%)	DFRmid	0.49 (73%)	10x	0.23 (35%)	DFRmid	-0.14 (2%)
10y	0.22 (82%)	DFRlast	0.15 (7%)	6x	-0.23 (35%)	DFRlast	-0.32 (10%)
6y	0.22 (82%)			1x	0.23 (33%)		
11y	0.22 (79%)			7x	-0.22 (33%)		
21y	-0.21 (73%)			21x	0.22 (31%)		
Body-Anal PLS							
First CV Pair (r = 0.72)				Second CV Pair (r = 0.64)			
Variable	CV1 Body Loading	Variable	CV1 Anal Loading	Variable	CV2 Body Loading	Variable	CV2 Anal Loading
8y	0.23 (91%)	Alength	0.36 (44%)	26y	0.32 (55%)	Alength	0.63 (44%)
7y	0.23 (88%)	AFS1	0.29 (30%)	1x	0.28 (41%)	AFS1	-0.61 (41%)
18y	-0.23 (87%)	AFSmid	0.45 (70%)	12x	0.28 (40%)	AFSmid	-0.24 (6%)
17y	-0.23 (87%)	AFSlast	0.51 (90%)	4y	-0.27 (39%)	AFSlast	0.02 (0%)
22y	-0.23 (87%)	AFR1	0.48 (81%)	5y	-0.24 (30%)	AFR1	0.04 (0%)
9y	0.22 (83%)	AFRmid	0.36 (47%)	3y	-0.23 (27%)	AFRmid	-0.28 (9%)
10y	0.22 (81%)	AFRlast	0.05 (1%)	25x	-0.22 (26%)	AFRlast	-0.35 (14%)
6y	0.22 (80%)			26x	-0.22 (25%)		
11y	0.22 (80%)			18x	-0.22 (25%)		
21y	-0.21 (77%)			21x	-0.21 (24%)		

Table 2.4 (Continued)

Caudal-Dorsal PLS							
First CV Pair (r = 0.69)				Second CV Pair (r = 0.38)			
Variable	CV1 Caudal Loading	Variable	CV1 Dorsal Loading	Variable	CV2 Caudal Loading	Variable	CV2 Dorsal Loading
CFR1	-0.36 (31%)	Dlength	-0.13 (5%)	CFR1	-0.70 (65%)	Dlength	0.76 (56%)
CFR3	-0.49 (58%)	DFS1	0.02 (0%)	CFR3	-0.53 (37%)	DFS1	-0.64 (40%)
CFR5	-0.62 (93%)	DFSmid	-0.39 (46%)	CFR5	0.12 (2%)	DFSmid	-0.33 (10%)
CFR8	-0.53 (68%)	DFSlast	-0.53 (84%)	CFR8	0.46 (28%)	DFSlast	-0.04 (0%)
		DFR1	-0.53 (85%)			DFR1	0.06 (0%)
		DFRmid	-0.52 (81%)			DFRmid	0.08 (1%)
		DFRlast	-0.22 (14%)			DFRlast	0.05 (0%)
Caudal-Anal PLS							
First CV Pair (r = 0.72)				Second CV Pair (r = 0.39)			
Variable	CV1 Caudal Loading	Variable	CV1 Anal Loading	Variable	CV2 Caudal Loading	Variable	CV2 Anal Loading
CFR1	0.39 (38%)	Alength	0.30 (32%)	CFR1	-0.67 (57%)	Alength	-0.05 (0%)
CFR3	0.51 (64%)	AFS1	0.33 (39%)	CFR3	-0.50 (31%)	AFS1	-0.01 (0%)
CFR5	0.60 (91%)	AFSmid	0.45 (73%)	CFR5	0.19 (5%)	AFSmid	-0.23 (6%)
CFR8	0.49 (60%)	AFSlast	0.49 (86%)	CFR8	0.53 (35%)	AFSlast	-0.25 (7%)
		AFR1	0.47 (78%)			AFR1	-0.16 (3%)
		AFRmid	0.39 (54%)			AFRmid	0.40 (19%)
		AFRlast	0.08 (2%)			AFRlast	0.87 (87%)
Dorsal-Anal P LS							
First CV Pair (r = 0.88)				Second CV Pair (r = 0.64)			
Variable	CV1 Dorsal Loading	Variable	CV1 Anal Loading	Variable	CV2 Dorsal Loading	Variable	CV2 Anal Loading
Dlength	0.16 (8%)	Alength	0.30 (32%)	Dlength	0.58 (36%)	Alength	0.52 (32%)
DFS1	0.02 (0%)	AFS1	0.31 (34%)	DFS1	-0.29 (9%)	AFS1	-0.25 (8%)
DFSmid	0.40 (50%)	AFSmid	0.45 (72%)	DFSmid	-0.19 (4%)	AFSmid	0.04 (0%)
DFSlast	0.53 (87%)	AFSlast	0.49 (87%)	DFSlast	0.17 (3%)	AFSlast	0.23 (6%)
DFR1	0.52 (85%)	AFR1	0.46 (76%)	DFR1	0.17 (3%)	AFR1	0.18 (4%)
DFRmid	0.48 (73%)	AFRmid	0.39 (55%)	DFRmid	-0.23 (6%)	AFRmid	-0.38 (17%)
DFRlast	0.19 (11%)	AFRlast	0.13 (6%)	DFRlast	-0.73 (57%)	AFRlast	-0.69 (58%)

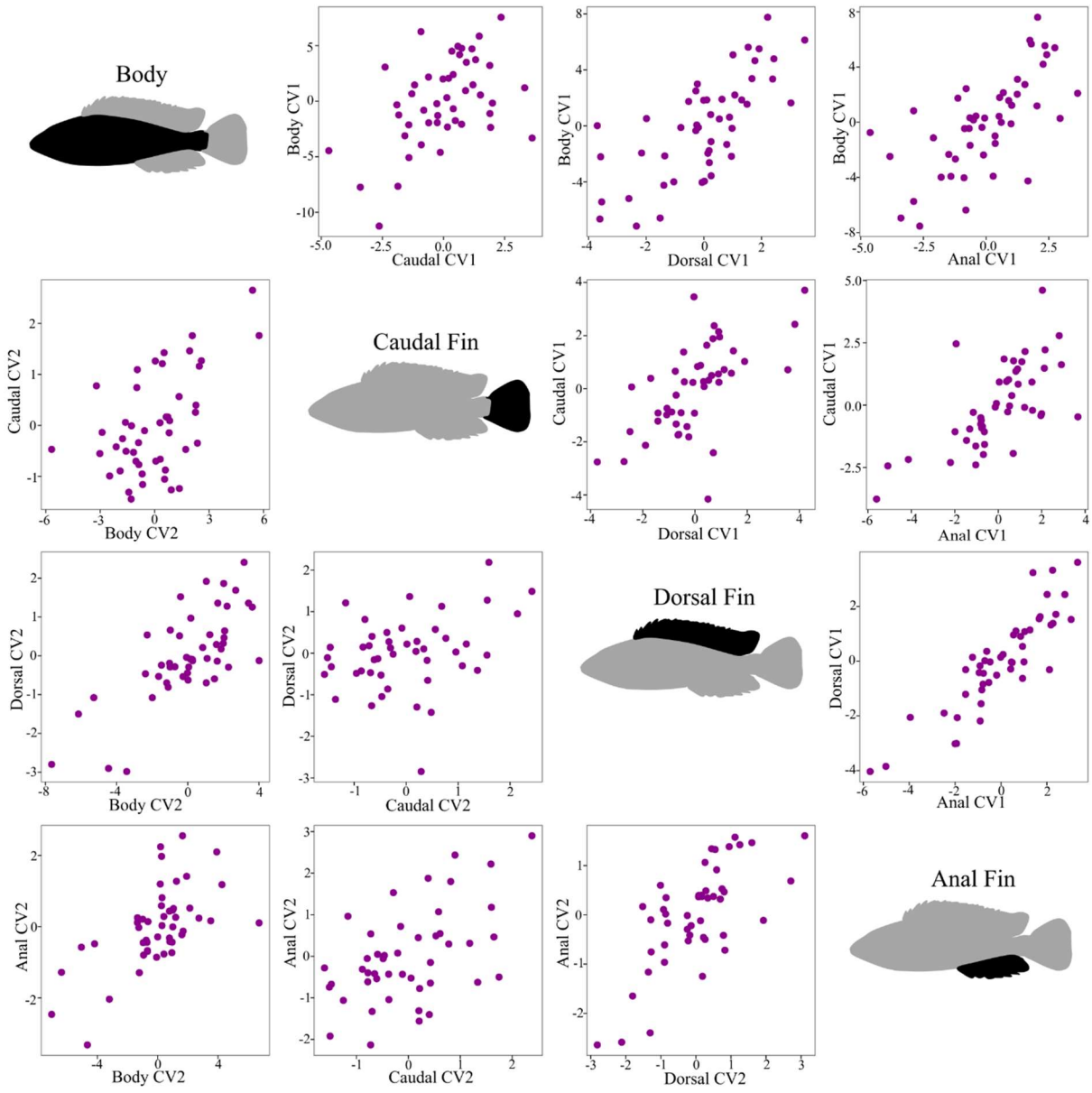

Figure 2.6. Partial least-squares canonical variates displaying covariation of independent contrasts of body and median fin shapes on the McMahan et al. (2013) phylogeny.

(Wanek and Sturmbauer, 2015), geophagines (Astudillo-Clavijo et al., 2015), and others (Clabaut *et al.,* 2007, Muschick *et al.,* 2012). In most lineages the chief axis of body shape diversification was one of body depth, spanning from elongate narrow-bodied forms to deep-bodied, rounded forms; in the one exception (Wanek and Sturmbauer, 2015), body depth variation still explained a substantial amount of morphological variation. While body shape is one of the chief factors governing swimming performance, fins and bodies interact in tandem when fishes swim. Despite the wealth of knowledge concerning body shape evolution in the cichlids, little is known about how the fins vary across the clade, or how fin morphology relates to body morphology. The present study demonstrates that body shape evolution does not occur independently of the fins, but rather among a suite of morphological changes that potentially augment body shape's contribution to locomotor specialization.

2.5.1 *Body and fin shape variation encompasses specialist forms*

PCAs of fin and body shape reflect the hypothesized specializations of each structure, with morphological variation of the fins and the bodies falling on spectra that span between specialized forms (Figure 2.2). More than 33% of the variation in body shape was explained by differences in body depth (Figure 2.2, Table 2.3), which is frequently associated with trade-offs in pelagic versus littoral habits. Specifically, streamlined forms are considered adaptive for economical open water swimming (pelagic), whereas deep-bodied forms are considered specialists for maneuverability in structurally complex environments (littoral). The association between deep-bodied forms and maneuvering performance, and slender-bodied forms and cruising performance has been demonstrated in a few studies (Ohlberger *et al.,* 2006, Ellerby and

Gerry, 2011); though some studies reveal little relationship between body shape and swimming performance (Webb *et al.,* 1996, Gerstner, 1999).

Most of the variation in cichlid caudal fins was explained by a single axis ranging from fishes with long caudal fin elements to fishes with short caudal fin elements relative to body size (Figure 2.2, CPC1; Table 2.3). Typically, long, high-surface-area fins are associated with maneuvering performance, and this axis may in part distinguish maneuvering specialists. Greater than 30% of the variation in caudal fins reflected the spectrum between forked or concave tails and convex, rounded tails. Forked tails— semi-lunate tails in particular—are ascribed a thrust enhancing function with minimal additional cost, a hallmark of thunniform swimmers of high economy. Broad rounded tails, on the other hand, are employed by burst accelerators to use recoil to generate high thrust (at considerable energetic cost), and by maneuverers to generate pitching moments.

It is more difficult to relate variation in the median fins to specific hydrodynamic functions, in large part due to the lack of research on median fin hydrodynamics. Prior studies suggest that the dorsal and anal fins combined produce balancing torques to support roll stability and perhaps function as a "double-tail" to produce thrust during slow-speed swimming (Drucker and Lauder, 2001, Standen and Lauder, 2005). Both median fins are also actively spread and manipulated during maneuvers (Standen and Lauder, 2005). PCAs revealed a general trend with dorsal and anal fins both ranging from forms with longer anterior spines and shorter rays, to forms with shorter spines but greatly elongated central and posterior rays (Figure 2.2, Table 2.3). In terms of locomotor specialization, this may indicate a spectrum between short-finned but spiny forms for high-speed cruising, in which the median fins are typically collapsed, and lower speed maneuverers that may benefit from high fin surface area. For the haplochromine cichlids,

it is possible that specialization or constraint of anal fin morphology is related to sexual selection for the tribe's distinctive egg spots on the distal anal fin (Goldschmidt, 2010). The probability for sexual or other selection to confound the selective pressures of locomotor performance may be higher in the median fins than in the body or the caudal fin because these fins can be almost entirely collapsed in most species. The extent to which the median fins are shaped by locomotor demands is probably modulated by the extent to which these fins are employed in swimming relative to their importance in other behaviors.

In cichlids, variation in individual locomotor structures can be explained well by merely one or two PC axes. Variation along a spectrum between implied locomotor specializations forms a major proportion of the total variation in each structure, especially for the fins. In other words, cichlid fins are either characteristic of locomotor specialization or generalists, and there are few unexpected fin morphologies.

2.5.2 *Features associated with locomotor specializations exhibit correlated evolution*

There was little support for either of the two null hypotheses presented for cichlid morphological evolution (Table 2.1). Strong correlated evolution across structures contradicted the hypothesis of complete modularity between the fins and the body (null hypothesis 1, Table 2.1); but the correlations between structures were not perfect, and varied in their ability to explain each structure's morphology, invalidating null hypothesis 2, though to a lesser degree. In contrast, and in accordance with earlier studies of ecomorphology (following Webb, 1984), the correlated change of structures appears to support locomotor specialization as described by three of the four functional-linkage hypotheses in Table 2.1. Changes in the caudal peduncle region of the body are associated with changes in tail morphology, such that elongate, tapered peduncles

co-occur with concave, forked, or semi-lunate tails (Tables 2.1 [Link 1, Body–Caudal CV2], 2.4, Supp. Tables S2.4, S2.5; Figures 2.4-2.6, Supp. Figure S2.12). Median fin morphology was very strongly linked, (Tables 2.1 [Link 2, Dorsal-Anal CV1 and CV2], 2.4, Supp. Tables S2.4, S2.5; Figures 2.4-2.6, Supp. Figure S2.12). Changes in body depth are accompanied by changes in median fin length, such that deep-bodied fishes tend to have longer fins, and elongate fishes tend to have shorter fins, relative to body size (Table 2.1 [Link 4; Body–Dorsal, Body–Anal CV1], 2.4, Supp. Tables S2.4, S2.5; Figures 2.4-2.6, Supp. Figure S2.12). In general, these patterns are analogous to the single structure cases presented above (Figure 2.2): just as most individual structures vary between expected specialist forms and generalist forms with few anomalies, there are also few anomalous combinations of structures. Specialist fins are generally accompanied by appropriate specialist bodies, and generalist fins are typically accompanied by generalist bodies; with evolution toward morphological specializations occurring repeatedly throughout the cichlid phylogeny. There are few cichlid species with combinations of body shapes associated with one specialization and fins associated with a different specialization.

The underlying pattern of morphological integration among cichlids, in which functionally linked structures evolve in tight correspondence with each other, raises the possibility that correlated evolution of structures is typical of, or even characteristic of adaptive radiation. The study of triggerfish body and fin shape (Dornberg *et al.,* 2011) suggests that this may be the case in fishes, though to generalize this across fishes requires further study. Other taxa, while more remote from fishes, also demonstrate that adaptive radiation is associated with predictable patterns of correlated evolution in suites of functionally related structures. In the lizard genus *Anolis*, for example, habitat-specific ecomorphs show correlated body, leg length, and tail length evolution: the ectomorphs are not defined by single structure modification (Losos,

1990, Losos, 1992, Mahler *et al.,* 2010). Similar patterns of ecomorphological multitrait change have been described in frogs (Blackburn *et al.,* 2013). If patterns of covarying morphology are constrained by or adaptive for locomotor function, perhaps other aspects of morphology and physiology also change together to support locomotion. The evidence from Lake Tanganyika showing that trophic niche, pharyngeal jaw structure, and body shape are all interrelated suggests a broad link among ecology, locomotor habits, and gross morphology (Muschick *et al.,* 2012). While covariation of morphology and ecological niche does not necessarily ascribe a given trait change adaptive value, it does strongly suggest that natural selection acts on both ecology and morphology together. Further research into the biomechanical means by which body and fin morphology affect swimming performance is necessary to bridge the morphology–performance gap, let alone determine the consequences of morphological correlations on fitness. Nevertheless, the tightly correlated nature of cichlids' multistructure morphological evolution reflects an underlying principle of functional morphology: organisms function as integrated units, and structures must covary to function together within the context of the organism.

2.5.3 *Cichlid morphology is dictated by neither ancestry nor convergence*

The fact that cichlid morphology is overdispersed relative to a BM model could suggest either that cichlid morphology is not restricted by ancestry, or that there is strong convergent evolution toward optimal forms. This is also supported by the finding that the major axes of evolutionary morphological diversification in cichlids parallel the axes of morphological variation determined in the absence of phylogenetic information (Table 2.3). However, there was no evidence of convergent evolution beyond that expected under random BM evolution (Supp. Figures S2.7–S2.10). This suggests that the diversity observed is not driven by shared ancestry

following a single early diversification, nor by evolution toward particular optimal forms, but rather that the same trajectories of morphological evolution have occurred repeatedly across the cichlid phylogeny without reaching the same end point. The trends of varying body depth, relative fin length, and fin concavity characterize morphological disparity throughout cichlid evolution, and regions of morphospace that are empty may be so due to selection against deleterious configurations. Alternatively, common trajectories of morphological evolution may be dictated by canalized developmental linkages across structures. This is likely true for median fin shape, where there are known symmetries in the development of those structures (Mabee *et al.,* 2002).

2.5.4 *Diversification of locomotor structures coincides with adaptive radiation and speciation*

DTT plots for body shape and all three fins exhibit peaks above the 95% confidence interval for a neutral model of BM evolution around 45 myr for both phylogenetic datasets, and around 5 myr for the Friedman dataset (Figure 2.3, Supp. Figure S2.11). These dates correspond loosely with the divergence of Cichlinae and Pseudocrenilabrinae (Friedman *et al.* 2013, McMahan *et al.,* 2013) and the explosive radiation of the haplochromine cichlids (Genner *et al.,* 2007, Friedman *et al.,* 2013), respectively. The McMahan dataset only included a single haplochromine, and would not be expected to show diversification within that group. Both DTT analyses indicate that peaks in disparity occurred after major events in the biogeographic history of cichlids (such as possible vicariance or dispersal), but before any desiccation events that may have contributed to the speciation of haplochromines in Lake Victoria (Vences *et al.,* 2001, Seehausen, 2002)—which would explain the low disparity of the haplochromines compared to other groups.

The coincidence of speciation and morphological diversification reinforces the importance of morphology in adaptive radiations either as a result of species radiation, or a driver of speciation. Morphological diversification occurs concurrently with species radiation in fishes (Rabosky *et al*., 2013). The fact that all four structures studied displayed increased disparity at simultaneous points in time also suggests that morphological diversification occurs across structures simultaneously. This interpretation is consistent with similar findings in studies looking at body profile and pharyngeal jaw morphology in cichlids (Muschick *et al.,* 2012).

The patterns of disparity through time indicate two major characteristics of the cichlid radiation. First, the simultaneous diversification of all locomotor structures suggests that it is unlikely that any one structure acts as a "key innovation" of locomotor morphology to release the others—or, if any structure did act as a morphological release, that the subsequent diversification of other structures happened over a short period of evolutionary time. Second, the correspondence of changes in locomotor structures with both species radiation and diversification of trophic structures demonstrates that the adaptive radiation of cichlids was holistic, incorporating morphological diversification in structures beyond those strictly associated with feeding behavior and trophic niche.

2.5.5 *Functional implications of correlated evolution*

The inferred patterns of correlated morphological evolution observed raise potential functional roles for correlated variation that may serve as the basis for selection for specific configurations as they affect locomotor performance. Biomechanical hypotheses and convergent morphological trajectories of distantly related lineages suggest that economical cruisers, burst accelerators, and maneuvering specialists each require a different suite of morphological traits to

be most effective at their specialization (Webb, 1982, Webb, 1984, Astudillo-Clavijo *et al.,* 2015), but few studies have looked at correlated evolution of body and fin shape (save Wright, 2000 and Dornburg *et al*., 2011 for such an analysis of triggerfishes). This study demonstrates correlated evolution of multiple locomotor traits in a macroevolutionary context, showing that these patterns are consistent with ecomorphological hypotheses.

Deep-bodied profiles with long fins, in accordance with linkage hypotheses 2 and 4, are thought to support maneuverability, providing long lever arms that can produce large turning moments. Similarly, the co-occurrence of narrow caudal peduncles and forked tails, following linkage hypothesis 1, is believed to support economical cruising, reducing drag and inertial recoil while potentially augmenting thrust. If the evolution of locomotor structures supports locomotor specialties as predicted, a nontrivial assumption given the increasing evidence of "many-to-one" mappings of morphology on performance (Wainwright *et al.,* 2005, Collar and Wainwright ,2006, Wainwright, 2007), one would expect that swimming performance changes in accordance with multistructure morphology. Hence, measuring performance in phylogenetic context should be a means of testing the hypothesis that patterns of correlated morphological evolution support locomotor specialization.

The patterns presented here propose specific, testable hypotheses about performance benefits that may be accrued due to morphological covariation. For economical cruising, a narrow, elongate caudal peduncle may require a forked caudal fin to maintain thrust while reducing energetic costs. For a quick acceleration, a rounded torpedo-shaped body may be insufficient for thrust production without large median and caudal fins. Future research could determine whether the observed combinations of traits result in their hypothesized outcomes. For linkage hypothesis 1, one would expect lower cost of transport at high speeds for fishes with

narrow caudal peduncles and forked tails, perhaps by hydrodynamic development of leading edge vorticity and wake recapture. For linkage hypotheses 2 and 4, one would expect fishes with deep bodies and long median fins to exhibit high maneuverability, either in terms of small turning radius or high agility. Comparison of actual performance measures with respect to economical swimming (e.g., maximum sustainable speed, cost of transport), acceleration (e.g., maximum accelerations), and maneuvering (e.g., angular accelerations) will aid in efforts to determine whether morphological specialists exhibit performance tradeoffs in accordance with assumptions about locomotor specialization.

In conclusion, body shape does not evolve in isolation of other traits. Rather, morphological evolution in the cichlids is characterized by correlated change across a spectrum of traits that likely contribute to differences in performance and life history. These findings call for a more nuanced appreciation of both the processes of morphological evolution and development as to how correlated change comes about, and the biomechanics underlying swimming ecomorphology. In the case of cichlid morphological evolution, both the body and the fins change together, likely supporting locomotor specialization, in a pattern of tight multistructural correlation that may be the norm for adaptive trait evolution.

2.6 Data archiving

Copies of MCZ specimen radiographs have been published online at MCZbase, (http://www.mczbase.mcz.harvard.edu). Morphometric coordinates, measurements, and code have been uploaded to Data Dryad Digital Repository: http://doi.org/10.5061/dryad.h4k6f.

2.7 References

Adams, D. C. (2014). A generalized K statistic for estimating phylogenetic signal from shape and other high-dimensional multivariate data. *Syst. Biol.* 63: 685-697.

Adams, D. C. and E. Otarola-Castillo. (2013). geomorph: an R package for the collection and analysis of geometric morphometric shape data. *Methods Ecol. Evol*. 4: 393-399.

Affleck, R. J. (1950). Some points in the function, development, and evolution of the tail in fishes. *Proc. Zool. Soc. Lond*. 120: 349-368.

Albertson, R. C., J. A. Markert, P. D. Danley, and T. D. Kocher. (1999). Phylogeny of a rapidly evolving clade: the cichlid fishes of Lake Malawi, East Africa. *Proc. Natl. Acad. Sci. USA* 96: 5107-5110.

Albertson, R. C., J. T. Streelman, and T. D. Kocher. (2003). Directional selection has shaped the oral jaws of Lake Malawi cichlid fishes. *Proc. Natl. Acad. Sci. USA* 100: 5252-5257.

Akhtar, I., R. Mittal, G. V. Lauder, and E. Drucker. (2007). Hydrodynamics of a biologically inspired tandem flapping foil configuration. *Theor. Comput. Fluid Dyn*. 21: 155-170.

Antonucci, F., C. Costa, J. Aguzzi, and S. Cataudella. (2009). Ecomorphology of morpho-functional relationships in the family of Sparidae: a quantitative statistic approach. *J. Morphol.* 270: 843-855.

Arbour, J. H. and H. Lopez-Fernandez. (2014). Adaptive landscape and functional diversity of Neotropical cichlids: implications for the ecology and evolution of Cichlinae (Cichlidae; Cichliformes*). J. Evol. Biol*. 27: 2431-2442.

Arbuckle, K., C. M. Bennett, and M. P. Speed. (2014). A simple measure of the strength of convergent evolution. *Methods Ecol. Evol.* 5: 685-693.

Arbuckle, K. and A. Minter. (2015). windex: analyzing convergent evolution using the Wheatsheaf Index in R. *Evol Bioinform Online*. 11: 11-14.

Astudillo-Clavijo, V., J. H. Arbour, and H. Lopez-Fernandez. (2015). Selection towards different adaptive optima drove the early diversification of locomotor phenotypes in the radiation of Neotropical geophagine cichlids. *BMC Evol. Biol*. 15: 77.

Benjamini, Y. and Y. Hochberg. (1995). Controlling the false discovery rate: a practical and powerful approach to multiple testing. *J. R. Stat. Soc. Series B* 57: 289-300.

Blackburn, D. C., C. D. Siler, A. C. Diesmos, J. A. McGuire, D. C. Cannatella, and R. M. Brown. (2013). An adaptive radiation of frogs in a southeast Asian island archipelago. *Evolution*. 67: 2631-2646.

Blake, R. W., J. Li, and K. H. S. Chan. (2009). Swimming in four goldfish *Carassius auratus* morphotypes: understanding functional design and performance employing artificially selected forms. *J. Fish Biol*. 75: 591-617.

Borazjani, I., and M. Daghoogi. (2013). The fish tail motion forms an attached leading edge vortex. *Proc. R. Soc. Lond. B.* 280: 20122071.

Chakrabarty, P. (2005). Testing conjectures about morphological diversity in cichlids of Lakes Malawi and Tanganyika. *Coepia.* 2005: 359-373.

Clabaut, C., P. M. E. Bunje, W. Salzburger, and A. Meyer. (2007). Geometric morphometric analyses provide evidence for the adaptive character of the Tanganyikan cichlid fish radiations. *Evolution*. 61: 560-578.

Claverie, T., and P. C. Wainwright. (2014). A morphospace for reef fishes: elongation is the dominant axis of body shape evolution. *PLoS One*. 9: e112732.

Collar, D. C. and P. C. Wainwright. (2006). Discordance between morphological and mechanical diversity in the feeding mechanism of centrarchid fishes. *Evolution.* 60: 2575-2584.

Dornburg, A., B. Sidlauskas, F. Santini, L. Sorenson, T. J. Near, and M. E. Alfaro. (2011). The influence of an innovative locomotor strategy on the phenotypic diversification of triggerfish (Family: Balistidae). *Evolution.* 65-67: 1912-1926.

Drucker, E. G. and G. V. Lauder. (2001). Locomotor function of the dorsal fin in teleost fishes: experimental analysis of wake forces in sunfish. *J. Exp. Biol.* 204: 2943-2958.

Ehlinger, T. J. and D. S. Wilson. (1988). Complex foraging polymorphism in bluegill sunfish. *Proc. Natl. Acad. Sci. USA*. 85: 1878-1882.

Ellerby, D. J. and S. P. Gerry (2011). Sympatric divergence and performance trade-offs of bluegill ecomorphs. *Evol. Biol.* 38, 422-433.

Feilich, K. L. and G. V. Lauder. (2015). Passive mechanical models of fish caudal fins: effects of shape and stiffness on self-propulsion. *Bioinspir. Biomim.* 10: 036002.

Friedman, M. (2010). Explosive morphological diversification of spiny-finned teleost fishes in the aftermath of the end-Cretaceous extinction. *Proc. R. Soc. Lond. B*. 277: 1675-1683.

Friedman, M., B. P. Keck, A. Dornburg, R. I. Eytan, C. H. Martin, C. D. Hulsey, P. C. Wainwright, and T. J. Near. (2013). Molecular and fossil evidence place the origin of cichlid fishes long after Gondwanan rifting. *Proc. R. Soc. Lond. B.* 280: 20131733.

Friedman, M., B. P. Keck, A. Dornburg, R. I. Eytan, C. H. Martin, C. D. Hulsey, P. C. Wainwright, and T. J. Near. 2013. Data from: Molecular and fossil evidence place the origin of cichlid fishes long after Gondwanan rifting. Dryad Digital Repository. doi: 10.5061/dryad.48f62.

Genner, M. J., O. Seehausen, D. H. Lunt, D. A. Joyce, P. W. Shaw, G. R. Carvalho, and G. F. Turner. (2007). Age of cichlids: new dates for ancient lake fish radiations. *Mol. Biol. Evol.* 24: 1269-1282.

Gerstner, C. L. (1999). Maneuverability of four species of coral reef fish that differ in body and pectoral-fin morphology. *Can. J. Zool*. 77: 1102-1110.

Goldschmidt, T. (2010). Egg mimics in Haplochromine cichlids (Pisces, Perciformes) from Lake Victoria. *Ethology* 88: 177-190.

Harmon, L. J., J. A. Schulte II, A. Larson, and J. B. Losos. (2003). Tempo and mode of evolutionary radiation in iguanian lizards. *Science.* 301: 961-964.

Harmon, L. J., J. T. Weir, C. D. Brock, R. E. Glor and W. Challenger. (2008). GEIGER: investigating evolutionary radiations. *Bioinformatics* 24: 129-131.

Ingram, T., and D. L. Mahler. (2013). SURFACE: detecting convergent evolution from comparative data by fitting Ornstein-Uhlenbeck models with stepwise Akaike Information Criterion. *Methods Ecol. Evol.* 4: 416-425.

Joliffe, I. T. (2002). Principal Components Analysis. 2nd ed. Springer-Verlag, New York, U.S.A.

Klingenberg, C. P. (2011). MorphoJ: an integrated software package for geometric morphometrics. *Mol. Ecol. Resour.* 11: 353-357.

Kocher, T. D., J. A. Conroy, K. R. McKaye and J. R. Stauffer. (1993). Similar morphologies of cichlid fish in lakes Tanganyika and Malawi are due to convergence. *Mol. Phylogenet. Evol.* 2: 158-165.

Kusche, H., H. Recknagel, K. R. Elmer and A. Meyer. (2014). Crater lake cichlids specialize along the benthic-limnetic axis. *Ecol. Evol*. 4: 1127-1139. doi: 10.1002/ece3.1015

Lai, Y.-C. 1963. Effects of several preservatives on proportional measurement of the fat-headed minnow, *Pimephales promelas.* M.A. thesis, University of Kansas, Lawrence. 40 pp.

Lauder, G. V. and E. G. Drucker. (2004). Morphology and experimental hydrodynamics of fish fin control surfaces. *IEEE J. Ocean. Eng*. 29: 556-571.

Lauder, G. V., B. Flammang and S. Alben. (2012). Passive robotic models of propulsion by the bodies and caudal fins of fish. *Integr. Comp. Biol.* 52: 576-587.

Lauder, G. V., J. C. Nauen and E. G. Drucker. (2002). Experimental hydrodynamics and evolution: function of median fins in ray-finned fishes. *Integr. Comp. Biol.* 42: 1009-1017.

Liem, K. F. (1973). Evolutionary strategies and morphological innovations: cichlid pharyngeal jaws. *Syst. Zool.* 22: 425-441.

Lighthill, M. J. (1970). Aquatic animal propulsion of high hydrodynamical efficiency. *J. Fluid Mech.* 44: 265-301.

López-Fernández, H., K. O. Winemiller, C. Montaña and R. L. Honeycutt. (2012). Diet-morphology correlations in the radiation of South American geophagine cichlids (Perciformes: Cichlidae: Cichlinae). *PLoS ONE*. 7: e33997.

Losos, J. B. (1990). Ecomorphology, performance capability, and scaling of West Indian Anolis lizards: an evolutionary analysis. *Ecol. Monograph.* 60: 369-388.

Losos, J. B. (1992). The evolution of convergent structure in Caribbean Anolis communities. *Syst. Biol.* 41: 403-420.

Mabee, P. M., P. L. Crotwell, N. C. Bird, and A. C. Burke. (2002). Evolution of median fin modules in the axial skeleton of fishes. *J. Exp. Zool. (Mol. Dev. Evol*.) 294: 77-90.

Mahler, D. L., L. J. Revell, R. E. Glor and J. B. Losos. (2010). Ecological opportunity and the rate of morphological evolution in the diversification of Greater Antillean anoles. *Evolution.* 64: 2731-2745.

McMahan, C. D., P. Chakrabarty, J. S. Sparks, W. L. Smith and M. P. Davis. (2013). Temporal patterns of diversification across global cichlid biodiversity. *PLoS ONE.* 8: e71162.

Montaña, C. G., K. O. Winemiller and A. Sutton. (2014). Intercontinental comparison of fish ecomorphology: null model tests of community assembly at the patch scale in rivers. *Ecol. Monogr.* 84: 91-107.

Muschick, M., A. Indermaur and W. Salzburger. (2012). Convergent evolution within an adaptive radiation of cichlid fishes. *Curr. Biol.* 22: 2362-2368.

Ohlberger, J., G. Staaks and F. Hölker. (2006). Swimming efficiency and the influence of morphology on swimming costs in fishes. *J. Comp. Physiol. B*. 176: 17-25.

Paradis, E., J. Claude and K. Strimmer. (2004). APE: analyses of phylogenetics and evolution in R language. *Bioinformatics*. 20: 289-290.

Rabosky, D. L., F. Santini, J. Eastman, S. A. Smith, B. Sidlauskas, J. Chang and M. E. Alfaro. (2013). Rates of speciation and morphological evolution are correlated across the largest vertebrate radiation. *Nat. Commun.* 4: 1958.

Revell, L. J. (2009). Size-correction and principal components for interspecific comparative studies. *Evolution.* 63: 3258-3268.

Revell, L. J. (2012). phytools: an R package for phylogenetic comparative biology (and other things). *Methods Ecol. Evol*. 3: 217-223. doi: 10.1111/j.2041-210X.2011.00169.x

Rohlf. F. J. (2013). tpsDig, digitize landmarks and outlines, version 2.17. Department of Ecology and Evolution, State University of New York at Stony Brook.

Rüber, L. and D. C. Adams. (2001). Evolutionary convergence of body shape and trophic morphology in cichlids from Lake Tanganyika. *J. Evol. Biol.* 14: 325-332.

Salzburger, W., T. Mack, E. Verheyen and A. Meyer. (2005). Out of Tanganyika: genesis, explosive speciation, key-innovations and phylogeography of the haplochromine cichlid fishes. *BMC Evol. Biol*. 5: 17.

Sanchez, G. (2012). plsdepot: Partial least squares data analysis methods. R package version 0.1.17.

Schindelin, J., I. Argansa-Carreras, E. Frise, V. Kaynig, M. Longair, T. Pietzsch, S. Preibisch, C. Rueden, S. Saalfeld, B. Schmid, J. Y. Tinevez, D. J. White, V. Hartenstein, K. Eliceiri, P. Tomancak and A. Cardona. (2012) Fiji: an open-source platform for biological-image analysis. *Nature Methods*. 9: 676-682.

Schneider, C. A., W. S. Rasband and K. W. Eliceiri. (2012). NIH Image to ImageJ: 25 years of image analysis. *Nature Methods*. 9: 671-675.

Schwarzer, J., A. Lamboj, K. Langen, B. Misof, and U. K. Schliewen. (2015). Phylogeny and age of chromidotilapiine cichlids (Teleostei: Cichlidae). *Hydrobiologia.* 748: 185-199.

Seehausen, O. (2002). Patterns in fish radiation are compatible with Pleistocene desiccation of Lake Victoria and 14600 year history for its cichlid species flock. *Proc. R. Soc. Lond. B.* 269: 491-497.

Snorrason, S. S., S. Skulason, B. Jonsson, P. M. Jonasson, H. J. Malmquist, P. M. Jónasson, O. T. Sandlund and T. Lindem (1994). Trophic specialization in arctic charr *Salvelinus alpinus* (Pisces; Salmonidae): morphological divergence and ontogenetic niche shifts. *Biol. J. Linnean Soc.* 52: 1-18.

Standen, E. M and G. V. Lauder. (2005). Dorsal and anal fin function in bluegill sunfish Lepomis macrochirus: three-dimensional kinematics during propulsion and maneuvering. *J. Exp. Biol.* 208: 2753-2763.

Stauffer, J. R., N. J. Bowers, K. A. Kellogg and K. R. McKaye. (1997). A revision of the blue-black *Pseudotropheus zebra* (Teleostei: Cichlidae) complex from Lake Malawi, Africa, with a description of a new genus and ten new species. *Proc. Acad. Nat. Sci. Philadelphia* 148: 189-230.

Tenenhaus, M. (1998). La régression PLS: Théorie et pratique. Paris, France: Editions Technip.

Thorsen, D. H. and M. W. Westneat. (2005). Diversity of pectoral fin structure and function in fishes with labriform propulsion. *J. Morphol.* 263: 133-150.

Triantafyllou, M. S., G. S. Triantafyllou and D. K. P. Yue. (2000). Hydrodynamics of fishlike swimming. *Annu. Rev. Fluid Mech*. 32: 33-53.

Tytell, E. D., E. M. Standen, and G. V. Lauder. (2008). Escaping Flatland: three-dimensional kinematics and hydrodynamics of median fins in fishes. *J. Exp. Biol.* 211: 187-195.

Vences, M., J. Freyhof, R. Sonnenberg, J. Kosuch and M. Veith. (2001). Reconciling fossils and molecules: Cenozoic divergence of cichlid fishes and the biogeography of Madagascar. *J. Biogeogr.* 28: 1091-1099.

Wainwright, P. C., M. E. Alfaro, D. I. Bolnick and C. D. Hulsey. (2005). Many-to-one mapping of form to function: a general principle in organismal design? *Integr. Comp. Biol*. 45: 256-262.

Wainwright, P. C. (2007). Functional versus morphological diversity in macroevolution. *Ann. Rev. Ecol. Evol. Syst.* 38: 381-401.

Walker, J. A. and M. W. Westneat. (2002). Performance limits of labriform propulsion and correlates with fin shape and motion. *J. Exp. Biol.* 205: 177-187.

Wanek, K. A. and C. Sturmbauer. (2015). Form, function and phylogeny: comparative morphometrics of Lake Tanganyika's cichlid tribe Tropheini. *Zool. Scr.* 44: 362-373.

Ward, A. B. and R. S. Mehta. (2010). Axial elongation in fishes: using morphological approaches to elucidate developmental mechanisms in studying body shape. *Integr. Comp. Biol.* 50: 1106-1119.

Webb, P. W. (1982). Locomotor patterns in the evolution of actinopterygiian fishes. *Amer. Zool.* 22: 329-342.

Webb, P. W. (1984) Body form, locomotion and foraging in aquatic vertebrates. *Amer. Zool.* 24: 107-120.

Webb, P. W., G. D. LaLiberte and A. J. Schrank. (1996). Does body and fin form affect the maneuverability of fish traversing vertical and horizontal slits? *Environ. Biol. Fishes.* 46: 7-14.

Weihs, D. (1989). Design features and mechanics of axial locomotion in fish. *Amer. Zool*. 29: 151-160.

Winemiller, K. O., L. C. Kelso-Winemiller and A. L. Brenkert. (1995). Ecomorphological diversification and convergence in fluvial cichlid fishes. *Environ. Biol. Fishes.* 44: 235-261.

Wright, B. (2000). "Form and function in aquatic flapping propulsion: morphology, kinematics, hydrodynamics, and performance of the triggerfishes (Tetraodontiformes: Balistidae)" Ph. D. Dissertation, Organismal Biology and Anatomy, U Chicago, Chicago, IL.

Young, K. A., J. Snoeks and O. Seehausen. (2009). Morphological diversity and the roles of chance and determinism in African cichlid radiations. *PLoS ONE.* 4: e4740.

Page intentionally left blank

Chapter 3

Swimming with multiple propulsors: measurement and comparison of swimming gaits in three species of neotropical cichlids

Kara L. Feilich

3.1 Summary

Comparative studies of fish swimming have been limited by the lack of quantitative definitions of fish gaits. Traditionally, swimming gaits have been defined categorically by the fin or region of the body that is used as the main propulsor and named after major fish clades (e.g. carangiform, anguilliform, balistiform, labriform). This method of categorization is limited by lack of explicit measurements, the inability to incorporate contributions of multiple propulsors, and the inability to compare gaits across different categories. I propose an alternative framework for the definition, comparison, and categorization of fish gaits based on the propulsive contribution of each structure (body and/or fin) being used as a propulsor relative to locomotor output, and demonstrate the effectiveness of this framework by comparing three species of neotropical cichlids with different body shapes. This approach is modular with respect to the number of propulsors considered, flexible with respect to the definition of the propulsive inputs and the locomotor output of interest, and designed explicitly to handle combinations of propulsors. Using this approach, gait can be defined as a trajectory through propulsive space, and gait-transitions can be defined as discontinuities in the gait trajectory. By measuring and defining gait in this way, patterns of clustering corresponding to existing categorical definitions of gait may emerge, and gaits can be rigorously compared across categories.

3.2 Background

Fishes are diverse and effective swimmers. There is much to be learned from the study of their swimming biomechanics, including different means of thrust generation and maneuvering, morphological design strategies, and effective kinematic motions for propulsion. The study of fish swimming, however, has been hampered by the lack of effective means of measuring and comparing fish gaits. There are myriad combinations of propulsive motions that fishes use across and within any given body shapes (Breder, 1926, Webb, 1973, Lindsey, 1978, Webb, 1984, Lauder and Madden, 2006, Korsmeyer *et al*., 2002, Arreola and Westneat, 1997, Lauder, 2006 and others). Typically, these steady swimming gaits are described using qualitative categories defined by the main propulsive structure, and named based on an exemplar fish taxon that uses that category (reviewed in Sfakiotakis *et al.* 1999). For example, some "body-caudal fin" swimmers use the "anguilliform" mode, undulating almost the entire length of the body (named for the eel order Anguilliformes*)*. Some others use the "thunniform" mode, undulating only the posterior-most part of the body and the tail (named for tuna genus *Thunnus*). Some "median-paired fin" swimmers use the "labriform" gait, oscillating their pectoral fins (named for wrasses, family Labridae); others might use "balistiform" locomotion, undulating both median fins, (named for triggerfishes, family Balistidae). There are at least 13 of these named gait categories (Sfakiotakis *et al.* 1999), but without the ability to quantitatively measure and compare these kinematic gaits, it is virtually impossible to disentangle the effects of fish morphology and that of gait itself on swimming performance.

Efforts to create a means of gait measurement and comparison in swimming fish are aided by this rich literature in both descriptive classifications of fish gaits, and by quantitative methods for comparing tetrapod gaits. The existing classification scheme for fish gaits provides

easily identifiable categorical gait designations and identifies defining characteristics of different swimming modes, but precludes comparisons across these categories (e.g. Breder, 1926, Lindsay, 1979, Webb, 1984, Sfakiotakis *et al*., 1999). Any effective means of comparing gaits should be able to distinguish (and ideally, quantify) differences contributing to these existing classifications. The long history of gait study in terrestrial biomechanics (e.g. Hildebrand, 1965, Hildebrand, 1976, Hildebrand, 1977, Hildebrand, 1989, Alexander, 1984, Alexander, 1989) provides several means of comparison and suggests variables of interest that can be adapted for application to swimming gaits. The first goal of the present study was to integrate these two bodies of literature to create and test a means of measuring and comparing fish gaits across taxa.

Fish gait classifications are, as described above, traditionally based on differences in which anatomical structures (e.g. fins, body undulations) are used in propulsion, and whether these propulsors are used in an oscillatory versus an undulatory motor pattern. Within a particular gait category, the magnitude of the frequency and amplitude of the undulation or oscillation determines swimming speed. Any suitable gait measurement system should then rightly include these kinematic parameters, and perhaps also the swimming speed for which they are used. In addition, the ability of fishes to use multiple propulsive elements at a given speed—a fact typically not incorporated into gait classifications—should be explicitly incorporated into any new gait measurement. For example, the traditional understanding of body-caudal undulatory gaits ignores the fact that median fins are often active in addition to body undulation (Tytell *et al.,* 2008, Standen and Lauder, 2005), and that the pattern of median fin activity changes as swimming speed increases (Drucker and Lauder, 2005, Standen and Lauder, 2005).

Here, I compare three species of neotropical cichlids of different body and fin morphology with respect to their gaits and steady swimming performance. These species, *Cichla*

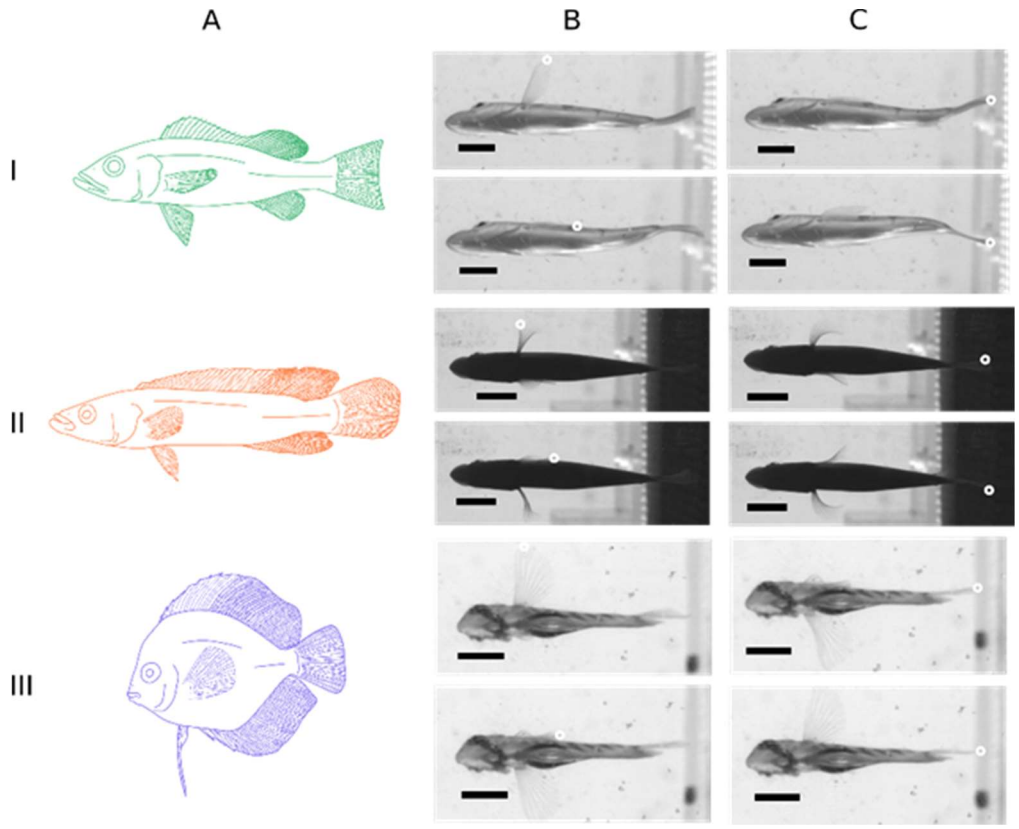

Figure 3.1. Lateral profiles (A) and representative pectoral (B) and caudal (C) fin beats at 1.5 BL s^{-1} for each of the three species used in this study: (I) *Cichla ocellaris*, (II) *Crenicichla saxatilis*, and (III) *Symphysodon aequifasciatus*. The points from which amplitude was calculated are shown in white circles. Colors shown for each fish correspond to those used for each species in Figures 3.3 – 3.7.

ocellaris, *Crenicichla saxatilis*, and *Symphysodon aequifasciatus*, have body shapes that are typically associated with specific locomotor modes and performance capacities (see below, and Figure 3.1A; hereafter these species will be referred to by genus only). This provides an excellent opportunity to test specific ecomorphological hypotheses of morphology-swimming mode linkages, as well as to determine whether different kinematics confound the effects of shape on steady swimming performance. *Cichla* has a typical perciform body shape: it is slightly laterally compressed, has a tapered caudal peduncle, and what could be considered "generalist" fin morphology (Webb, 1984). It was therefore predicted to have the best cruising (= steady swimming) performance, measured as maximum prolonged swimming speed, and to use chiefly a body-caudal fin undulatory gait as opposed to labriform-pectoral fin- based propulsion. *Crenicichla* has an "acceleration-specialist" morphology, with a very cylindrical muscular body and caudally-positioned fin area. Based on the hypothesized tradeoff between acceleration and cruising performance (Webb, 1984), it was predicted that *Crenicichla* would have the lowest steady swimming performance. *Symphysodon* has an extreme body shape associated with maneuvering performance (Webb, 1984): it is extremely laterally compressed, and has a deep disc-shaped body with large median fins, and was therefore predicted to have a labriform gait and intermediate swimming performance in terms of maximum sustainable speed. The likelihood of these species to have different gaits made them an appropriate test case for a new approach to comparing swimming gaits.

3.3 Materials and Methods

3.3.1 *Fish care and maintenance*

Five specimens each of *Symphysodon aequifasciatus* Pellegrin 1904 (SL = 8.5 ± 0.5 cm, mean ± s.d.), *Crenicichla saxatilis* Linnaeus 1758 (10.9 ± 0.1 cm), and *Cichla ocellaris* Bloch & Schneider 1801 (9.8 ± 1.2 cm) were obtained through the pet trade, and housed at 28ºC with a 12h:12h light:dark cycle for at least 2 weeks in the lab before the beginning of experiments. *Symphysodon* and *Cichla* were maintained at pH 7, and *Crenicichla* were maintained at pH 6.2. *Symphysodon* are typically maintained at a lower pH, but these specimens were bred and raised by the breeder at pH 7. Experiments were conducted in water matching that used to house each species at 28ºC. Experimental and fish care protocols were approved by the Harvard University Institutional Animal Care and Use Committee under protocol 20-03 to George Lauder.

3.3.2 *Steady swimming performance trials and analysis*

Three trials from each fish were used to measure steady swimming kinematics and performance. Trials were conducted in a 600 L swimming flume with the working section restricted to 26 cm x 26 cm x 28 cm. For each trial, the fish swam for step increases from 0.5 body lengths (BL, measured as standard length) per second, increasing by 0.2 BLs^{-1} until burst and coast swimming was observed, following the procedure of Ellerby and Gerry (2011). Each swimming speed interval lasted 15 min, until anaerobic burst-and coast behavior was observed. Increases in speed were gradual over 30 s between 15 min intervals.

Steady swimming performance was measured using two different metrics: pectoral-caudal gait-transition speed (Drucker, 1996) and maximum prolonged swimming speed (He, 2010). Gait-transition speed (U_{trans}) was recorded as the speed at which a fish began to employ its caudal fin for propulsion. Maximum prolonged swimming speed (U_{max}) was calculated as a function of the fastest speed that could be sustained for 15 min (U_{last}) and the length of time

spent at the subsequent speed before anaerobic burst-and-coast behavior was observed (t_{final}) (Ellerby and Gerry, 2011) as follows:

(3.1) $U_{max} = U_{last} + \frac{t_{final}}{15\text{min}}(0.2\ \text{BLs}^{-1})$

Performance metrics were best represented by a normal distribution, and each were compared using a linear mixed-effects model fit by REML with species as a fixed factor and specimen as a random factor using the R package *lme4* (Bates *et al.*, 2015). Post-hoc Tukey HSD tests were conducted using R package *multcomp* (Hothorn *et al.*, 2008) to determine which species had significantly different performance.

3.3.3 *Kinematic data collection and analysis*

From each trial, for each speed interval where possible, 10 s of steady swimming were recorded in lateral and ventral view at 250 fps with 1024 x 1024 pixel resolution using two digital high-speed cameras (FASTCAM-1024PCI, Photron USA Inc., San Diego, CA, USA), with one pointed at a 45º angle front-faced mirror positioned under the flume working section. For some intervals, the fish position in the flume made video unattainable. For *C. saxatilis,* successful trials were only obtained for 3 out of more than 20 attempts, and only with a black screen covering the wall of the flume: therefore, for this species, only ventral view videos were possible. Because of the variability in the ability to film different individuals of the three species, the breakdown of how many trials were conducted using each individual, and which analyses were conducted on those trials, are provided in Supp. Table S3.1.

Videos were calibrated using a 1 cm x 1 cm grid pattern photographed at multiple positions in the working section in both lateral and ventral views. From measurements of these

images, two linear equations were fitted to find pixel-to-cm conversion factors in both the vertical and horizontal plane.

Pectoral and caudal fin frequency and amplitude were recorded from the ventral view videos. Caudal fin amplitude was defined as the tip-to-tip displacement of the ventral tip of the posterior fin margin perpendicular to the direction of flow. Pectoral fin amplitude was measured in two ways: pectoral fin sweep angle, the arc in degrees through which the fin tip moved in one fin beat, and pectoral fin tip displacement, the displacement of the tip of the pectoral fin from the position closest to the body during the fin beat (shown in Fig. 3.1). All three amplitude measurements were made from the video in pixels using ImageJ, then converted to cm using the calibration factors for the fish's position in the working section (ImageJ v.1.51f, Fiji distribution; Schindelin *et al.*, 2012, Schneider *et al*., 2012). Amplitude was measured as displacement of the fin tip at the extrema of the fin beat, shown in Figure 3.2. From the kinematic measurements, Strouhal number (*St*) was calculated for each propulsor as follows:

(3.2) $St = fL/U$,

where *f* is the propulsor's average fin beat frequency and *L* is the propulsor's average amplitude at speed *U*. Fin beat frequencies amplitudes, and the product of these were compared using linear mixed effects models fit by restricted maximum likelihood (REML) with species as a fixed factor and individual as a random factor, using unnormalized speed as a covariate using R package *lme4* (Bates *et al.,* 2015).

Body midline kinematics were traced from ventral view video for representative individuals of *Cichla* and *Symphysodon*. For *Crenicichla*, midline traces were taken only from those rare trials where the fish actually swam, which were probably not "representative" of typical behavior in the field. The midlines were taken from single body undulation cycles at

every 10% of the undulatory cycle from 0%, resulting in 10 midline traces per speed. Midlines were compared qualitatively.

3.3.4 *Parameterization of gait as a trajectory though a propulsive space*

Traditionally, fish gaits have been classified categorically and qualitatively, with little regard for the nuances of how a fish's gait may change with speed, or the employment of multiple propulsive structures (i.e. pectoral fins, caudal fins, body undulations, median fins). This prohibits quantitative comparison of gaits across fishes that use different categories of gait.

Here, I propose a different means of defining gait that allows for the treatment of multiple propulsors and quantitative analysis and comparison. Gait can be thought of as the combination of propulsive inputs, be they from legs, bodies, or fins, to produce a given locomotor output (i.e. speed or thrust). To quantify gait, then, one needs to parameterize those propulsive inputs, and the output of interest (Eqn. 3.3), where *n* is the number of propulsors.

(3.3) $Output = \sum_{i=1}^{n} Input_i$

The question arises, how does one parameterize the extent to which a given propulsor contributes to the locomotor output? One intuitive candidate for this is the product of frequency (*f*) and amplitude (*A*) of a propulsor, as in Webb, 1973. For a fin, this is effectively the distance that fin travels per second to achieve a particular speed. If we define the input, propulsor effort (*Eff*), for a given propulsor *i* as

(3.4) $Eff_i = f_i * A_i$,

and speed (*U*) as the propulsive output, then, we can express gait as the proportionality:

(3.5) $U \propto \sum_{i=1}^{n} Eff_i$.

For a fish in which the propulsors of interest are the pectoral fins and the caudal fins, we can then think of gait as the series of inputs producing each speed:

(3.6) $U \propto Eff_{pectoral} + Eff_{caudal}$,

where $Eff_{pectoral}$ assumes symmetric input of pectoral fins. If pectoral fins are not used symmetrically, each fin could be treated independently.

Note that this approach is modular, and easily modified to examine different output variables, different numbers of propulsors, and different effort/input equations. For instance, given data on fin area, one could just as easily define propulsive effort as the product of frequency, amplitude, and fin area.

If we restrict ourselves to the two-propulsor case, this also provides an easy means of visually characterizing and comparing gait in a quantitative framework, by plotting the output as a function of the propulsive inputs. In this context, gait is the trajectory through a 3D propulsive space, and a true "gait transition" would be represented as a discontinuity in this trajectory. For example, Figure 3.2 demonstrates three possible gait trajectories that one would expect of traditional swimming modes. A "perfectly labriform" fish would increase steady swimming speeds by increasing only pectoral input (black points); a "perfectly carangiform" fish would increase speed by increasing only caudal input (medium grey points); and a fish with a typical paired-fin to body-caudal gait transition would have a bend in its trajectory through propulsive space, as it begins to favor the latter propulsive system (light grey points) (Figure 3.2). When considering only the input axes, as in the top graph of Figure 3.2, it is apparent that these hypothetical fish occupy different regions of gait space.

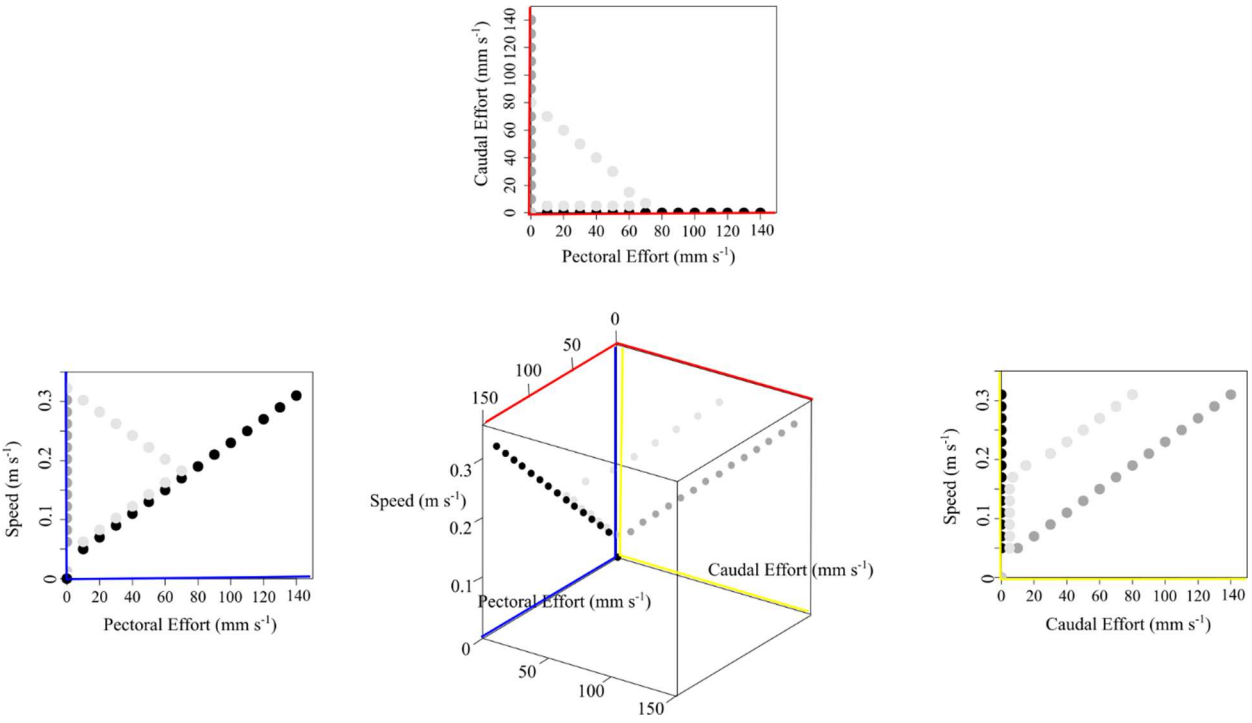

Figure 3.2. Hypothetical "gait trajectories" and 2-D isometric projections of three potential swimming "types": perfectly labriform (black), perfectly carangiform (medium grey), and a type transitioning from labriform to body-caudal swimming (light grey). The projection on blue axes shows the contribution of the pectoral fins with speed. The projection on the yellow axes shows the contribution of the caudal fin with speed. The projection on the red axes can be considered the occupation of gait space, showing what combinations of propulsive movements are used by the fish. Note that the light grey trace has been shifted slightly in the y-axis to avoid overlap.

The above proportionality and graphing scheme was used to visually compare the trajectory through propulsor space (gait) of the three species examined here. Note that this approach still holds for more than two propulsors, but visualization would require projection of the multidimensional propulsor space into a lower-dimensional (3 or less) space for plotting. This could be accomplished by means of dimension reduction techniques, or by focusing on only two propulsors at a time.

3.3.5 *Note on body size and scaling*

There are some problems with methods accounting for the effects of scaling by simply dividing swimming speed by body length (Drucker and Jensen, 1996). While the individuals used in this study were all of very similar length, *Crenicichla* individuals were slightly larger than the others, and did not overlap with the other two species along the size domain, precluding their inclusion in a regression-based analysis with size as a covariate. Therefore, I chose to compare midline kinematics, gait transition speed, and maximum prolonged speed by normalizing swimming speed to standard length. Gait transition speed and maximum prolonged swimming speeds are also given without normalization, but these values were not considered comparable for statistical testing. Kinematic parameters (i.e. frequency, amplitude, "effort" as defined) and gait trajectories were compared and plotted without normalization, as there was no *a priori* expectation of how they will scale. That being said, use of this approach in the future can explicitly test for allometric effects on gait, given appropriate experimental design.

3.4 Results

3.4.1 *Differences in kinematic strategy*

The three species of cichlids used different kinematic strategies to propel themselves at increasing speeds. Generally, all three species changed caudal fin beat frequencies rather than caudal fin beat amplitudes at different speeds, but varied both pectoral fin beat frequency and amplitude (Figure 3.3, Table 3.1). Speed and species had interacting effects on all measures of pectoral fin use; but independent effects on caudal fin use, i.e. different species had similar slopes of the curves of caudal kinematics against speed, but different intercepts (Table 3.1, Figure 3.3). The changes across species typically involved which fins were being used at any given speed. At low speeds, *Cichla* used the pectoral fins as its primary propulsors, increasing pectoral fin beat frequency to speed up. At the gait-transition speed, *Cichla* began to use body-caudal fin propulsion, increasing caudal fin beat frequency while reducing pectoral fin beat frequency (Figure 3.3, Table 3.1). *Symphysodon* used an alternative kinematic strategy, increasing both pectoral fin beat frequency and amplitude, and eventually employing the caudal fin to increase speed. There was no discrete gait transition in *Symphysodon*, rather, this was recorded as the speed at which the fish began to use the caudal fin. *Crenicichla*, when it swam at all, increased pectoral fin beat frequency with increasing speed (Figure 3.3, Table 3.1). Data from *Crenicichla* however, may be unreliable, as the fishes tended to "swim" in contact with the bottom of the flume. The inability to elicit reliable steady swimming in *Crenicichla* raises the question as to whether this species has the physiological or behavioral capacity for steady swimming at all.

Patterns of body undulation also varied across species (Figure 3.4), and in the case of *Cichla* also varied with speed. Neither *Symphysodon* nor *Crenicichla* had any observable body bending while steady swimming at any speed. This was notable in *Crenicichla*, which has both

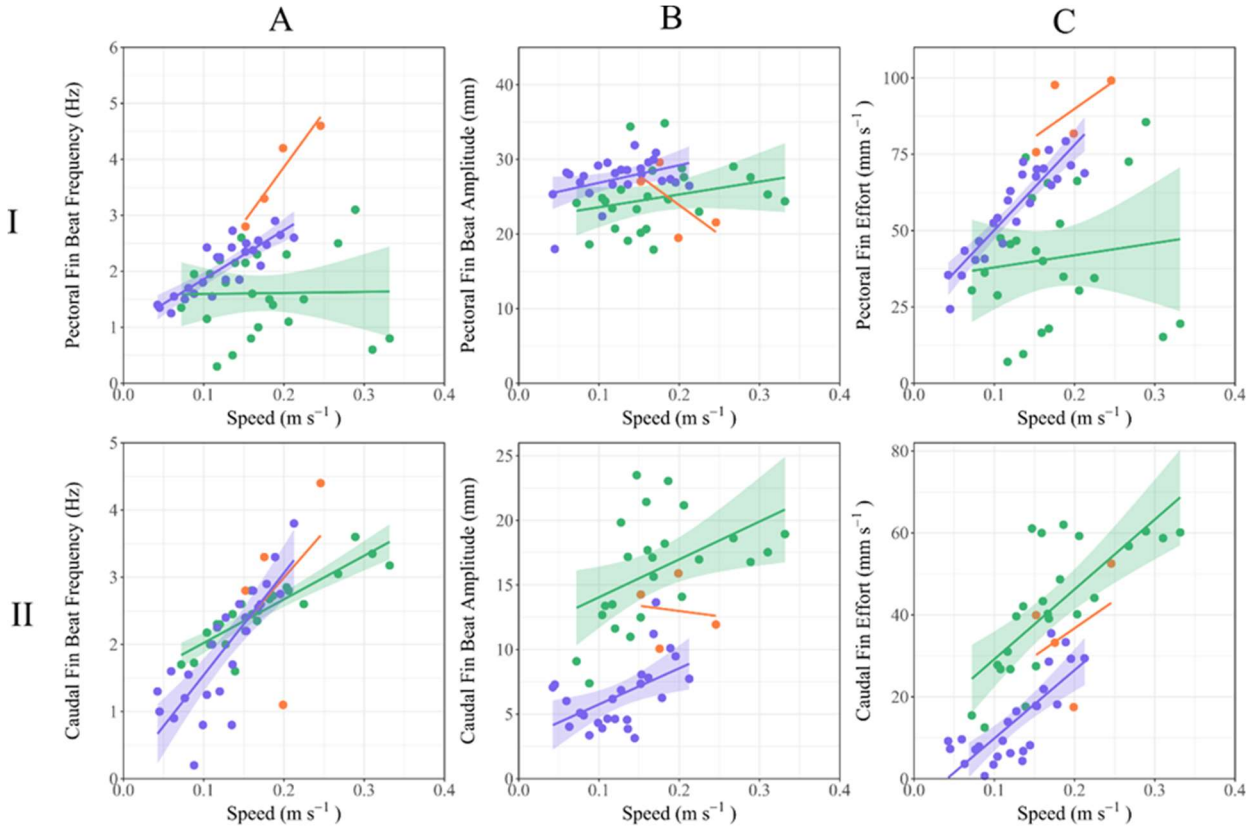

Figure 3.3 Pectoral (I) and Caudal (II) fin beat frequencies (A), amplitudes (B), and "effort" (C) as a function of steady swimming speed. Each point is the mean average of all trials at that speed for a given fish. Linear regressions for each species are shown with 95% confidence intervals shaded. There was insufficient sampling to calculate confidence intervals for *Crenicichla*. Species are indicated by color as in Fig. 3.1. Statistical comparisons are presented in Table 3.1. *Cichla*: n = 4; *Crenicichla*: n = 2; *Symphysodon:* n = 3.

Table 3.1. Linear mixed effects models to determine variation in fin beat frequency, amplitude, and "effort" with respect to speed and species (fixed effects) while accounting for individual variation (random effect). Data correspond with that depicted in Figure 3.3. Where there was a significant interaction effect, single factor effects are not reported. Statistics are reported from Type II Wald Chi-square tests of linear mixed effects models.

Response Variable	Speed:Species (df =2)	Speed (df = 1)	Species (df = 2)
Pectoral Fin Frequency	**$\chi^2 = 19.78,\ p < 0.001$**	-	-
Pectoral Fin Amplitude	**$\chi^2 = 8.18,\ p = 0.017$**	-	-
Pectoral Fin Effort	**$\chi^2 = 28.20,\ p = 0.003$**	-	-
Caudal Fin Frequency	$\chi^2 = 3.17,\ p = 0.205$	**$\chi^2 = 58.08,\ p < 0.001$**	$\chi^2 = 6.33,\ p = 0.042$
Caudal Fin Amplitude	$\chi^2 = 1.73,\ p = 0.421$	**$\chi^2 = 16.59,\ p < 0.001$**	**$\chi^2 = 19.96,\ p < 0.001$**
Caudal Fin Effort	$\chi^2 = 0.76,\ p = 0.685$	**$\chi^2 = 55.98,\ p < 0.001$**	**$\chi^2 = 15.10,\ p < 0.001$**

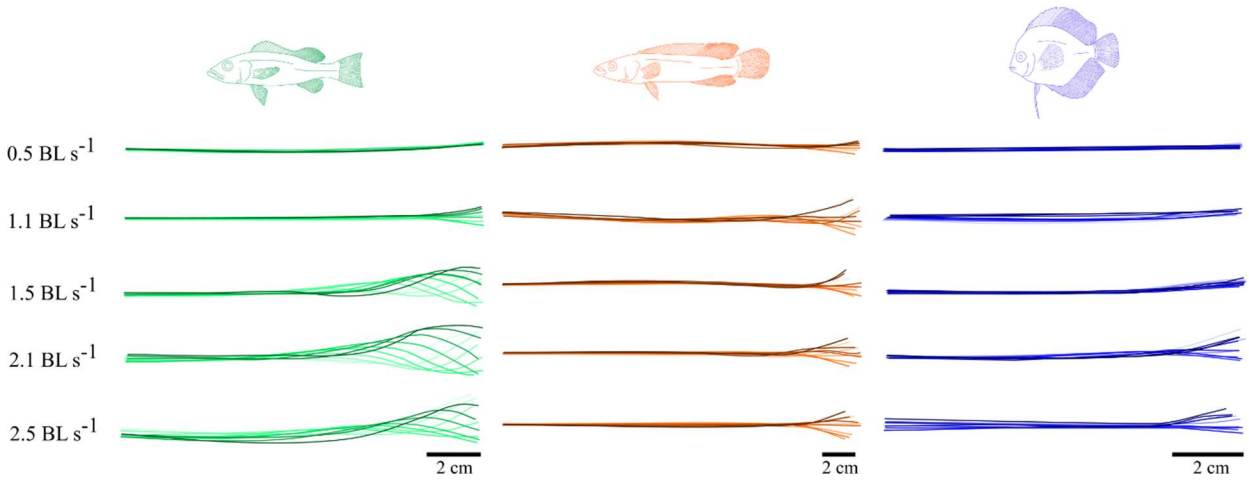

Figure 3.4. Representative midline kinematics of each species at 0.5, 1.1, 1.5, 2.1, and 2.5 BL s^{-1}. Species are indicated by color as in Figure 3.1. 0% of caudal fin beat cycle is shown in the lightest hue, and 90% is shown in the darkest hue for each kinematic envelope. Midlines are scaled to unit body length across species, and scale bars are presented for each species.

the most elongate, anguilliform, body shape, and can bend with very low radius of curvature when maneuvering (K. Feilich, personal observation). If *Crenicichla* swam steadily according to predictions based on its morphology, it would have used a more anguilliform gait (Webb, 1973). Instead, when it swam, it did so with a gait very similar to that of *Symphysodon* (Figures 3.3 and 3.4). *Cichla* used no body bending at low speeds, but increased its body bending as speed increased, maintaining almost a full sinusoidal wavelength along its body at the fastest speeds measured (Figure 3.4).

3.4.2 *Differences in morphology do not necessarily impose differences in performance*

Despite the marked differences in morphology, and in some cases, kinematics, across the three species, differences in steady swimming performance were small to negligible (Figures 3.5 and 3.6). There was a significant effect of species on both normalized gait transition speed and normalized maximum prolonged swimming speed (U_{trans}: Type II Wold $\chi^2 = 6.33$, $df = 2$, $p = 0.042$*; U_{max}: Type II Wold $\chi^2 = 8.66$, $df = 2$, $p = 0.013$*). Post-hoc testing did not reveal significant pairwise differences among gait transition speeds (Tukey Contrasts: *Crenicichla – Cichla*: $p = 0.083$; *Symphysodon – Cichla*: $p = 0.093$; *Symphysodon – Crenicichla*: $p = 0.897$). The only significant difference across species was between the maximum prolonged swimming speed of *Cichla* and *Symphysodon*, with *Cichla* having a significantly higher maximum prolonged speed (Figure 3.6; Tukey Contrasts: *Crenicichla – Cichla*: $p = 0.234$; *Symphysodon – Cichla*: $p = 0.011$*; *Symphysodon – Crenicichla*: $p = 0.934$). When this result is considered in conjunction with gait-transition speed (defined as the speed at onset of caudal fin use), it showed that *Cichla* uses caudal fin-based propulsion for a broader speed range than *Symphysodon*, which may contribute to its steady swimming performance.

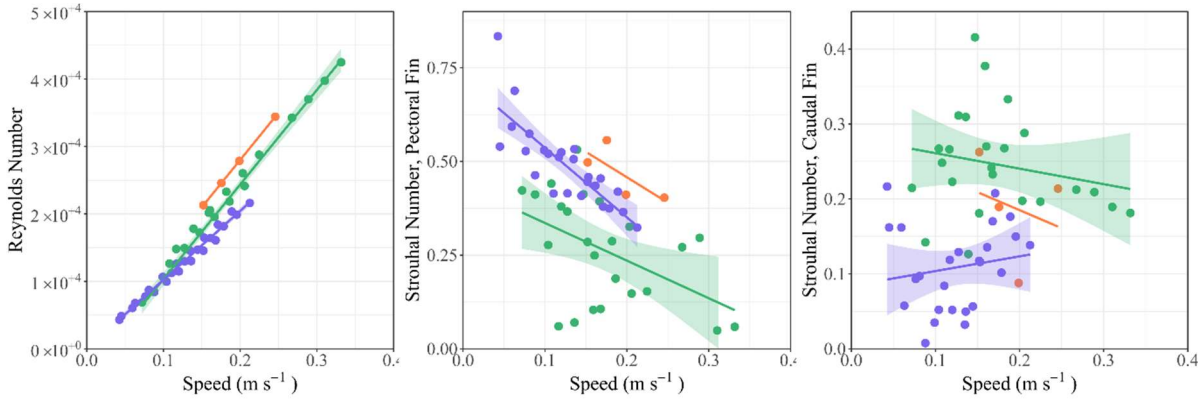

Figure 3.5. Mean Reynolds number and Strouhal number as a function of steady swimming speed. Strouhal numbers are calculated separately for each of the left pectoral fin and the caudal fin (see Eqn. 3.2). Linear regressions for each species are shown with 95% confidence intervals shaded. There was insufficient sampling to calculate confidence intervals for *Crenicichla*, due to its inconsistent swimming. Species are indicated by color as in Figure 3.1. *Cichla*: n = 5; *Crenicichla*: n = 2; *Symphysodon*: n = 5.

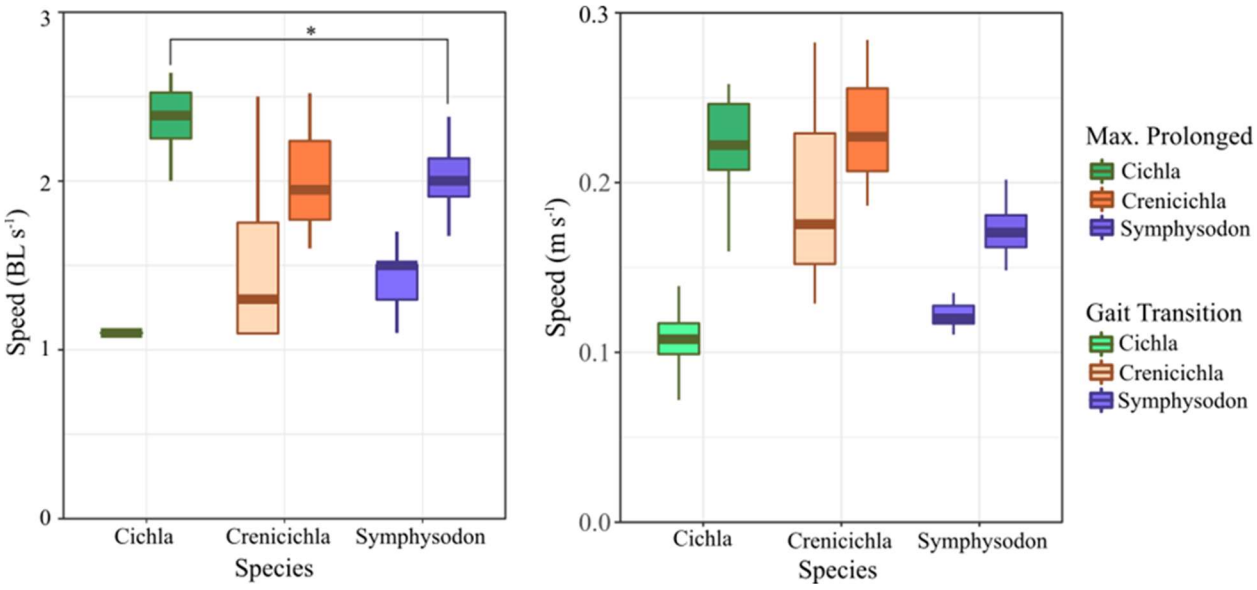

Figure 3.6. Pectoral-caudal gait transition speed and maximum prolonged swimming speed. Note that gait transition speed is defined as the onset of caudal fin use; almost all fishes continued to use their pectoral fins in addition to the caudal fin after the gait transition. Left: Speeds normalized to body length. Right: Raw speed. Note that statistical comparisons were only conducted for the normalized speeds. * indicates significant differences with $p <$ 0.05 following mixed factor modeling and post-hoc Tukey HSD. Bars indicate mean, 25% and 75% quartiles, and lines indicate the range of the data. Sample sizes for these data are presented as n = (U_{trans}, U_{max}), *Cichla*: n = (5,5); *Crenicichla*: n = (3,2); *Symphysodon*: n = (5,5).

3.4.3 *High variation in use of the non-primary propulsor*

For the two species that swam consistently, the gait trajectories reveal that one propulsor had a much noisier relationship with speed than the other (Figure 3.7). For *Cichla*, the pectoral fins were used inconsistently with increasing speed, and for *Symphysodon*, caudal fin use was inconsistent, though less variable than the use of the pectoral fins of *Cichla*. This likely reflects the contribution of each system to propulsion overall, with the non-primary propulsors having more variability. In most of the fishes studied, however, even the non-primary propulsor was almost always being used, often substantially, and probably played an important role in swimming. The median species trajectories also suggest that *Cichla* used the typical paired-fin to body-caudal fin gait transition (the curve in the median trajectory), but *Symphysodon* is not (Figure 3.7). In contrast to trading one propulsor for another, once *Symphysodon* began to use its caudal fin, it increased both pectoral and caudal fin effort with increasing speed—less a "transition" than an augmentation (Figure 3.7). In addition, the projection of these gait trajectories can be used as an analog to Hildebrand-type tetrapod "gait spaces" (Hildebrand, 1976) —showing that *Cichla* and *Symphysodon* occupy distinct areas of gait space (Figure 3.7).

Differences in individual patterns of steady swimming kinematics are further highlighted and reinforced by the depiction of each individual fish's gait trajectory (Figure 3.8). All of the

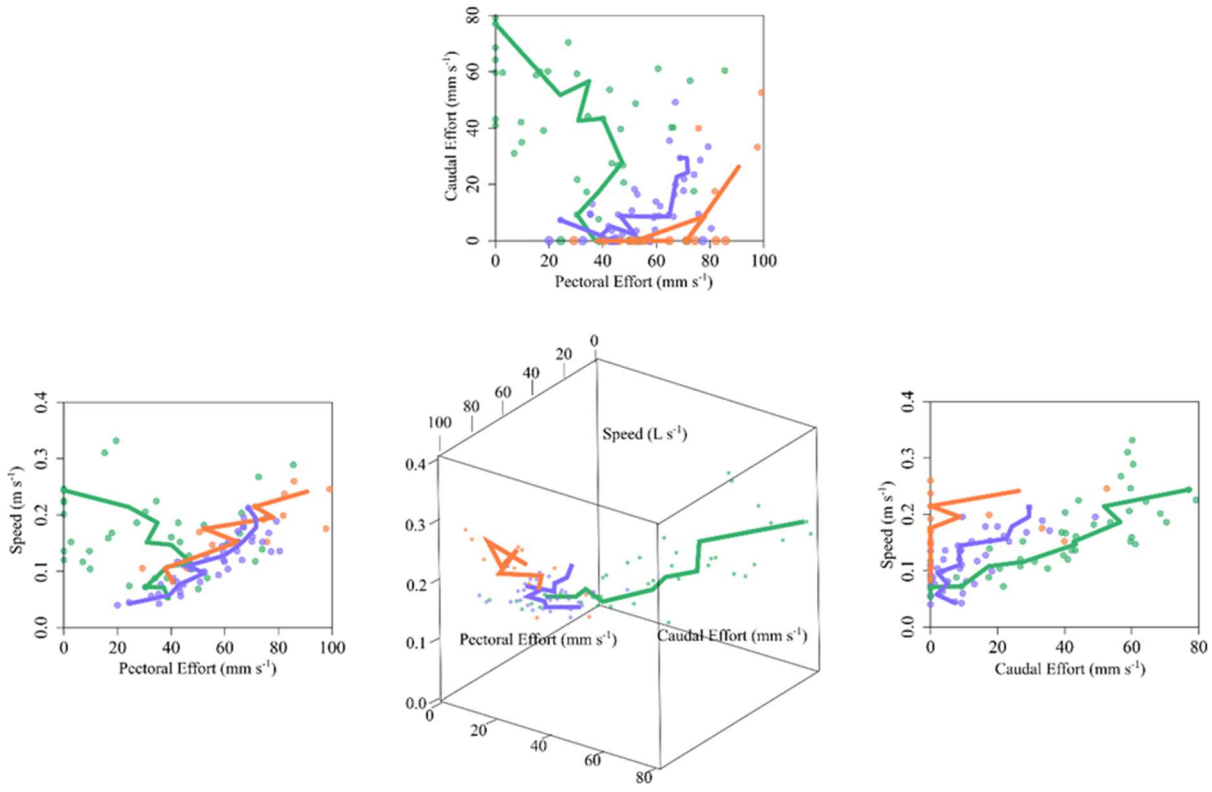

Figure 3.7. Gait trajectories and gait space occupation for the individual fishes of three species used in this study. Points show average of 5 fin beats for caudal effort and pectoral effort for a given fish-trial. For each species, the median values for each speed are connected by straight line segments. Species are indicated by color as in Figure 3.1. *Cichla*: n = 4; *Crenicichla*: n = 2; *Symphysodon*: n = 3.

Symphysodon individuals followed almost the exact same path through gait space, indicating consistency across individuals in the use of both pectoral and caudal propulsion to increase speed. *Cichla* individuals, however, had more erratic, zig-zagging trajectories through gait space (Figure 3.8). This suggests that, perhaps, *Cichla* is capable of using multiple kinematic patterns to achieve the same or similar speeds, supplementing low caudal fin use with pectoral fin use or vice versa.

3.5 Discussion

3.5.1 *Context for comparison of propulsive gaits*

Despite the widespread use of swimming gait categories in the fish biomechanics literature, studies that have examined the kinematics of more than one propulsor often demonstrate that fishes are not constrained to any one category, and can use aspects of multiple categories at any given speed (Lauder, 2006). For example, fishes using body-caudal undulations may also use pectoral fin movements at the same time. The median fins can also, simultaneously, contribute to steady swimming propulsion, though their roles are comparatively understudied (Lauder, 2006). In addition, the lack of a framework to explore the diversity of "non-standard" swimming modes has restricted the possible utility of existing data to address comparative questions about fishes using different swimming modes. The main goal of this study was to test a new method of defining and characterizing fish gaits that provides for both quantitative inclusion of combinations of propulsors, and that allows for standardized comparisons of the many diverse swimming gaits. This method was used to compare the gaits and steady swimming performance of three species of cichlid with body shapes associated with swimming specializations.

Fish swimming is in some respects more complicated than quadrupedal terrestrial

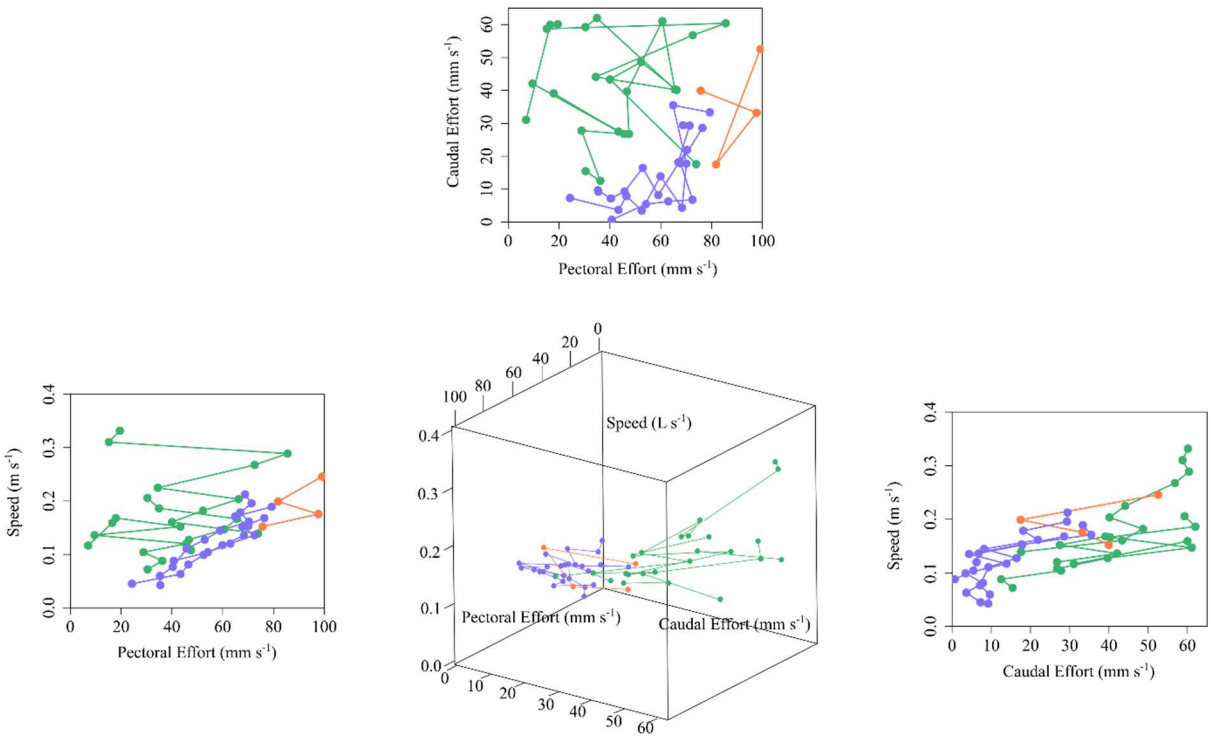

Figure 3.8. Average gait trajectories and gait space occupation for the individual fishes of three species used in this study. Lines connect average values for an individual fish at different speeds. Species are indicated by color as in Figure 3.1. *Cichla*: n = 4; *Crenicichla*: n = 2; *Symphysodon*: n = 3.

locomotion: it is currently impossible to directly measure the forces produced during aquatic locomotion, there are often more degrees of freedom in the movement of aquatic bodies and fins than in terrestrial quadruped bodies and limbs, and the current state of fluid dynamic modeling severely limits application of inverse or forward dynamic approaches to aquatic systems. Therefore, the historical comparative methods that exist to address terrestrial locomotion have informed the approach taken here. Specifically, Milton Hildebrand's insight that "gaits can be expressed numerically and analyzed graphically to reveal their nature and relationships" (Hildebrand, 1965), and similar work by Vladimir Sukhanov and Petr Gambaryan parameterizing the movements of the legs, can be applied to the propulsive elements of swimming fish (Hildebrand, 1965, Hildebrand, 1976, Sukhanov, 1974, Gambaryan, 1974).

Hildebrand's and others' "gait-space" provided for new kinds of comparative questions about gait (many proposed by Hildebrand himself), allowing researchers to formally describe gait variability, the extent of hypothetical gait diversity, and how variables of interest (development, allometry, etc.) affect gait (e.g. Hildebrand, 1976, Peters, 1983, Lemelin *et al.,* 2003). However, the tetrapod symmetrical "gait formula" as is cannot be applied to fishes, because it considers stride duty factor and phase lag. For the former, it is difficult to define a consistent duty factor for the multiple fish propulsors that can be used in the absence of information about when in a fin beat or in a body undulation thrust is being produced. While these data are starting to become available (e.g. Lucas *et al.,* 2015), it is unlikely that they will exist for the vast diversity of fish morphologies and swimming modes in the near future. For the latter, whether or not different propulsors are used with the same period, or with periods that are in phase with one another, is still largely unknown.

The existing literature on fish swimming provided likely candidates for incorporation into a fish "gait formula". Virtually every fish propulsor operates with some (near-constant) frequency and some (near-constant) amplitude during steady swimming at any given speed (Bainbridge, 1958). Values for fin beat frequency in particular are reported in almost every study of steady swimming, though usually only for one propulsor of interest. These data are readily available, and much easier to collect at present than more sophisticated hydrodynamic information. Combined, these two parameters can summarize the movement of a given swimming propulsor reasonably effectively (Webb, 1973).

3.5.2 *Quantifying kinematic strategy provides a means of isolating and comparing gaits*

As swimming performance (or in fact, all locomotor performance) is the product of the combined and interacting effects of morphology, kinematics, and physiology, it is impossible to understand how each of these factors individually affects performance without having some way of isolating the variation in each (Arnold, 1983). By parameterizing gait kinematics, it is possible to explicitly measure the association between kinematics and other variables of interest, and compare kinematics across a range of species and conditions. The three species in this study have fairly archetypal body morphology with respect to hypotheses of swimming eco-morphology, but any attempt to attribute differences in their swimming performance to shape would be confounded without knowledge of any variation in their steady swimming gait (and physiology, but that is beyond the scope of this study).

The gait trajectory analysis defined and used here largely isolates movement patterns from gross morphology (though see below for concerns and possible future approaches). For instance, even though *Crenicichla* and *Symphysodon* have different body shapes, their kinematic

gaits are similar (Figures 3.3 and 3.4). And although the maximum prolonged speed in *Crenicichla* is similar to that of *Cichla*, their kinematics are different. In fact, the kinematics for *Crenicichla* were in contrast with what was hypothesized for its body form: when *Crenicichla* did swim, it did so using a more stereotypically labriform gait than anguilliform.

3.5.3 *Potential for many-to-one mapping of morphology and kinematics on performance*

If species differ in both morphology and gait, these factors will confound the effects of one another on performance. In this case, the higher steady swimming performance of *Cichla* in terms of maximum sustainable speed may be the product of either its "cruising" morphology, its body undulating kinematics, or some combination of the two—the contributions of either to performance and the interaction between the two is confounded. While the gait trajectory approach successfully described variation in movement patterns, its application to these three species highlighted the potential for multiple-to-one mappings of morphological and kinematic traits on swimming performance. These three species, with three different morphologies used two kinematic strategies. Despite these differences, there was surprisingly little variation in steady swimming capacity among the three species. Two species (*Cichla* and *Crenicichla*) obtained remarkably similar maximum prolonged swimming speeds, despite having different morphology and different kinematics. This demonstrates how tenuous the links between morphology, kinematics, and performance can be in the case of a function as multifaceted as steady swimming capacity. Without direct observation and measurement of function, these results suggest caution in the application of swimming mode assumptions based on morphology.

3.5.4 *Choices and refinement of the gait trajectory approach*

The gait trajectory approach as tested here successfully described the kinematic patterns of the species tested, depicting the changing and variable use of two distinct propulsive structures with speed. It successfully demonstrated how some variation in performance as defined can be attributable to differences in gait and morphology, and also how performance can be similar in the face of distinctly different gait and morphology (suggestive of underlying physiological variation). The approach can be extended to incorporate additional propulsive elements with little modification. Any fish that swims steadily can be plotted in this multi-dimensional gait space. The incorporation of additional propulsors, such as the dorsal fin or anal fin merely requires the addition of more axes, which can be analyzed quantitatively with no change in approach. While these cannot all be visualized in 3 dimensions, projections of the multiple axes into lower dimensional space, or dimension reduction techniques can be applied for visualization. For example, a gymnotiform swimmer would probably fall largely on an anal fin axis, with little to no caudal input.

That being said, there are several choices and refinements of the method that can be made going forward. First, the choice of propulsive input function ("effort", here) can be modified based on the researcher's intent. An obvious modification would be to incorporate morphological variables such as fin area and fin angle into the input function. However, to do so would be to explicitly incorporate morphological variation into a function meant to isolate kinematics, which, depending on one's research aims, may be undesirable. For this same reason, it may be desirable to normalize amplitude to some length parameter, though again, this would require caution with respect to the unintended inclusion of morphological variation. For pectoral fin beats, measuring amplitude as the fin sweep angle avoids the effects of fin length; however,

there is currently no consistent definition for a sweep angle of the caudal fin, as the base of the fin typically moves in both heave and pitch.

An additional challenge is how to account for the effects of allometry on both amplitude and frequency, aside from differences in morphological configuration. When the fish being compared are of similar size, this is not an issue, but there are likely non-linear allometric relationships between frequency, amplitude and body size. Perhaps the best way of accounting for this variation is to first measure it empirically, and experimentally determine the nature of such allometric relationships for a number of individual species, before attempting to generalize across all fishes.

Finally, it is worth noting that the gait trajectory approach as defined here does not account for differences in propulsive phase relationships (e.g. phase differences between the pectoral and caudal fins, or between pectoral fins; Hale *et al.*, 2006). These can be described categorically and plotted on top of a trajectory; or treated separately from the trajectory itself.

3.5.5 *Future directions for the study of swimming gaits*

Given the ability to quantitatively compare swimming gait trajectories as defined here, there are many questions about swimming gait that can be addressed. The gait trajectory approach can be applied to treat gait as a response variable, and determine the effects of other important biological factors such as size, fatigue, or flow conditions on gait itself. The explicit measurement of multiple propulsors' movements can be incorporated into metabolic studies and hydrodynamic studies, determining the economy of a particular gait, or a particular propulsor. In conjunction with dimension reduction techniques, gait trajectories may also assist in the identification of kinematic parameters that covary, or that may have otherwise be considered

unimportant. The isolation of kinematic variables as presented here is another step towards understanding how morphology, kinematics, and physiology interact to produce performance.

3.6 References

Alexander, R. M. (1984). The gaits of bipedal and quadrupedal animals. *J. Robotics. Res.* 3: 49-59.

Alexander, R. M. (1989). Optimization and gaits in the locomotion of vertebrates. *Physiol. Rev.* 69:1199-1227.

Arnold, S. J. (1983). Morphology, performance, fitness. *Amer. Zool.* 23: 347-361.

Arreola, V. I. and M. W. Westneat. (1996). Mechanics of propulsion by multiple fins: kinematics of aquatic locomotion in the burrfish (*Chilomycterus schoepfi*). *Proc. R. Soc. B.* 263: 1689-1696.

Bainbridge, R. (1958). The speed of swimming of fish as related to size and to the frequency and amplitude of the tail beat. *J. Exp. Biol.* 35: 109-133.

Bates, D., M. Mächler, B. Bolker, and S. Walker. (2015). Fitting linear mixed-effects models using lme4. *J. Stat. Softw*. 67: 1-48.

Breder, C. M. (1926). The locomotion of fishes. *Zoologica*. 4: 159-297.

Drucker, E. G. (1996). The use of gait transition speed in comparative studies of fish locomotion. *Amer. Zool.* 36: 555-566.

Drucker, E. and J. Jensen (1996). Pectoral fin locomotion in the striped surfperch. II. Scaling swimming kinematics and performance at a gait transition. *J. Exp. Biol.* 199: 2243-2252.

Drucker, E. G. and Lauder, G. V. (2005). Locomotor function of the dorsal fin in rainbow trout: kinematic patterns and hydrodynamic forces. *J. Exp. Biol.* 208: 4479-4494.

Ellerby, D. J. and S. P. Gerry (2011). Sympatric divergence and performance trade-offs of bluegill ecomorphs. *Evol. Biol.* 38, 422-433.

Gambaryan, P. P. (1974) How Mammals Run: Anatomical Adaptations. New York, John Wiley and Sons.

Hale, M. E., R. D. Day, D. H. Thorsen and M. W. Westneat. (2006). Pectoral fin coordination and gait transitions in steadily swimming juvenile reef fishes. *J. Exp. Biol*. 209: 3708-3718.

He, P. (2010). Swimming capacity of marine fishes and its role in capture by fishing gears. In Fish Locomotion: An Eco-Ethological Perspective (ed. P. Domenici and B. G. Kapoor). Enfield, NH: Science Publishers. pp. 484-512.

Hildebrand, M. (1965). Symmetrical gaits of horses. *Science.* 150: 701-708.

Hildebrand, M. (1976). Analysis of tetrapod gaits: general considerations and symmetrical gaits. In Neural Control of Locomotion (ed. R. Herman, S. Grillner, P. Stein, and D. Stuart), pp. 203-236. New York: Plenum Press.

Hildebrand, M. (1977). Analysis of asymmetrical gaits. *J. Mammal.* 58: 131-156.

Hildebrand, M. (1989). The quadrupedal gaits of vertebrates. *BioScience.* 39: 766-775.

Hothorn, T., F. Bretz and P. Westfall. (2008). Simultaneous inference in general parametric models. *Biom. J.* 50: 346-363.

Korsmeyer, K., J. Steffensen and J. Herskin. (2002). Energetics of median and paired fin swimming, body and caudal fin swimming, and gait transition in parrotfish (*Scarus schlegeli*) and triggerfish (*Rhinecanthus aculeatus*). *J. Exp. Biol.* 205: 1253-1263.

Lauder, G. V. (2006). Locomotion. In The Physiology of Fishes, 3rd Ed. (ed. D. H. Evans and J. B. Claiborne), pp. 3-46. Boca Raton: CRC Press.

Lauder, G. V. and P. G. A. Madden. (2006). Fish locomotion: kinematics and experimental hydrodynamics for roboticists. *Int. J. Automat. Comput.* 3: 325-335.

Lemelin, P., D. Schmitt and M. Cartmill. (2003). Footfall patterns and interlimb co-ordination in opossums (Family Didelphidae): evidence for the evolution of diagonal-sequence walking gaits in primates. *J. Zool., Lond*. 260: 423-429.

Lindsey, C. C. (1978). Form, function, and locomotory habits in fish. In Fish Physiology, Vol. 7. Locomotion (ed. W. S. Hoar and D. J. Randall), pp. 1-100. New York: Academic Press.

Lucas, K. N., J. Dabiri and G. V. Lauder. (2015). Application of PIV-based pressure measurements to the study of aquatic propulsion. APS Division of Fluid Dynamics (Fall), abstract #R38.001.

Peters, S. E. (1983). Postnatal development of gait behavior and functional allometry in the domestic cat (*Felis catus*). *J. Zool., Lond.* 199: 461-486.

Schindelin, J., I. Arganda-Carreras, E. Frise, V. Kaynig, M. Longair, T. Pietzsch, S. Preibisch, C. Rueden, S. Saalfeld, B. Schmid, et al. (2012). Fiji: an open-source platform for biological image analysis. *Nature Methods*. 9: 676-682.

Schneider, C. A., W. S. Rasband and K. W. Eliceiri. (2012). NIH Image to ImageJ: 25 years of image analysis. *Nature Methods*. 9: 671-675.

Sfakiotakis, M., D. M. Lane and J. B. C. Davies. (1999). Review of swimming modes for aquatic locomotion. *IEEE J. Ocean. Eng.* 24: 237-252.

Standen, E. M and G. V. Lauder. (2005). Dorsal and anal fin function in bluegill sunfish Lepomis macrochirus: three-dimensional kinematics during propulsion and maneuvering. *J. Exp. Biol.* 208: 2753-2763.

Sukhanov, V. B. (1974). General System of Symmetrical Locomotion of Terrestrial Vertebrates and Some Features of Movement of Lower Tetrapods. Washington, DC: Smithsonian Institution and National Science Foundation.

Tytell, E. D., E. M. Standen, and G. V. Lauder. (2008). Escaping Flatland: three-dimensional kinematics and hydrodynamics of median fins in fishes. *J. Exp. Biol.* 211: 187-195.

Webb, P. W. (1973). Kinematics of pectoral fin propulsion in *Cymatogaster aggregata. J. Exp. Biol.* 59: 697-710.

Webb, P. W. (1984) Body form, locomotion and foraging in aquatic vertebrates. *Amer. Zool.* 24: 107-120.

Page intentionally left blank

Chapter 4

Unsteady locomotion in fishes: do fish use alternative kinematic paths to the same higher-speed endpoint?

Kara L. Feilich, Valentina di Santo, George. V. Lauder

4.1 Summary

Unsteady swimming is an important and understudied aspect of fish behavior. For unsteady swimming to be more effectively studied, there need to be methods for parameterizing the range of unsteady kinematics used by fishes, to facilitate comparison among fishes and behaviors, and to associate kinematics with their performance outcomes. However, aside from the well-studied C-start escape response, we have little means of quantitatively describing unsteady movements—and in turn, little knowledge about inherent variation in kinematic strategies to produce accelerations. In this study, we use a suite of methods to parameterize the caudal fin kinematics of unsteady swimming by bass and trout during linear and burst accelerations, and to determine the potential for fishes to use multiple kinematics strategies to accelerate. Acceleration kinematics tended to vary with initial speed, with linear accelerations at lower speeds and burst accelerations at higher speeds. Linear accelerations were virtually indistinguishable from steady swimming in terms of caudal fin movement—indicating non-caudal fin thrust producing or drag minimizing mechanisms. Burst accelerations were characterized by a single distinct fin beat, typically with low period and high amplitude. Several of the methods tested provided quantitative means of comparing unsteady behaviors, especially if extended to include additional propulsors (i.e. pectoral and median fins). These methods provide an interesting perspective from which to study unsteady swimming and speed changes in fishes.

4.2 Background

Studies of fish swimming kinematics have, with good reason, chiefly focused on steady swimming biomechanics. Steady swimming can be used as a baseline for other hydrodynamic behaviors (Tytell, 2004), can be (relatively) easily elicited in a laboratory setting, and by virtue of its consistency, can be parameterized with minimal difficulty (Gray, 1933, Bainbridge, 1958, Webb, 1973, Eloy, 2012). Alternatively, studies of unsteady kinematic behaviors (with the exception of the well-studied C-start, which is relatively stereotypical across fishes (reviewed in Domenici and Blake, 1997) are scarce, and more difficult. Unsteady swimming has a number of important functions, including feeding, escaping (Domenici and Blake, 1997), and potentially energy savings (Weihs, 1974). Unsteady swimming may even be the dominant mode of locomotion for many fishes, as opposed to steady swimming (Webb, 1991, Mueller et al 2000). Though the importance of unsteady locomotor performance is recognized (Langerhans and Reznick, 2010), the transient nature and variability of unsteady behaviors makes it difficult to derive functionally meaningful descriptive kinematic parameters. Without a framework for consistently describing unsteady acceleratory behaviors, it is also difficult to study acceleratory kinematics in comparative contexts.

Acceleration performance—which is important as a means of feeding, energy savings and of escape, likely contributes to fitness, and thereby, is a subject of natural selection. Variation in acceleration performance raises the follow-up question of how fishes vary in the production of those accelerations. For instance, variation in acceleration performance may arise from underlying differences in kinematics; or there could be many-to-one mappings of kinematics on performance. Further study of acceleration kinematics may shed light on the flexibility of underlying motor control systems and inform the design of biomimetic propulsion. In addition,

having a means of parameterizing kinematics during these behaviors would facilitate, eventually, answering questions of how different traits (e.g. kinematics, morphology, physiology) can each individually affect performance. The major challenges to parameterizing acceleration stem from its inherent variability. Unlike steady swimming, it is inaccurate to ascribe a single average value in frequency and amplitude to any given sequence of fin beats, as these vary over the duration of the behavior. The time-course of fin beat variation is also of interest, as is the range of steady swimming speeds from which fishes initiate acceleration. Furthermore, acceleration behaviors can be "linear" in nature, where fish change velocity for a brief period before settling in to a steady higher speed (Tytell, 2004), or more dramatically unsteady as when fishes use a burst-and-coast strategy to swim at high speeds.

From existing studies of non-escape acceleration in fishes, tail tip kinematics seem to be an important driver of acceleration. Tytell (2004) found that tail tip velocity was a good predictor of acceleration performance. Muller and colleagues (2000) also noted that most burst-and-coast swimming bouts consisted of a single tail-flick—highlighting the potential need for a fin beat by fin beat analysis. Many other studies indicate "phases" of fast-starts (e.g. Webb, 1978, Tytell and Lauder, 2008), but how these phases correspond with other unsteady movements is unknown. A framework for comparing all of these behaviors would prove valuable in assessing context-specific kinematics and performance.

The goals of this study were (1) to develop a suite of methods to examine caudal fin kinematics during acceleratory locomotion in fishes, and (2) to demonstrate their utility for studying unsteady swimming by analyzing data from both largemouth bass and rainbow trout. Our main interest was to determine if there are kinematic signatures of different unsteady behaviors: i.e., is there more than one set of kinematics for producing a given acceleration? Can

and do fish use alternative kinematic paths to the same higher-speed endpoint (see Figure 4.1)? The methods presented here were adapted from procedures for parameterizing steady swimming behavior in terms of propulsive inputs (Feilich, 2017a), and by statistical methods for analyzing the degree of variation in cyclical signals.

4.3 Materials and Methods

4.3.1 *Animal care and maintenance*

Juvenile rainbow trout *Oncorhynchus mykiss* (n = 2; standard lengths = 9 cm, 8.5 cm), were obtained from the Blue Stream Hatchery (Barnstable, MA, USA), largemouth bass *Micropterus salmoides* (n = 1, standard length = 15 cm), were collected with seine nets in the Charles River (Cambridge, MA, USA). All fishes were transported to the Museum of Comparative Zoology Laboratories at Harvard University in a well-aerated, and temperature controlled tank. Once in the laboratory fishes were individually housed in 40-L tank at 16°C and under a 12 h:12 h light:dark photoperiod. Fishes were fed a diet of fresh earthworms three times per week, but were fasted for 24 h prior to each trial. All experiments and care procedures were performed under the approved Harvard University IACUC protocol (no. 20-03 to GVL).

4.3.2 *Swimming trials and behavior categorization*

Fishes were recorded while swimming steadily (prior to acceleration behavior) at varying speeds (1-6 body lengths per second (BL s^{-1})) in a flow tank with a total working section of 28×28×80 cm as previously described by Tytell and Lauder (2004), at a constant temperature (16 ± 0.5°C). Most trials were < 3 BL s^{-1}. We only recorded swimming sequences where fishes were

Figure 4.1. Schematic diagram with simulated data showing multiple kinematic pathways to accelerate to the same final speed, assuming caudal fin propulsion only. A. Relationship between steady swimming speed and caudal fin beat period. B. The relationship between steady swimming speed and caudal fin beat amplitude. C. A three-dimensional representation of a caudal steady swimming gait trajectory—the composite relationship resolved from A and B. Paths 1, 2, and 3, are a few of infinitely many different kinematic possibilities for accelerating between the two speeds highlighted in red. Path 1 represents a gradual kinematic transition where acceleration kinematics mirror the kinematics used during steady locomotion at the intermediate speeds. Path 2 represents acceleration by keeping period constant, jumping to a larger caudal fin beat amplitude to speed up, before decreasing amplitude slightly to settle in to the new steady swimming speed. Path 3 represents acceleration by keeping fin beat amplitude constant, jumping to a shorter fin beat period to accelerate, before increasing period slightly to settle into the new steady swimming speed. Data are simulated such that fin beat period has an inverse linear relationship with swimming speed, and amplitude has a sigmoidal relationship with speed. These hypothesized relationships are in keeping with the experimental observations that speed varies linearly with fin beat frequency (i.e. 1/period), and amplitude is mostly invariant with speed.

Figure 4.1 (Continued)

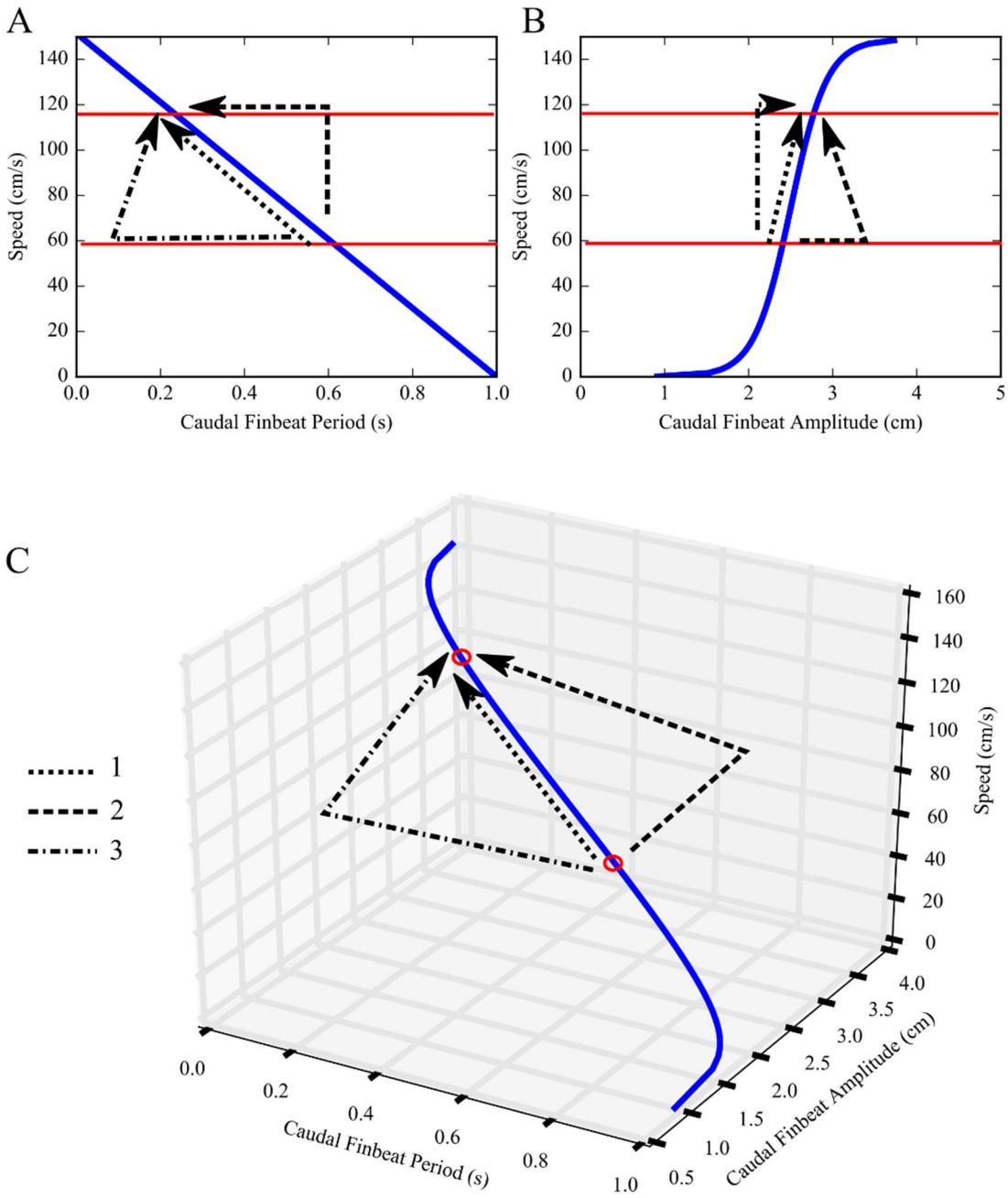

swimming in the center and away from all flow tank walls and flow-straighteners (at either end of the working section). Lateral and ventral views of steady swimming, burst and linear acceleration were recorded by two synchronized 1-megapixel high-speed video cameras (FASTCAM 1024 PCI; Photron USA, San Diego, CA, USA) at 1000 frames s^{-1}. The ventral view was recorded using a 45º mirror under the swim tunnel. Videos from the two cameras were calibrated and aligned to recreate the images in three-dimensional space using direct linear transformation in MATLAB (MathWorks, Natick, MA, USA) and using a calibration program developed by Hedrick (2008).

We recorded three different behaviors: steady swimming, burst-and-coast, and linear acceleration. Steady swimming was defined as the forward swimming of the fish at the speed that matched that of the incoming flow (i.e. fish maintained position in the tunnel). The burst-and-coast behavior was defined as having two forward swimming phases: during the first preparatory phase the fish beats its tail with increased amplitude and increases body angle with respect to the mean direction of forward travel. In the second phase the fish body assumes a stretched straight posture in a glide forward. We defined as linear accelerations those swimming sequences in which fish maintained a straight forward motion and increase in speed with respect to the incoming flow, while maintaining regular (i.e. periodic, uninterrupted) caudal fin beat kinematics. Note that this definition does not necessarily imply a constant rate of speed increase—only the continuous nature of caudal kinematics and forward advance in position relative to oncoming flow.

4.3.3 *Measurement of kinematics and fin beat parameters*

For each trial, the positions of the tip of the snout and the tip of the caudal fin were digitized using DLTv6 (Hedrick, 2008). For the tip of the snout, automatic tracking with the default parameters (Autotrack predictor: extended Kalman, Autotrack search area: 9, Autotrack threshold: 9) was sufficient for accurate tracking, as confirmed by manual assessment of the tracked position. In the few cases where the autotracking algorithm was inaccurate, frames were digitized manually within DLTv6. For the tail tip, autotracking was almost never sufficient, and the frames were all manually digitized. Data were saved from DLT in flat format, and all subsequent processing was done using custom written code in Python 3.4 (Python Software Foundation, http://www.python.org). The code used for processing, and all subsequently described analyses, takes advantage of several existing Python packages (Supp. Table 4.1), and can be found in a GitHub repository maintained by K. Feilich (Feilich, 2017b).

To permit the calculation of velocity and acceleration from the slightly noisy position data, position traces were smoothed using a 2nd order Savitzky-Golay filter with a window length corresponding to 121 ms. This procedure was found to smooth the data enough for differentiation without diminishing maxima and minima more than 2%. For each trial, net instantaneous velocity and acceleration of the swimming fish were calculated as the first- and second-derivative of the snout position data. A second smoothing with the same parameters was used in between the velocity and the acceleration differentiation.

To determine the period and amplitude for each fin beat in every trial, we isolated the y-axis position (yaw-axis) of the caudal fin tip. These position traces were detrended by fitting a 3rd order polynomial to the position data before using the peak-detection algorithm implemented in the open-source python package PeakUtils v.1.0.3 (L. Negri. available at https://bitbucket.org/lucashnegri/peakutils). Each peak was designated the start of a caudal fin

beat. However, this choice is arbitrary, so all analyses were also conducted using each trough as the start of a fin beat. The y-position data were multiplied by -1, and the peak finding process repeated to find the troughs in the data. Doing the analyses with peaks-first and with troughs-first allowed us to get a sense of the effect of fin beat cycle start choice on the relationships between measured fin beat parameters and performance. There was minimal difference between the peak-first and the trough-first fin beat analyses, so for the rest of this manuscript, we refer only to the peaks-first data. Troughs-first data are presented for comparison in the supplemental materials. Fin beat period was calculated as the time from the starting peak to the subsequent peak for each fin beat. Amplitude was calculated as the y-position distance between the starting peak, and the subsequent trough for each fin beat. Absolute instantaneous tail tip accelerations were calculated from these detrended data using the smoothing and differentiation procedure adopted for the calculation of body acceleration from the snout position.

In order to associate each fin beat with performance measures for further analyses, the maximum instantaneous velocity and acceleration during the duration of each fin beat was also recorded.

4.3.4 *Statistical analysis of kinematic parameters*

Multiple linear regression models were fit to the data to relate fin beat period and amplitude to the maximum instantaneous speed and acceleration for each fish, for a total of 3 models using statsmodels (v. 0.6.1, available at https://github.com/statsmodels/statsmodels) in Python 3.4. The data did not match the assumption of normality of residuals, so we conducted 2000 bootstrap analyses by resampling residuals to estimate 95% confidence intervals of the regression coefficients and their pseudo-p values using custom scripts to store the outputs of the

bootstrapped trials (Feilich, 2017b). Where interaction terms were found to be insignificant, a second model (with bootstrapping) was fitted without the interaction term.

4.3.5 *Sinusoidal regression as estimate of steadiness*

In order to compare the "steadiness" of the caudal kinematics in different behaviors, it was necessary to devise a means of measuring steadiness. One potential means of doing this is to compare the kinematics to a perfectly steady signal, such as a perfect sine wave, as the lateral movement of the tail tip during steady swimming is very nearly a sine wave (Videler and Wardle, 1978).

To assess the degree to which any given kinematic series matched "steadiness", first we needed an estimate of what completely steady would look like for that series. To do this, we used least squares optimization to estimate the three parameters of a sine wave: amplitude (A), frequency (*f*), phase (φ); and offset (C), to best fit the data using the following equation for optimization:

(4.1) $0 = A\sin(2\pi f t + \varphi) + C - y(t)$,

where *y(t)* is the detrended lateral tail tip position (as calculated for peak finding, see Section 4.3.3). Then, the Pearson's calculation coefficient (*r*) between the detrended position data and the best fit sine wave was calculated for each trial. This provided a crude but effective measure of steadiness, where trials with r = 1 are very well modeled by a sine wave (and presumably "steady", and are less steady with decreasing r—though this is an unpredictable relationship at low r. When r < 0.5 or so, that trial was quite removed from a sine wave function. This calculation, however, is entirely dependent on how well-fit the sine wave approximation is. Least-squares optimization can be sensitive to initial conditions in cases where there are multiple

local minima (Bock *et al.* 2007), which could result in a spuriously low correlation coefficient. To avoid this possibility, initial guesses for the sine wave amplitude and frequency (A_0 and f_0, respectively) were obtained empirically from the data:

(4.2) $f_0 = 1/\bar{\tau}$

(4.3) $A_0 = \bar{A}$,

where τ is fin beat period and A is tail beat amplitude as measured above. For trials with greater than four available fin beats, the fin beats with the lowest and highest values of period and amplitude were excluded from the calculation of the initial conditions – this always increased the fit in trials with more heterogeneous fin beats, and did not change the best fit parameters in other trials. For trials with less than four available fin beats, all fin beats were used to calculate these initial values. All of these analyses were done using least squares optimization as implemented in SciPy (v. 0.18.1; Jones *et al.,* 2001-) within custom scripts (Feilich, 2017b).

4.3.6 *Cross-correlation of Fourier transforms to compare across and within behaviors*

In addition to estimating overall steadiness of the three behaviors studied, we wanted to determine if the behaviors might have specific kinematic signatures. Examining the shapes of the Fourier transform of the detrended tail beat data was one way to test this hypothesis. If Fourier transforms of trials of a given behavior exhibited high maximum cross correlations, but trials of different behaviors exhibited low cross-correlations, that would indicate specific characteristics of the shape of the frequency distribution were specific to each behavior. Shape of the Fourier transform contains information about the number of frequencies found in a signal, so one might expect steady trials to have single narrow peaks, but burst accelerations to have broad peaks.

Because Fourier transforms were to be used in pairwise cross-correlations, the detrended tail tip position data for the shorter-duration trial in each pairwise trial comparison was extended on either end with the mean fin tip position, to equal the length of the longer trial, before calculating Fourier transforms. Fast Fourier transforms of these data were calculated using NumPy v. 1.11.3 (Ascher *et al.,* 1999), and the first portion of the transformed data, corresponding to the 0-1 Hz frequency domain was discarded. This was a necessary pre-processing step, as each trace had its largest peak at 0 Hz (representing non-periodic trends in the data; see Smith, 2003), and without removing this part of the Fourier transformed data, any cross-correlation would be dominated by that peak in the trace, instead of those parts of the transform resulting from fin beat motion. Cross-correlations were conducted on these modified transforms of each pair of trials using SciPy.signal (Jones *et al.,* 2001-, Feilich, 2017b). The maximum cross-correlation is reported for each comparison.

4.4 Results

4.4.1 *General observations of acceleratory kinematics*

Among the three behaviors studied, there was little difference in the kinematics of steady swimming versus an acceleration, and even the maximum instantaneous accelerations across the two behaviors were similar (Figure 4.2, Figure 4.3). The highest maximum accelerations were only achieved during bursts, which had more variable tail beat kinematics across and within trials (Figures 4.2-4.3). Fin beats during linear acceleration varied little from their counterparts during steady swimming at the same initial speed (Figure 4.2-4.3). Qualitatively, the three different behaviors appeared kinematically consistent between Bass 1, Trout 1 and Trout 2.

Figure 4.2 Observed caudal fin beat kinematics for swimming behaviors initially coded as steady swimming, linear acceleration, and burst acceleration. Left Column: Largemouth Bass (n=1, SL = 15 cm, n_trials = 23), Right Column: Rainbow Trout (n = 2; SL = 9 cm, 8.5 cm, 8 cm; n_trials = 21). Top: All fin beats against maximum instantaneous acceleration. Middle: Fin beats with maximum instantaneous accelerations < $5x10^{-4}$ cm/s^2, to show variation. Bottom: Fin beats against maximum instantaneous velocity. (Circles: steady swimming trials, +: linear acceleration trials, Star: burst acceleration trials. Points are colored by initial speed of trial.)

Figure 4.2 (Continued)

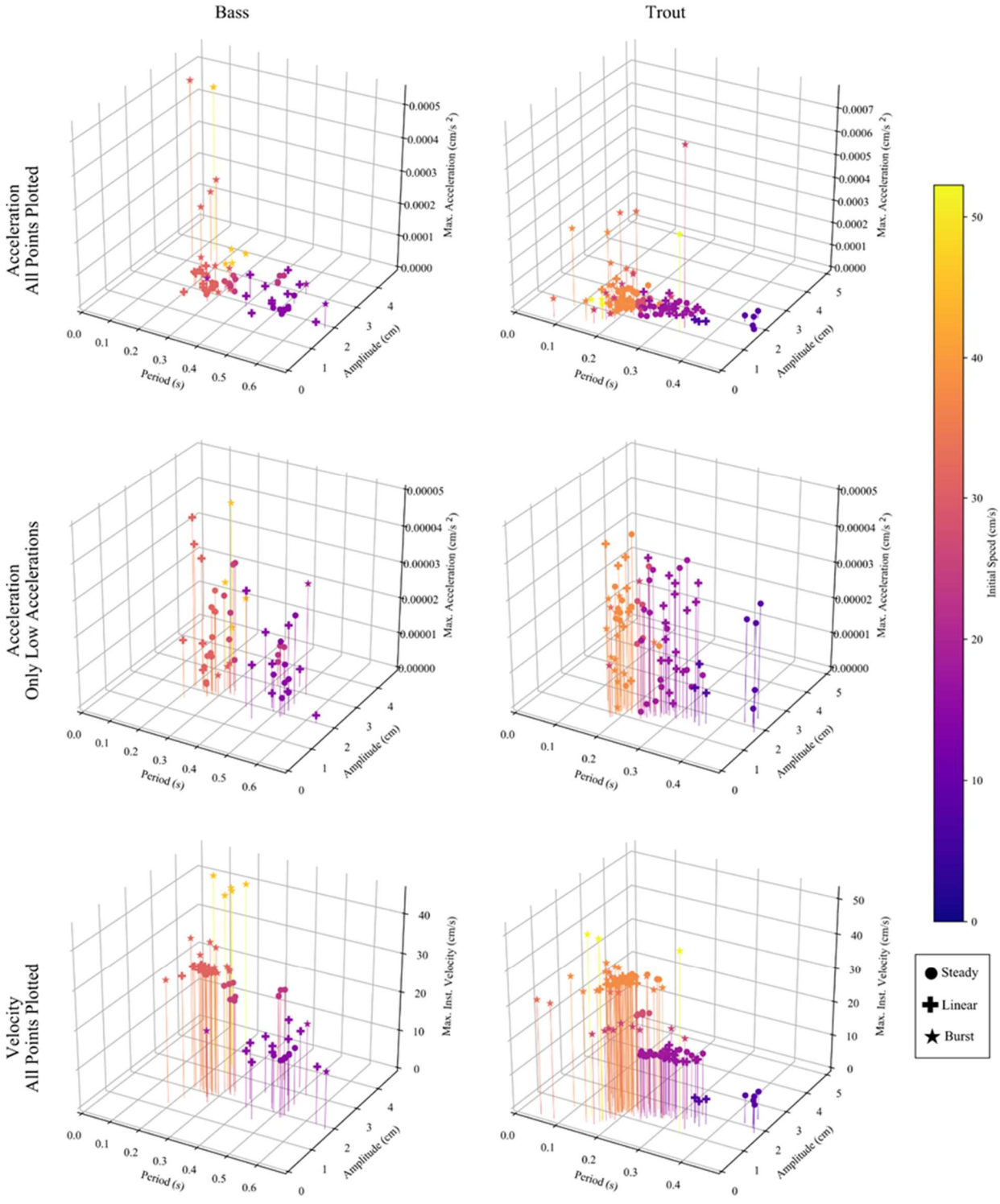

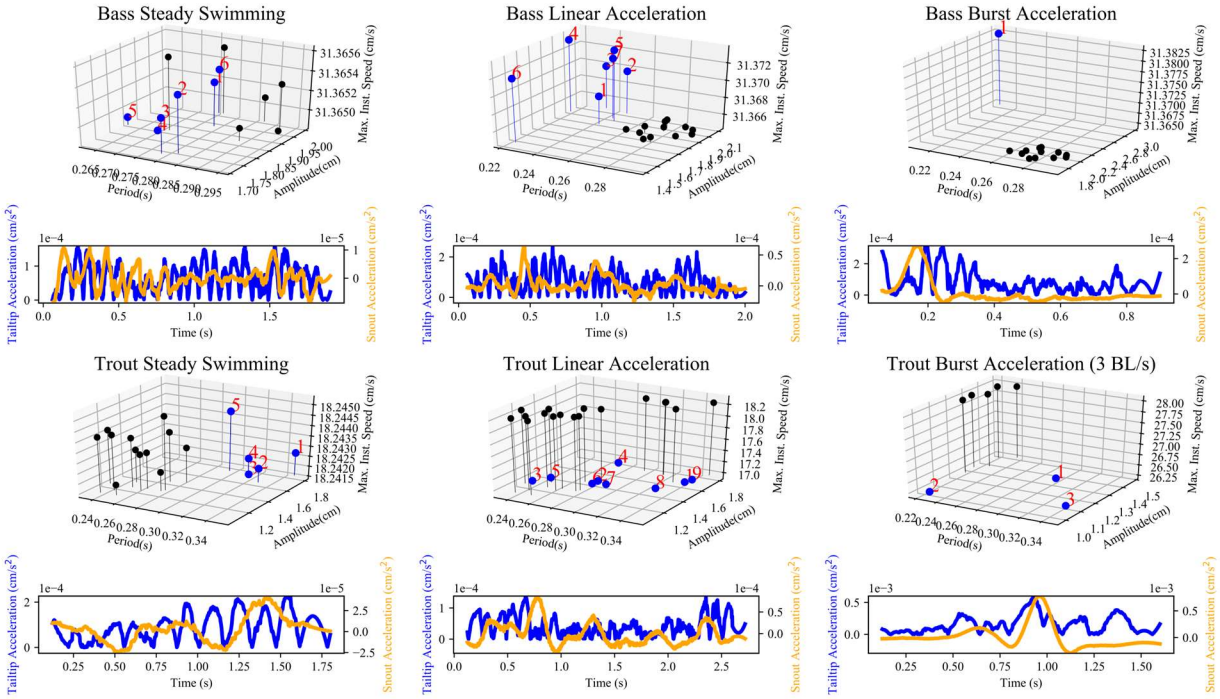

Figure 4.3. Fin beat parameters and body and tail tip accelerations during three swimming behaviors with initial speeds of 2 BL s^{-1}, compared to those during steady swimming at similar speeds. Three-dimensional plots show fin beat parameters as in Figure 2 for a single trial of the given behavior (blue), compared to all steady swimming fin beats at the same initial speed (black). Numbers in red give the temporal order of fin beats detected in the trial. Below each fin beat plot are the absolute value of the tail tip acceleration for the focal trial (blue, left axis) plotted against the forward acceleration of the tip of the snout (orange, right axis). Trials depicted are the same as in Figures 4.4 and 4.5.

4.4.2 *Period and amplitude variation with maximum instantaneous speed and acceleration*

There was a negative relationship between period and maximum instantaneous speed—in keeping with the well-established relationship between frequency and steady swimming speed (Figure 4.2). Multiple linear regression analyses indicated that, for two of three fishes studied (one of each species) there was no significant interaction effect between period and amplitude on speed, and the effect of period on maximum instantaneous speed agreed with the prediction of increasing speed with decreasing period (Bass: $F = 91.81$ with $p_{boot} < 0.001$, β_τ CI (-68.3, -50.3) with $p_{boot} < 0.001$, adj. $R^2 = 0.728$; Trout 1: $F = 67.48$ with $p_{boot} = 0.003$, β_τ CI (-125.7, -63.4) with $p_{boot} < 0.001$, adj. $R^2 = 0.627$). Only for the bass data did amplitude have a small but significant relationship with maximum instantaneous speed, where higher amplitudes were associated with higher speeds (Bass: β_A CI (0.9, 4.9) with $p_{boot} = 0.004$; Trout 1: β_A CI (-37.8, 12.7) with $p_{boot} = 0.035$). For Trout 2, there was a significant interaction between period and amplitude, and only amplitude had a significant effect after accounting for the interaction term (Trout 2: $F = 40.70$ with $p_{boot} = 0.009$, $\beta_{\tau:A}$ CI (-108.30, -25.81) with $p_{boot} = 0.011$, β_A CI (6.46, 21.48) with $p_{boot} = 0.002$, adj. $R^2 = 0.709$). Full regression model outputs are reported in Supp. Tables S4.2-S4.4.

In general, the relationships between fin beat kinematics and maximum instantaneous acceleration were poorly modeled by linear regression. Multiple linear regressions of period and amplitude on maximum instantaneous accelerations only fit the data well for the Bass (Bass: $F = 32.77$ with $p_{boot} = 0.009$, $\beta_{\tau:A}$ CI ($-94.0*10^{-5}$, $-52.6*10^{-5}$) with $p_{boot} < 0.001$, adj. $R^2 = 0.728$; Trout1: $F = 5.61$ with $p_{boot} = 0.100$, adj. $R^2 = 0.149$; Trout2: $F = 2.329$ with $p_{boot} = 0.261$, adj. $R^2 = 0.075$). In this case, there was a significant interaction term between period an amplitude, making the modeled relationship between kinematics and acceleration difficult to interpret.

However, for the bass, both period and amplitude individually also had significant positive coefficients (Bass: β_τ CI ($85.4*10^{-5}$, $178.6*10^{-5}$) with $p_{boot} < 0.001$, β_A CI ($22.5*10^{-5}$, $36.5*10^{-5}$) with $p_{boot} < 0.001$). Full regression model outputs are reported in Supp. Tables S4.5-S4.7.

4.4.3 *Correlation with best-fit sine waves as indicator of steadiness*

The three swimming behaviors (steady swimming, linear acceleration, burst acceleration) were consistently different in their degree of steadiness as indicated by correlation with their best fit sine waves (Figure 4.4; Table 4.1). The correlation between steady swimming tail tip kinematics and their associated best-fit sine waves were consistently high with range = [0.83, 0.99], suggesting that steady swimming is very steady from the perspective of caudal kinematics (Table 4.1). Linear acceleration tail tip kinematics also were highly correlated with their best fit sine waves, with range = [0.69,0.97] (Table 4.1). Burst accelerations were typically only poorly correlated with their best fit sine waves, with correlation coefficients ranging between [0.26, 0.82], though the correspondence between the tail tip motion and the sine wave is probably unclear at correlations $r < 0.7$. This suggested that burst accelerations are characterized by instability—meaning, by inconsistent caudal kinematics.

4.4.4 *Fourier transform shape is not a good indicator of behavior*

Fourier transforms of tail tip kinematics did little to distinguish between acceleratory and steady swimming behaviors (Figures 4.5-4.7). Burst behaviors tended to show higher correlations with themselves than other behaviors; but for bass, maximum cross-correlation was a better indicator of initial speed than of behavior (see Figure 4.6A compared to 4.6B). This did

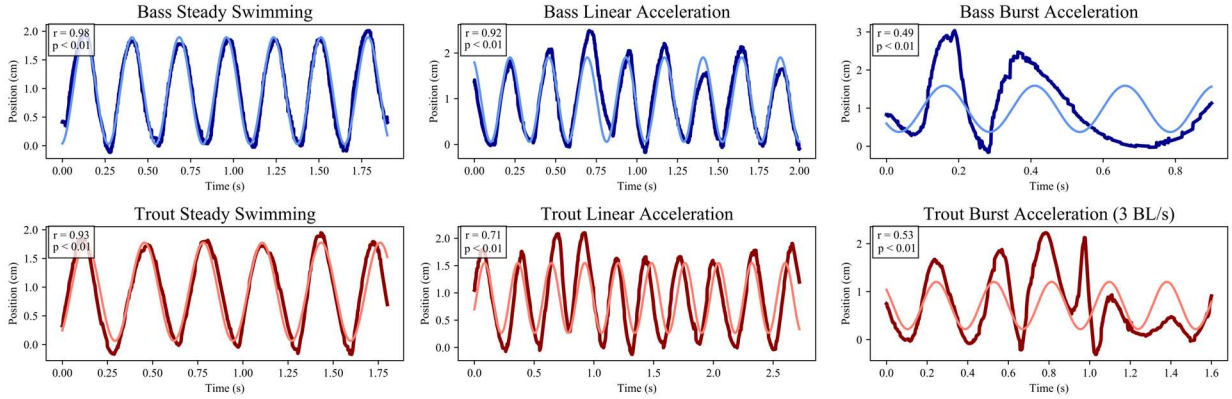

Figure 4.4. Representative traces of detrended tail tip motion during three swimming behaviors with initial speeds of 2 BL s^{-1}, and the best fit sine waves for those traces.

Blue: Largemouth Bass (SL = 15 cm), Red: Rainbow Trout (mean SL = 8.75 cm). The dark curve is the detrended raw data for that trial and the light curve is the sine wave fitted to that trial using least squares optimization. The correlation coefficient between the detrended raw position data and the best fit sine wave is shown in the top left corner of each plot, with its associated p-value. The burst acceleration trace for trout is from a trial at an initial speed of 3 BL s^{-1}, as we were unable to elicit burst accelerations below this speed. Trials depicted are the same as in Figures 4.3 and 4.5.

Table 4.1. Pearson's correlation coefficients and associated p-values for each trial when correlated with its best fit sine wave, grouped by speed and behavior.

Bass								
Steady Swimming			Linear Acceleration			Burst Acceleration		
Trial	Initial Speed (cm/s)	r	Trial	Initial Speed (cm/s)	r	Trial	Initial Speed (cm/s)	r
Bass1S04	14.7	0.91	Bass1S19	14.7	0.94	Bass1S05	14.7	-
Bass1S16	14.7	0.93	Bass1S20	14.7	0.88	Bass1S15	14.7	0.82
Bass1S17	14.7	0.98	Bass1S14	14.7	0.85	Bass1S07	18.5	0.60
Bass1S23	23.5	0.98	Bass1S18	14.7	0.69	Bass1S03	31.4	0.49
Bass1S01	24.6	0.96	Bass1S08	31.4	0.92	Bass1S06	31.4	0.70
Bass1S02	27.1	0.99	Bass1S09	31.4	0.77	Bass1S10	31.4	0.32
Bass1S11	31.4	0.98				Bass1S13	31.4	0.59
Bass1S12	31.4	0.99				Bass1S21	31.5	0.65
						Bass1S22	45.6	0.74
Trout								
Steady Swimming			Linear Acceleration			Burst Acceleration		
Trial	Initial Speed (cm/s)	r	Trial	Initial Speed (cm/s)	r	Trial	Initial Speed (cm/s)	r
BTrout1S09	8.2	0.99	BTrout2S14	7.5	0.97	BTrout2S03	26.3	0.53
BTrout1S04	8.37	0.97	BTrout2S02	17.0	0.84	BTrout2S04	26.3	0.33
BTrout1S01	18.2	0.91	BTrout2S01	17.0	0.71	BTrout2S05	26.3	-
BTrout1S02	18.2	0.97	BTrout1S08	37.9	0.78	BTrout2S07	33.5	0.37
BTrout1S03	18.2	0.93				BTrout2S08	33.5	0.49
BTrout1S05	28.0	0.97				BTrout2S09	35.7	0.49
BTrout1S06	37.9	0.84				BTrout1S10	37.9	0.80
BTrout1S07	37.9	0.83				BTrout2S10	38.0	0.50
						BTrout1S11	52.2	0.26

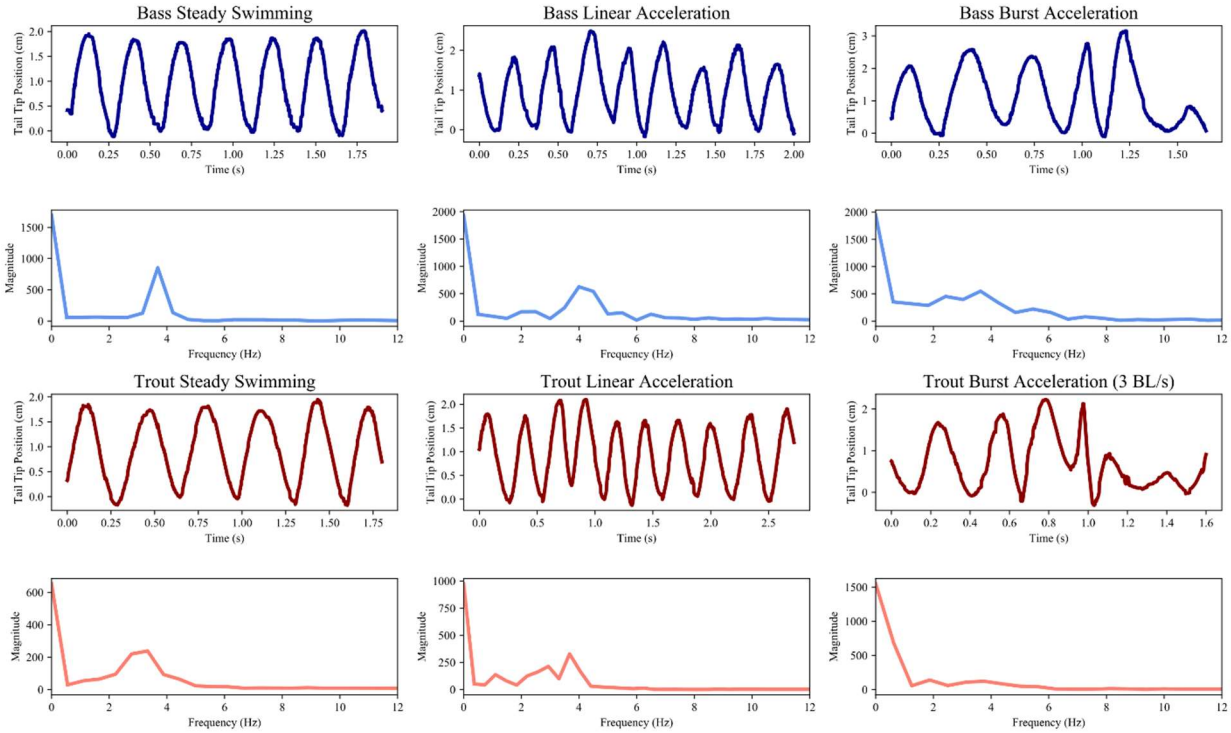

Figure 4.5. Representative traces of detrended tail tip motion during three swimming behaviors with initial speeds of 2 BL s^{-1}, and the fast Fourier transforms (FFT) of those traces. Blue: Largemouth Bass (SL = 15 cm), Red: Rainbow Trout (mean SL = 8.75 cm). Top row of each species shows tail tip position in the axis perpendicular to the direction of swimming, with background trend removed. Bottom row for each species shows an FFT of the tail tip trace immediately above. The burst acceleration trace for trout is from a trial at a speed of 3 BL s^{-1}, as we were unable to elicit burst accelerations below this speed. Trials depicted are the same as in Figures 4.3 and 4.4.

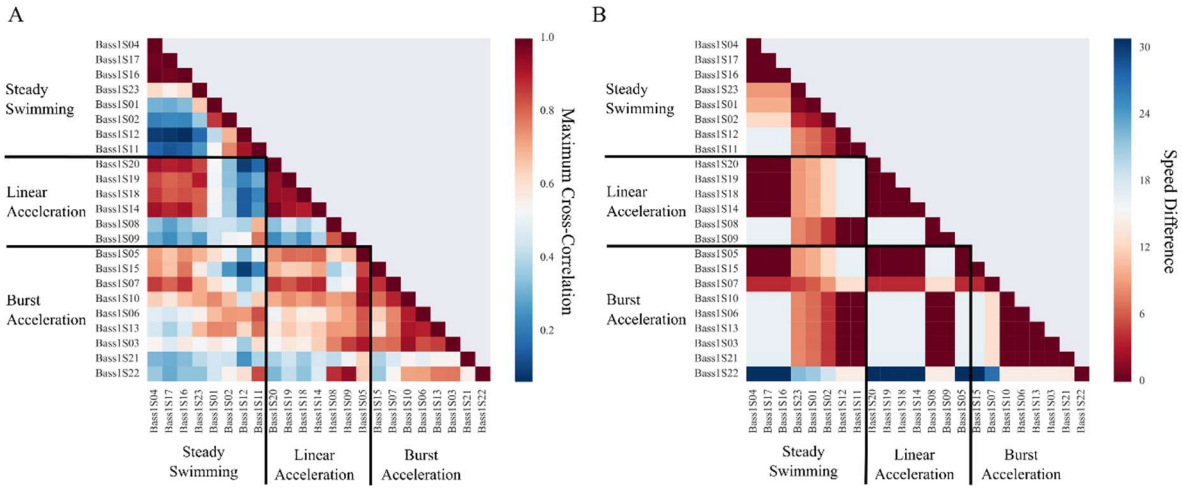

Figure 4.6. Heat-map showing maximum normalized pairwise cross-correlations between the Fourier transforms of detrended tail beat motions for all Bass trials, and pairwise initial speed differences between trials. For each pairwise comparison, the detrended raw tail tip position data (as shown in Figure 4.3) for the shorter length of the two trials was padded on either end with its mean value to equal the length of the longer trial before Fourier transform convolution. This made the lengths of the two Fourier transforms suitable for the purposes of cross-correlation. A: Maximum cross-correlations of FFTs. B: Pairwise speed differences between trials. Similar correlation values in individual cells or groups of cells between A and B indicates that swimming speed is a major factor driving the shape of the fin beat frequency distribution.

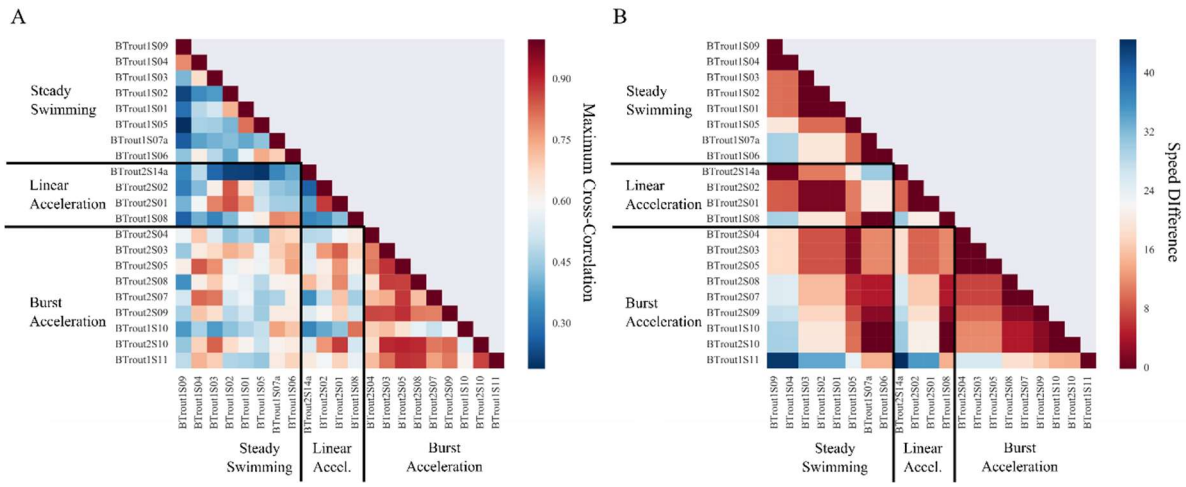

Figure 4.7. Heat-map showing maximum normalized pairwise cross-correlations between the Fourier transforms of detrended tail beat motions for all Trout 1 and 2 trials and pairwise initial speed differences between trials. For each pairwise comparison, the detrended raw tail tip position data (as shown in Figure 4.3) for the shorter length of the two trials was padded on either end with its mean value to equal the length of the longer trial before Fourier transform convolution. This made the lengths of the two Fourier transforms suitable for the purposes of cross-correlation. A: Maximum cross-correlations of FFTs. B: Pairwise speed differences between trials. Similar correlation values in individual cells or groups of cells between A and B indicates that swimming speed is a major factor driving the shape of the fin beat frequency distribution.

not appear to be the case for the trout studied, however, and it was unclear what may be driving any similarity between trials in that dataset other than "burst" or "non-burst" categorization.

4.5 Discussion

The goal of this study was to evaluate potential methods for the description and comparison of caudal-fin driven acceleration behaviors, and to assess their utility in analyzing kinematic trajectories (Figure 4.1). While none of the methods used were sufficient in and of themselves to quantitatively characterize the kinematic differences among these diverse behaviors, some may prove useful for thinking about unsteady movements more broadly, while others may provide insight into the different means by which fishes accelerate on a routine basis. Specifically, the approach used here indicated that fish probably are able to use alternative kinematic acceleration strategies to reach the same high speed endpoint—but, given the strong relationship between initial speed and kinematics—that they might not actually do so.

Multiple linear regression revealed that, while swimming speed is governed chiefly by fin beat frequency/period, instantaneous acceleration has a complicated non-linear relationship with caudal fin beat period and amplitude (Supplemental Tables S4.2-S4.7). Even the relationship between tail tip acceleration and body acceleration is not clear (Figure 4.3), likely due to the confounding influence of fin extension and body curvature. Generally higher fin tip accelerations were associated with higher instantaneous body accelerations, with the highest fin tip accelerations observed during bursts, but the temporal relationship between peak tail tip acceleration and peak body acceleration was unclear (Figure 4.3). These combined results suggest that analysis of the caudal fin tip alone is not sufficient for comparing acceleration

kinematics – which is not surprising, given the multiple propulsive options available to a fish to generate an acceleration.

Despite the limitations of the approaches considered here, this approach indicates that not all aspects acceleration kinematics need to deviate much from steady swimming. Caudal fin beat kinematics for linear accelerations were no different than those for steady swimming at the same initial speeds. Neither did linear accelerations differ much from steady swimming in their degree of steadiness—virtually all of them were very well modeled by a sine wave function (Table 4.1). This suggests that something other than caudal fin beat kinematics are facilitating linear accelerations. In other words, caudal kinematics are not the chief determinants of acceleration in linear acceleration behaviors, some other factor must be driving the change in acceleration. Linear acceleration may be produced using steady kinematics if there is a concurrent reduction in drag, perhaps by retracting the median fins. If so, this runs counter to the idea that special kinematics (markedly different from steady swimming) are needed to produce an acceleration. Altered surface area of median and paired fins (dorsal, anal, pelvic, and pectoral) may well also play a role in acceleration behavior (by altering area to reduce drag, or by increasing posterior surface area so that similar amplitudes of body motion generate increased thrust), although to date only extremely limited data are available on non-caudal fin function during acceleration behaviors.

Burst accelerations appear to be unique when compared to linear accelerations and steady swimming. As noted by Müller et al. (2000), burst accelerations typically occurred over a single fin beat cycle. This single propulsive fin beat usually differs from the surrounding fin beats—but the manner of this difference varies; it is usually shorter in period, and may be higher in amplitude as well (Figures 4.2 and 4.4). Variance among fin beats also appears to be higher in

burst accelerations, and is corroborated by low values for the sinusoidal correlations of these trials (Table 4.1). In addition, burst accelerations could only be elicited at relatively high initial speeds, 2 BL s^{-1} or more in the bass, and only 3 BL s^{-1} or more in the trout. It is possible that underlying muscle physiology drives this pattern of occurrence, as well as the fin kinematics for the different acceleratory behaviors (Wardle, 1975). Specifically, linear accelerations and steady swimming are most likely driven by slow oxidative muscle, but the single burst fin beat (and its associated short period and high acceleration) may only be produced by fast glycolytic muscle recruitment (Jayne and Lauder, 1994). That the occurrence of burst accelerations was restricted to high initial speeds suggests that fast glycolytic muscle recruitment may be necessary to overcome the high drag forces experienced at high speeds, even to produce similar net accelerations.

In answer to the question posed in the title of this study: "do fish use alternative kinematic paths to the same higher-speed endpoint?", these data suggest that no, in the restricted case studied here, body-caudal fin swimming fishes do not use more than one kinematic strategy for a given initial speed. Fishes appeared to be constrained to using specific acceleration kinematics depending upon the initial speed. At low initial speeds, (< ~3 BL s^{-1}), the fishes studied here used linear accelerations, and we were incapable of eliciting burst behavior. At higher initial speeds, only burst accelerations were used, which may indicate the necessity of recruiting fast glycolytic muscle fibers to produce thrust at these speeds. It is unclear why burst accelerations are not used at low speeds, or why fast glycolytic muscle does not seem to be recruited during linear accelerations. Given the restricted occurrence of burst accelerations at only high speeds, it seems that fish preferentially use slow oxidative muscle to accelerate when

fast glycolytic muscle is not required. This may reflect an underlying energetic savings, or even a fundamental aspect of motor control.

An alternative question to that posed by the title is not whether fishes "do" use alternative kinematics, but whether or not they "can" use alternative kinematics to accelerate. It is certainly possible for fishes to be physiologically capable of burst accelerations at low initial speeds, and that they preferentially do not do so. In addition, one can imagine alternative kinematics that employ other fins and body movements in addition to the caudal fin, permitting a fish to use steady-swimming caudal fin kinematics, while increasing thrust with the other propulsors. Hypothetically, with comprehensive data on fin use across all fins over a range of initial speeds and behaviors, one could discern the extent to which a fish's kinematic repertoire is constrained.

Ultimately, these results suggest that fish may be able to accelerate using different combinations of kinematic parameters, and that a given end point speed may be achieved in more than one way as hypothesized schematically in Figure 4.1, but that these fish do not appear to use multiple kinematic strategies at a given initial speed within the context of caudal fin use. This suggestion is likely to be further strengthened by future studies that can simultaneously quantify the amplitude and frequency of motion for each of the median and paired fins simultaneously, creating a multidimensional gait space through which fish kinematics track (Feilich, 2017a). The approach documented here also indicates future areas of research and suggests other possible methods for categorizing unsteady movement. The successful approach of fitting a sine function as a "null model" of a cyclical motion may be modified for use with other propulsors, provided one can find an appropriate base function. With additional sampling for higher speed resolution, it may be possible to resolve distinct kinematic strategies that provide flexibility for modulating speed. Coupled with studies of muscle fiber recruitment, this may also reveal why (or if) fast

glycolytic fiber is restricted to escape and high-initial speed acceleratory behaviors. We feel this is an interesting perspective from which to study unsteady swimming and speed changes in fishes, and that further study will reveal the extent of kinematic flexibility across fishes' locomotor repertoire.

4.6 References

Ascher, D., P. F. Dubois, K. Hinsen, J. Hugunin and T. Oliphant. (1999). Numerical Python. Technical Report UCRL-MA-128569. Lawrence Livermore National Laboratory.

Bainbridge, R. (1958). The speed of swimming of fish as related to size and to the frequency and amplitude of the tail beat. *J. Exp. Biol.* 35: 109-133.

Bock, H. G., E. Kostina, and J. P. Schlöder. (2007). Numerical methods for parameter estimation in nonlinear differential algebraic equations. *GAMM-Mitt.* 30: 376-408.

Domenici, P. and R. W. Blake. (1997). The kinematics and performance of fish fast start swimming. *J. Exp. Biol.* 200: 1165-1178.

Eloy, C. (2012). Optimal Strouhal number for swimming animals. *J. Fluids. Struct.* 30: 205-218.

Feilich, K. L. (2017a). Swimming with multiple propulsors: measurement and comparison of swimming gaits in three species of neotropical cichlids. In revision.

Feilich, K. L. (2017b). Fish Track Processing. GitHub repository: https://github.com/kfeilich/FishTrackProcessing

Hedrick, T. L. (2008). Software techniques for two- and three-dimensional kinematic measurements of biological and biomimetic systems. *Bioinsp. Biomim.* 3: 034001.

Jayne, B. C. and G. V. Lauder. (1994). How swimming fish use slow and fast muscle fibers: implications for models of vertebrate muscle recruitment. *J. Comp. Physiol. A*. 175: 123-131.

Jones, E., E. Oliphant, P. Peterson *et al.* (2001-). SciPy: Open Source Scientific Tools for Python: http://www.scipy.org/

Langerhans, R. B. and D. N. Reznick. (2010). Ecology and evolution of swimming performance in fishes: predicting evolution with biomechanics. In Fish Locomotion: an Eco-Ethological Perspective. (eds. P. Domenici and B. G. Kapoor). Enfield, NH: Science Publishers. pp. 484-512.

Müller, U. K., Stamhuis, E. J. and J. J. Videler. (2000). Hydrodynamics of unsteady fish swimming and the effects of body size: comparing the flow fields of fish larvae and adults. *J. Exp. Biol.* 203: 193-206.

Smith, S. W. (2003). "Chapter 8: The Discrete Fourier Transform." Digital Signal Processing: A Practical Guide for Engineers and Scientists. Boston, MA: Newnes. pp. 141-168.

Tytell, E. D. (2004). Kinematics and hydrodynamics of linear acceleration in eels, *Anguilla rostrata*. *Proc. R. Soc. B.* 271: 2535-2540.

Tytell, E. D. and G. V. Lauder (2008). Hydrodynamics of the escape response in bluegill sunfish, *Lepomis macrochirus*. *J. Exp. Biol.* 211, 3359-3369.

Videler, J. J. and C. S. Wardle. (1978). New kinematic data from high speed cine film recordings of swimming cod (*Gadus morhua*). *Neth. J. Zool*. 28: 465-484.

Wardle, C. S. (1975). Limits of fish swimming speed. *Nature.* 255: 725-727.

Webb, P. W. (1973). Kinematics of pectoral fin propulsion in *Cymatogaster aggregata*. *J. Exp. Biol*. 59: 697-710.

Webb, P. W. (1978). Fast-start performance and body form in seven species of teleost fish. *J. Exp. Biol.* 74: 211-226.

Webb, P. W. (1991). Composition and mechanics of routine swimming of Rainbow Trout, *Oncorhynchus mykiss*. *Can. J. Fish. Aquat. Sci*. 48: 583-590.

Weihs, D. (1974). Energetic advantages of burst swimming of fish. *J. Theor. Biol.* 48: 215-229.

Appendix to Chapter 2

Supplemental Table S2.1. Specimens used, clade assignments for graphing, including referenced trees used to determine clade assignment, and the data blocks in which each specimen was included. Inclusion in phylogenetic analyses is indicated by the trees on which the genus of the specimen is included. Clade reference is coded as follows: 1: Friedman et al 2013, 2: McMahan et al 2013, 3: Moran et al 1994, 4: Joyce et al 2011, 5: Salzburger et al 2005, 6: Day et al 2008, 7: Klett and Meyer 2002, 8: Allender et al 2003, 9: Schwarzer et al 2009, 10: Clabaut et al 2005, 11: Smith et al 2008, 12: Schwarzer et al 2014, 13: Seehausen et al 2003. All species without a listed clade reference were assigned by locality to the Haplochromines, and therefore to clade 10.

Table S2.1 (Continued)

Species	Catalog No.	Clade	CladeRef	Body	Caudal	Dorsal	Anal	Ftree	Mtree
Acarichthys heckelii	MCZ90937	Geophagini	2,11	X	X	X	X		X
Acaronia nassa	MCZ34140	Cichlasomatini	2,11	X	X	X	X		X
Aequidens tetramerus	MCZ15953	Cichlasomatini	1,2,11	X		X	X	X	X
Amphilophus citrinellus	MCZ15412	Heroini	2,11	X	X	X	X		X
Apistogramma steindachneri	MCZ57339	Geophagini	2,11	X	X	X	X		X
Apistogrammoides pucallpaensis	MCZ51736	Geophagini	2,11	X	X	X	X		X
Aristochromis christyi	MCZ49522	10	3	X	X		X		
Astatoreochromis alluaudi	MCZ100525	10	2,5,6,10	X	X	X	X		X
Astatotilapia elegans	MCZ148145	10	1,3,4,5	X	X	X	X	X	
Astronotus ocellatus	MCZ57046	Astronotini	1,2,11	X	X	X	X	X	X
Aulonocara rostratum	MCZ131956	10	3,5	X		X	X		
Aulonocranus dewindti	MCZ49256	8	1,6,10	X	X	X	X	X	
Australoheros sp.	MCZ15404	Heroini	2,11	X	X	X	X		X
Bathybates fasciatus	MCZ98421	5	1,6,10	X	X	X	X	X	
Benitochromis cf. batesii	MCZ48132	2	1,12	X	X	X	X	X	

Table S2.1. (Continued)

Species	Catalog No.	Clade	CladeRef	Body	Caudal	Dorsal	Anal	Ftree	Mtree
Benthochromis tricoti	MCZ50834	7	1,6	X	X	X		X	
Biotodoma cupido	MCZ15628	Geophagini	2,11	X	X	X	X		X
Biotoecus sp.	MCZ16010	Geophagini	1,2,11	X	X	X		X	X
Boulengerochromis microlepis	MCZ32557	5	1,6	X	X	X	X	X	
Buccochromis lepturus	MCZ48900	10	3	X	X	X	X		
Bujurquina sp.	MCZ52157	Cichlasomatini	2,11	X	X	X	X		X
Callochromis pleurospilus	MCZ50826	8	6	X	X	X	X		
Caprichromis orthognathus	MCZ49461	10	3	X	X	X	X		
Caquetaia myersi	MCZ49322	Heroini	1,2,11	X	X	X	X	X	X
Cardiopharynx schoutedeni	MCZ50827	8	1,6	X	X	X	X	X	
Chaetobranchopsis orbicularis	MCZ15839	Chaetobranchini	2,11	X	X	X	X		X
Chaetobranchus semifasciatus	MCZ15704	Chaetobranchini	2,11	X	X	X	X		X

Table S2.1. (Continued)

Species	Catalog No.	Clade	CladeRef	Body	Caudal	Dorsal	Anal	Ftree	Mtree
Chalinochromis brichardi	MCZ49219	6	2,6,11	X	X	X	X		X
Champsochromis caeruleus	MCZ49533	10	3	X	X	X	X		
Chilotilapia rhoadesii	MCZ131953	10	1,3	X	X	X	X	X	
Chromidotilapia guntheri	MCZ48601	2	7,12	X	X	X	X		
Cichla monoculus	MCZ15276	Cichlini	1,2,11	X	X		X	X	X
Cichlasoma urophthalmus	MCZ59665	Heroini	1,2,	X	X	X	X	X	X
Copadichromis quadrimaculatus	MCZ49518	10	3,4,5	X	X	X	X		
Corematodus taeniatus	MCZ131702	10		X	X	X	X		
Crenicichla johanna	MCZ15020	Geophagini	1,2,11	X	X	X	X	X	X
Cryptoheros cutteri	MCZ88630	Heroini	1	X	X	X	X	X	
Ctenochromis horei	MCZ49278	10	5,6,10	X	X	X	X		
Ctenopharynx intermedius	MCZ49497	10		X	X	X	X		
Cunningtonia longiventralis	MCZ49243	10	6,10	X	X	X	X		
Cyathochromis obliquidens	MCZ49440	10	3	X	X	X	X		

Table S2.1. (Continued)

Species	Catalog No.	Clade	CladeRef	Body	Caudal	Dorsal	Anal	Ftree	Mtree
Cyathopharynx furcifer	MCZ50828	8	6,10	X	X	X	X		
Cyphotilapia frontosa	MCZ50837	7	1,5,6,10	X	X	X		X	
Cyrtocara moorii	MCZ96429	10	1,3,5	X	X	X	X	X	
Dicrossus maculatus	MCZ14855	Geophagini	1,2,11	X	X	X	X	X	X
Dimidiochromis comprecisseps	MCZ49499	10	3,4	X	X	X	X		
Diplotaxodon argenteus	MCZ135962	10	3,4,5	X		X	X		
Docimodus johnstoni	MCZ49541	10	3	X	X	X	X		
Ectodus descampsii	MCZ32618	8	5,6,10	X	X	X	X		
Eretmodus cyanostictus	MCZ50700	9	1,5,6,10	X	X	X	X	X	
Etroplus suratensis	MCZ4306	Etroplinae	1,2,11	X	X	X	X	X	X
Geophagus altifrons	MCZ15173	Geophagini	1,2,3	X	X	X	X	X	X
Gobiocichla ethelwynnae	MCZ58052	4	1,9,11	X	X	X	X	X	X
Grammatotria lemairii	MCZ49277	8	6,10	X	X	X			
Guianacara geayi	MCZ30140	Geophagini	2,11	X	X	X	X		X
Gymnogeophagus gymnogenys	MCZ88954	Geophagini	2,11	X	X	X	X		X

Table S2.1. (Continued)

Species	Catalog No.	Clade	CladeRef	Body	Caudal	Dorsal	Anal	Ftree	Mtree
Haplochromis lividus	MCZ100653	10	1,2	X	X	X	X	X	X
Hemibates stenosoma	MCZ49289	5	6	X	X	X	X		
Hemichromis fasciatus	MCZ31324	Hemichromini	1,2,11	X	X	X	X	X	X
Hemitilapia oxyrhyncha	MCZ49439	10	3	X	X	X	X		
Herichthys cyanoguttatus	MCZ15415	Heroini	2,11	X	X	X	X		X
Heroina isonycterina	MCZ49319	Heroini	11	X	X	X	X		
Heros severus	MCZ46095	Heroini	1,2,11	X	X	X	X	X	X
Heterochromis multidens	AMNH-I-241789	Heterochromini	1,2,10,11	X	X	X	X	X	X
Hypselecara temporalis	MCZ15344	Heroini	1,2,11	X	X	X	X	X	X
Julidochromis marlieri	MCZ48013	6	5,6,10	X	X	X	X		
Labeotropheus sp.		10	3,4,8	X	X	X	X		
Laetacara flavilabris	MCZ49316	Cichlasomatini	1,2,11	X	X	X	X	X	X
Lamprologus lemairii	MCZ49222	6	1,6	X	X	X	X	X	

Table S2.1. (Continued)

Species	Catalog No.	Clade	CladeRef	Body	Caudal	Dorsal	Anal	Ftree	Mtree
Lepidiolamprologus elongatus	MCZ49251	6	6	X	X	X	X		
Lestradea stappersii	MCZ32593	8	6	X	X				
Lethrinops furcifer	MCZ98601	10	3,4,5	X	X	X	X		
Limnochromis auritus	MCZ32324	7	5,6,10	X	X	X			
Limnotilapia dardennii	MCZ32584	10	1,6,10	X	X	X	X	X	
Lobochilotes labiatus	MCZ89094	10	5,6,10	X	X	X	X		
Maylandia aurora	MCZ98614	10	8	X	X	X	X		
Mbipia mbipi	MCZ100101	10	1,13	X	X	X	X	X	
Mesonauta festivus	MCZ90844	Heroini	1,2,11	X	X	X	X	X	X
Mylochromis sphaerodon	MCZ98605	10	3	X	X	X	X		
Naevochromis chrysogaster	MCZ60431	10		X	X	X	X		
Nanochromis dimidiatus	MCZ50588	2	1,9,12	X	X	X	X	X	
Neochromis greenwoodi	MCZ131287	10	13	X	X	X	X		

Table S2.1. (Continued)

Species	Catalog No.	Clade	CladeRef	Body	Caudal	Dorsal	Anal	Ftree	Mtree
Neolamprologus fasciatus	MCZ49250	6	1,2,6,11	X	X	X	X	X	X
Nimbochromis polystigma	MCZ135963	10	3,4	X	X	X	X		
Nyassachromis leuciscus	MCZ131954	10		X	X	X	X		
Ophthalmotilapia nasuta	MCZ50843	8	1,6,10	X	X	X	X	X`	
Oreochromis esculentus	MCZ100203	3	1,2,7	X	X	X	X	X	X
Otopharynx argyrosoma	MCZ131694	10	3	X	X		X		
Oxylapia polli	AMNH-I-97098	Ptychochromini	2,10	X	X	X	X		X
Parachromis managuensis	MCZ16086	Heroini	1,2,11	X	X	X	X	X	X
Parananochromis caudifasciatus	MCZ35398	2	12	X	X	X	X		
Paraneetroplus maculicauda	MCZ33281	Heroini	2,11	X	X	X	X		X
Paretroplus polyactis	MCZ165679	Etroplinae	1,2,11	X	X	X	X	X	X
Pelvicachromis pulcher	MCZ61101	2	2,7,11,12	X	X	X	X		X
Perissodus microlepis	MCZ49329	7	5,6,10	X	X		X		

Table S2.1. (Continued)

Species	Catalog No.	Clade	CladeRef	Body	Caudal	Dorsal	Anal	Ftree	Mtree
Petrochromis polyodon	MCZ49233	10	1,5,6,10	X	X	X	X	X	
Placidochromis subocularis	MCZ49451	10	3,4	X	X	X	X		
Plecodus paradoxus	MCZ32594	7	1,5,6,10	X	X	X	X	X	
Protomelas triaenodon	MCZ49467	10	3,4	X	X	X	X		
Pseudocrenilabrus multicolor	MCZ100465	10	1,5,10	X	X	X	X	X	
Pseudotropheus johannii	MCZ98611	10	2,5,8	X	X	X	X		X
Pterophyllum scalare	MCZ14989	Heroini	1,2,11	X	X	X	X	X	X
Ptychochromis oligacanthus	AMNH-I-225992	Ptychochromini	1,2,11	X	X	X	X	X	X
Pyxichromis orthostoma	MCZ153518	10	1,2,11	X	X	X	X		
Retroculus boulengeri	NMNH152111	Retroculini	3,4,5	X	X	X	X	X	X
Rhamphochromis	MCZ49542	10	5	X	X		X		
Sargochromis codringtonii	MCZ54346	10	1,2,7	X	X	X	X		
Sarotherodon occidentalis	MCZ63196	3	1,2,11	X	X	X	X	X	X
Satanoperca jurupari	MCZ90954	Geophagini	4	X	X	X	X	X	X
Schubotzia eduardiana	MCZ135771	10		X	X	X	X		

Table S2.1. (Continued)

Species	Catalog No.	Clade	CladeRef	Body	Caudal	Dorsal	Anal	Ftree	Mtree
Sciaenochromis spilostichus	MCZ49477	10		X	X	X	X		
Serranochromis robustus	MCZ32574	10	3,5	X	X	X	X	X	
Simochromis diagramma	MCZ50844	10	5,6,10	X	X	X	X		
Spathodus marlieri	MCZ50696	9	1,5,6,10	X	X	X	X	X	
Steatocranus gibbiceps	MCZ50479	4	1,2,9,11	X	X	X	X	X	X
Stigmatochromis woodi	MCZ49441	10		X	X	X	X		
Symphysodon discus	MCZ15834	Heroini	2,11	X	X	X	X		X
Taeniochromis holotaenia	MCZ98598	10	3	X	X	X	X		
Tangachromis dhanisi	MCZ50836	7		X	X	X	X		
Teleogramma gracile	MCZ50315	2	12	X	X	X	X		
Telmatochromis dhonti	MCZ49272	6	5,6	X	X	X	X		
Thysochromis ansorgii	MCZ48070	2	7,12	X	X	X	X		
Tilapia rendalli	MCZ98624	10	1,2,7	X	X	X	X	X	
Tramitichromis brevis	MCZ49452	10		X	X	X	X		

Table S2.1. (Continued)

Species	Catalog No.	Clade	CladeRef	Body	Caudal	Dorsal	Anal	Ftree	Mtree
Schubotzia eduardiana	MCZ135771	10		X	X	X	X		
Trematocara unimaculatum	MCZ49262	5	6	X	X	X	X		
Trematocranus placodon	MCZ49500	10	3	X	X	X	X		
Triglachromis otostigma	MCZ49275	7	5,6	X	X	X			
Tristramella simonis	MCZ25527	3	7	X	X	X	X		
Tropheus moorii	MCZ50847	10	5,6	X	X	X	X		
Tylochromis leonensis	MCZ63194	1	1,2	X	X	X	X	X	X
Tyrannochromis macrostoma	MCZ49534	10	1,3,5	X	X	X	X	X	

Supplemental Table S2.1 References:

1: Friedman, M., B. P. Keck, A. Dornburg, R. I. Eytan, C. H. Martin, C. D. Hulsey, P. C. Wainwright, and T. J. Near. (2013). Molecular and fossil evidence place the origin of cichlid fishes long after Gondwanan rifting. *Proc. R. Soc. Lond. B.* 280: 20131733.

2: McMahan, C. D., P. Chakrabarty, J. S. Sparks, W. L. Smith and M. P. Davis. (2013). Temporal patterns of diversification across global cichlid biodiversity. *PLoS ONE.* 8: e71162.

3: Moran, P., I. Kornfield and P. N. Reinthal. (1994). Molecular systematics and radiation of the haplochromine cichlids (Teleostei: Perciformes) of Lake Malawi. *Coepia* 1994: 274-288.

4: Joyce, D. A., D. H. Lunt, M. J. Genner, G. F. Turner, R. Bills and O. Seehausen. (2011). Repeated colonization and hybridization in Lake Malawi cichlids. *Curr. Biol.* 21: R108-R109.

5: Salzburger, W., T. Mack, E. Verheyen,and A. Meyer. (2005). Out of Tanganyika: Genesis, explosive speciation, key-innovations and phylogeography of the haplochromine cichlid fishes. *BMC Evol. Biol.* 5: 17.

6: Day, J. J., J. A. Cotton and T. G. Barraclough. (2008). Tempo and mode of diversification of Lake Tanganyika Cichlid Fishes. *PLoS ONE*. 3: e1730.

7: Klett, V. and A. Meyer. (2002). What, if anything, is a Tilapia?—Mitochondrial ND2 phylogeny of Tilapiines and the evolution of parental care systems in the African cichlid fishes. *Mol. Biol. Evol.* 19: 865-883.

8: Allender, C. J., O. Seehausen, M. E. Knight, G. F. Turner and N. Maclean. (2009). Divergent selection during speciation of Lake Malawi cichlid fishes inferred from parallel radiations in nuptial coloration. *Proc. Nat. Acad. Sci. USA.* 100: 14074-14079.

10: Clabaut, C., W. Salzburger and A. Meyer. (2005). Comparative phylogenetic analyses of the adaptive radiation of Lake Tanganyika cichlid fish: Nuclear sequences are less homoplasious but also less informative than mitochondrial DNA. *J. Mol. Evol.* 61: 666-681.

11: Smith, W., P. Chakrabarty and J. S. Sparks. (2008). Phylogeny, taxonomy, and evolution of Neotropical cichlids (Teleostei: Cichlidae: Cichlinae). *Cladistics.* 24: 625-641.

12: Schwarzer, J., A. Lamboj, K. Langen, B. Misof, and U. K. Schliewen. (2014). Phylogeny and age of chromidotilapiine cichlids (Teleostei: Cichlidae). *Hydrobiologia*.

13: Seehausen, O., E. Koetsier, M. V. Schneider, L. J. Chapman, C. A. Chapman, M. E. Knight, G. F. Turner, J. J. M. van Alphen and R. Bills. (2003). Nuclear markers reveal unexpected genetic variation and a Congolese-Nilotic origin of the Lake Victoria cichlid species flock. *Proc. Roy. Soc. B.* 270: 129-137.

Supplemental Table S2.2. List of geometric morphometric landmarks used to quantify body shape.

Landmark	Anatomical Description/ Location
1	Anterior tip of the premaxilla
2	Dorsal tip of the premaxilla
3	Anterior-most point on the orbit
4	Anterior-most point of the supraoccipital crest
5	Posterior-most point on the orbit
6	Dorsal tip of the supraoccipital crest
7	Base of dorsal fin spine I
8	Base of middle dorsal fin spine, or, if even number of spines (N), spine N/2
9	Base of posterior-most dorsal fin spine
10	Base of dorsal fin ray 1
11	Base of middle dorsal fin ray, or if even number of spines (N), spine N/2
12	Base of posterior-most dorsal fin ray
13	Base of dorsal-most caudal fin ray
14	Center of caudal fin ray base
15	Base of ventral-most caudal fin ray
16	Base of posterior-most anal fin ray
17	Base of anterior-most anal fin spine
18	Juncture of pelvic fin bases
19	Base of the ventral-most fin ray of the pectoral fin (left)
20	Base of the dorsal-mot fin ray of the pectoral fin (left)
21	Anterior tip of the pelvic girdle
22	Ventral tip of pectoral girdle
23	Articular-quadrate joint
24	Anterior margin of the first vertebra
25	Posterior margin of the 10^{th} vertebra
26	Posterior margin of the 20^{th} vertebra
27	Distal tip of posterior-most epural.

Supplemental Table S2.3. Linear regression analyses of principal component scores on body (centroid) size. Bold text indicates significance at 0.05 level.

Structure	PC1	PC2
Body	$\beta = -0.27$, adj. $R^2 = -0.01$	**$\beta = 1.61$, adj. $R^2 = 0.07$**
Caudal	$\beta = -0.26$, adj. $R^2 = -0.00$	$\beta = -0.07$, adj. $R^2 = -0.01$
Dorsal	**$\beta = 0.71$, adj. $R^2 = 0.03$**	$\beta = 0.48$, adj. $R^2 = 0.03$
Anal	$\beta = -0.69$, adj. $R^2 = 0.02$	$\beta = 0.03$, adj. $R^2 = -0.01$

Supplemental Table S2.4. PLS CV variable loadings for analyses conducted on PICs of the Friedman tree morphological dataset. Loadings are followed by the amount of variance in each variable explained by the CV (for second CV pairs, this is reported as the cumulative variation explained by CV pairs 1 and 2, less the variation explained by CV pair 1). For PLS including body shape data, only the 10 body shape variables with greatest magnitude loadings are reported. Correlation coefficients relating each pair of CVs are reported in parentheses.

Supplemental Table S2.4 (Continued)

Body-Caudal PLS							
First CV Pair (r = 0.61)				Second CV Pair (r = 0.57)			
Variable	CV1 Body Loading	Variable	CV1 Caudal Loading	Variable	CV2 Body Loading	Variable	CV2 Caudal Loading
22y	-0.25 (89%)	CFR1	0.36(31%)	10x	-0.39 (81%)	CFR1	0.68 (60%)
18y	-0.25 (86%)	CFR3	0.51 (61%)	9x	-0.38 (80%)	CFR3	0.48 (30%)
21y	-0.24 (81%)	CFR5	0.60 (86%)	11x	-0.32 (55%)	CFR5	-0.29 (10%)
17y	-0.24 (79%)	CFR8	0.52 (65%)	13x	0.28 (42%)	CFR8	-0.49 (32%)
7y	0.24 (77%)			14x	0.28 (41%)		
19y	-0.23 (76%)			27x	0.26 (37%)		
6y	0.23 (75%)			15x	0.26 (37%)		
16y	-0.23 (73%)			5x	0.24 (32%)		
8y	0.22 (69%)			13y	-0.19 (19%)		
9y	0.21 (60%)			6x	0.18 (18%)		
Body-Dorsal PLS							
First CV Pair (r = 0.71)				Second CV Pair (r = 0.87)			
Variable	CV1 Body Loading	Variable	CV1 Dorsal Loading	Variable	CV2 Body Loading	Variable	CV2 Dorsal Loading
18y	-0.24 (87%)	Dlength	0.11 (4%)	1x	0.30 (56%)	Dlength	0.86 (80%)
22y	-0.24 (83%)	DFS1	0.03 (0%)	12x	0.29 (54%)	DFS1	-0.40 (17%)
7y	0.23 (81%)	DFSmid	0.42 (52%)	14y	-0.24 (38%)	DFSmid	-0.18 (3%)
6y	0.23 (78%)	DFSlast	0.54 (87%)	7x	-0.24 (38%)	DFSlast	0.03 (1%)
8y	0.23 (77%)	DFR1	0.52 (82%)	13y	-0.24 (36%)	DFR1	0.04 (0%)
19y	-0.23 (76%)	DFRmid	0.50 (75%)	2y	-0.22 (32%)	DFRmid	0.08 (0%)
21y	-0.23 (76%)	DFRlast	0.19 (11%)	11x	0.22 (30%)	DFRlast	-0.29 (9%)
17y	-0.23 (75%)			25y	0.21 (29%)		
16y	-0.22 (69%)			26y	0.20 (27%)		
27x	-0.21 (66%)			3x	0.20 (25%)		
Body-Anal PLS							
First CV Pair (r = 0.60)				Second CV Pair (r = 0.76)			
Variable	CV1 Body Loading	Variable	CV1 Anal Loading	Variable	CV2 Body Loading	Variable	CV2 Anal Loading
18y	0.25 (88%)	Alength	-0.17 (9%)	14y	-0.31 (59%)	Alength	0.77 (79%)
22y	0.25 (88%)	AFS1	-0.39 (48%)	13y	-0.30 (55%)	AFS1	-0.52 (36%)
21y	0.24 (79%)	AFSmid	-0.46 (69%)	27y	-0.28 (45%)	AFSmid	-0.36 (17%)
7y	-0.24 (78%)	AFSlast	-0.52 (87%)	1x	0.26 (41%)	AFSlast	0.02 (0%)
17y	0.24 (77%)	AFR1	-0.48 (74%)	25y	0.26 (40%)	AFR1	0.13 (2%)
6y	-0.24 (76%)	AFRmid	-0.37 (46%)	15y	-0.26 (39%)	AFRmid	0.15 (3%)
19y	-0.23 (76%)	AFRlast	-0.08 (2%)	10y	0.23 (33%)	AFRlast	-0.04 (0%)
8y	-0.23 (70%)			9y	0.23 (32%)		
16y	0.22 (66%)			12x	0.23 (32%)		
27x	0.21 (58%)			26y	0.22 (30%)		

Supplemental Table S2.4 (Continued)

Caudal-Dorsal PLS							
First CV Pair (r = 0.73)				Second CV Pair (r = 0.43)			
Variable	CV1 Caudal Loading	Variable	CV1 Dorsal Loading	Variable	CV2 Caudal Loading	Variable	CV2 Dorsal Loading
CFR1	-0.25 (14%)	Dlength	-0.08 (2%)	CFR1	-0.78 (82%)	Dlength	0.28 (8%)
CFR3	-0.44 (44%)	DFS1	0.02 (0%)	CFR3	-0.57 (43%)	DFS1	-0.88 (80%)
CFR5	-0.64 (94%)	DFSmid	-0.40 (47%)	CFR5	0.12 (2%)	DFSmid	-0.35 (13%)
CFR8	-0.60 (81%)	DFSlast	-0.53 (84%)	CFR8	0.33 (14%)	DFSlast	-0.15 (3%)
		DFR1	-0.52 (83%)			DFR1	0.01 (0%)
		DFRmid	-0.52 (80%)			DFRmid	0.24 (6%)
		DFRlast	-0.22 (15%)			DFRlast	0.17 (3%)
Caudal-Anal PLS							
First CV Pair (r = 0.72)				Second CV Pair (r = 0.58)			
Variable	CV1 Caudal Loading	Variable	CV1 Anal Loading	Variable	CV2 Caudal Loading	Variable	CV2 Anal Loading
CFR1	0.32 (25%)	Alength	0.13 (6%)	CFR1	0.71 (65%)	Alength	0.08 (1%)
CFR3	0.50 (61%)	AFS1	0.42 (57%)	CFR3	0.49 (31%)	AFS1	-0.04 (0%)
CFR5	0.61 (90%)	AFSmid	0.47 (72%)	CFR5	-0.23 (7%)	AFSmid	0.11 (1%)
CFR8	0.54 (70%)	AFSlast	0.50 (82%)	CFR8	-0.45 (27%)	AFSlast	0.31 (12%)
		AFR1	0.45 (66%)			AFR1	0.37 (17%)
		AFRmid	0.39 (49%)			AFRmid	-0.40 (20%)
		AFRlast	0.10 (4%)			AFRlast	-0.78 (75%)
Dorsal-Anal P LS							
First CV Pair (r = 0.84)				Second CV Pair (r = 0.72)			
Variable	CV1 Dorsal Loading	Variable	CV1 Anal Loading	Variable	CV2 Dorsal Loading	Variable	CV2 Anal Loading
Dlength	0.08 (2%)	Alength	0.03 (0%)	Dlength	0.54 (32%)	Alength	0.69 (75%)
DFS1	0.04 (1%)	AFS1	0.42 (55%)	DFS1	-0.73 (58%)	AFS1	-0.29 (13%)
DFSmid	0.42 (55%)	AFSmid	0.47 (70%)	DFSmid	-0.26 (7%)	AFSmid	-0.28 (12%)
DFSlast	0.52 (85%)	AFSlast	0.50 (79%)	DFSlast	-0.08 (0%)	AFSlast	-0.18 (4%)
DFR1	0.50 (77%)	AFR1	0.44 (60%)	DFR1	0.03 (0%)	AFR1	-0.21 (7%)
DFRmid	0.49 (75%)	AFRmid	0.41 (52%)	DFRmid	0.27 (8%)	AFRmid	0.42 (27%)
DFRlast	0.25 (19%)	AFRlast	0.17 (9%)	DFRlast	0.24 (6%)	AFRlast	0.36 (20%)

Supplemental Table S2.5. PLS CV variable loadings for analyses conducted on PICs of the McMahan tree morphological dataset. Loadings are followed by the amount of variance in each variable explained by the CV (for second CV pairs, this is reported as the cumulative variation explained by CV pairs 1 and 2, less the variation explained by CV pair 1). For PLS including body shape data, only the 10 body shape variables with greatest magnitude loadings are reported. Correlation coefficients relating each pair of CVs are reported in parentheses

Supplemental Table S2.5 (Continued)

Body-Caudal PLS							
First CV Pair (r = 0.48)				Second CV Pair (r = 0.52)			
Variable	CV1 Body Loading	Variable	CV1 Caudal Loading	Variable	CV2 Body Loading	Variable	CV2 Caudal Loading
22y	0.25 (93%)	CFR1	-0.50 (70%)	8x	-0.36 (57%)	CFR1	0.55 (28%)
18y	0.24 (88%)	CFR3	-0.57 (89%)	13y	-0.33 (49%)	CFR3	0.21 (4%)
8y	-0.24 (86%)	CFR5	-0.54 (80%)	9x	-0.32 (47%)	CFR5	-0.40 (15%)
7y	-0.23 (79%)	CFR8	-0.41 (46%)	10x	-0.32 (46%)	CFR8	-0.73 (50%)
21y	0.23 (79%)			27y	-0.30 (40%)		
9y	-0.23 (77%)			11x	-0.27 (33%)		
6y	-0.22 (76%)			12y	-0.27 (32%)		
19y	0.22 (75%)			13x	0.26 (31%)		
17y	0.22 (74%)			15x	0.24 (25%)		
10y	-0.22 (73%)			27x	0.23 (24%)		
Body-Dorsal PLS							
First CV Pair (r = 0.72)				Second CV Pair (r = 0.73)			
Variable	CV1 Body Loading	Variable	CV1 Dorsal Loading	Variable	CV2 Body Loading	Variable	CV2 Dorsal Loading
17y	-0.26 (87%)	Dlength	0.33 (33%)	12x	0.31 (59%)	Dlength	0.60 (48%)
8y	0.26 (87%)	DFS1	0.02 (0%)	11x	0.29 (52%)	DFS1	-0.33 (14%)
7y	0.26 (85%)	DFSmid	0.36 (39%)	21x	-0.26 (42%)	DFSmid	-0.21 (6%)
18y	-0.25 (83%)	DFSlast	0.54 (89%)	1x	0.26 (41%)	DFSlast	-0.02 (0%)
9y	0.24 (76%)	DFR1	0.52 (83%)	2y	-0.25 (38%)	DFR1	-0.10 (1%)
22y	-0.24 (74%)	DFRmid	0.46 (64%)	4y	-0.23 (32%)	DFRmid	-0.31 (13%)
6y	0.24 (74%)	DFRlast	-0.02 (0%)	22x	-0.21 (26%)	DFRlast	-0.69 (62%)
10y	0.24 (73%)			12y	-0.20 (25%)		
19y	-0.23 (67%)			21y	0.20 (23%)		
20y	-0.22 (58%)			16x	0.19 (22%)		
Body-Anal PLS							
First CV Pair (r = 0.66)				Second CV Pair (r = 0.61)			
Variable	CV1 Body Loading	Variable	CV1 Anal Loading	Variable	CV2 Body Loading	Variable	CV2 Anal Loading
17y	-0.27 (90%)	Alength	0.34 (40%)	26y	0.27 (48%)	Alength	0.62 (48%)
18y	-0.27 (86%)	AFS1	0.31 (33%)	23y	0.27 (46%)	AFS1	-0.53 (35%)
8y	0.26 (82%)	AFSmid	0.45 (71%)	13x	0.26 (42%)	AFSmid	-0.20 (5%)
22y	-0.26 (79%)	AFSlast	0.51 (92%	27x	0.23 (34%)	AFSlast	0.01 (0%)
9y	0.26 (79%)	AFR1	0.48 (79%)	18x	-0.22 (32%)	AFR1	-0.01 (0%)
7y	0.25 (77%)	AFRmid	0.39 (54%)	13y	-0.22 (32%)	AFRmid	-0.46 (26%)
10y	0.25 (76%)	AFRlast	0.11 (4%)	14x	0.22 (31%)	AFRlast	-0.33 (14%)
19y	-0.24 (72%)			26x	-0.21 (28%)		
20y	-0.23 (66%)			5y	-0.21 (28%)		
6y	0.23 (65%)			25x	-0.21 (27%)		

Supplemental Table S2.5 (Continued)

Caudal-Dorsal PLS							
First CV Pair (r = 0.61)				Second CV Pair (r = 0.33)			
Variable	CV1 Caudal Loading	Variable	CV1 Dorsal Loading	Variable	CV2 Caudal Loading	Variable	CV2 Dorsal Loading
CFR1	-0.42 (50%)	Dlength	-0.09 (2%)	CFR1	0.69 (46%)	Dlength	0.21 (3%)
CFR3	-0.53 (78%)	DFS1	-0.14 (5%)	CFR3	0.41 (16%)	DFS1	0.84 (55%)
CFR5	-0.57 (91%)	DFSmid	-0.39 (38%)	CFR5	-0.20 (4%)	DFSmid	0.40 (12%)
CFR8	-0.48 (65%)	DFSlast	-0.52 (67%)	CFR8	-0.57 (31%)	DFSlast	0.20 (3%)
		DFR1	-0.57 (80%)			DFR1	0.01 (0%)
		DFRmid	-0.58 (83%)			DFRmid	-0.16 (2%)
		DFRlast	-0.21 (11%)			DFRlast	-0.36 (10%)
Caudal-Anal PLS							
First CV Pair (r = 0.67)				Second CV Pair (r = 0.52)			
Variable	CV1 Caudal Loading	Variable	CV1 Anal Loading	Variable	CV2 Caudal Loading	Variable	CV2 Anal Loading
CFR1	0.42 (48%)	Alength	0.18 (12%)	CFR1	0.70 (45%)	Alength	0.37 (17%)
CFR3	0.53(78%)	AFS1	0.38 (53%)	CFR3	0.44 (18%)	AFS1	-0.06 (0%)
CFR5	0.57 (91%)	AFSmid	0.45 (72%)	CFR5	-0.23 (5%)	AFSmid	0.23 (7%)
CFR8	0.48 (65%)	AFSlast	0.48 (82%)	CFR8	-0.58 (31%)	AFSlast	0.30 (12%)
		AFR1	0.44 (72%)			AFR1	0.28 (10%)
		AFRmid	0.45 (73%)			AFRmid	-0.35 (15%)
		AFRlast	0.17 (10%)			AFRlast	-0.75 (72%)
Dorsal-Anal P LS							
First CV Pair (r = 0.88)				Second CV Pair (r = 0.70)			
Variable	CV1 Dorsal Loading	Variable	CV1 Anal Loading	Variable	CV2 Dorsal Loading	Variable	CV2 Anal Loading
Dlength	0.28 (23%)	Alength	0.24 (22%)	Dlength	-0.49 (32%)	Alength	0.16 (3%)
DFS1	0.06 (1%)	AFS1	0.34 (46%)	DFS1	0.33 (15%)	AFS1	-0.14 (2%)
DFSmid	0.40 (48%)	AFSmid	0.44 (74%)	DFSmid	0.02 (0%)	AFSmid	-0.29 (9%)
DFSlast	0.53 (86%)	AFSlast	0.46 (83%)	DFSlast	-0.13 (2%)	AFSlast	-0.27 (7%)
DFR1	0.51 (79%)	AFR1	0.43 (71%)	DFR1	0.01 (0%)	AFR1	-0.14 (2%)
DFRmid	0.48 (69%)	AFRmid	0.44 (73%)	DFRmid	0.32 (14%)	AFRmid	0.36 (13%)
DFRlast	0.04 (0%)	AFRlast	0.22 (18%)	DFRlast	0.78 (82%)	AFRlast	0.84 (73%)

Supplemental Figure S2.1. Clade assignments based on Friedman et al 2013. Figure reproduced and modified with permission.

Supplemental Figure S2.1 (Continued)

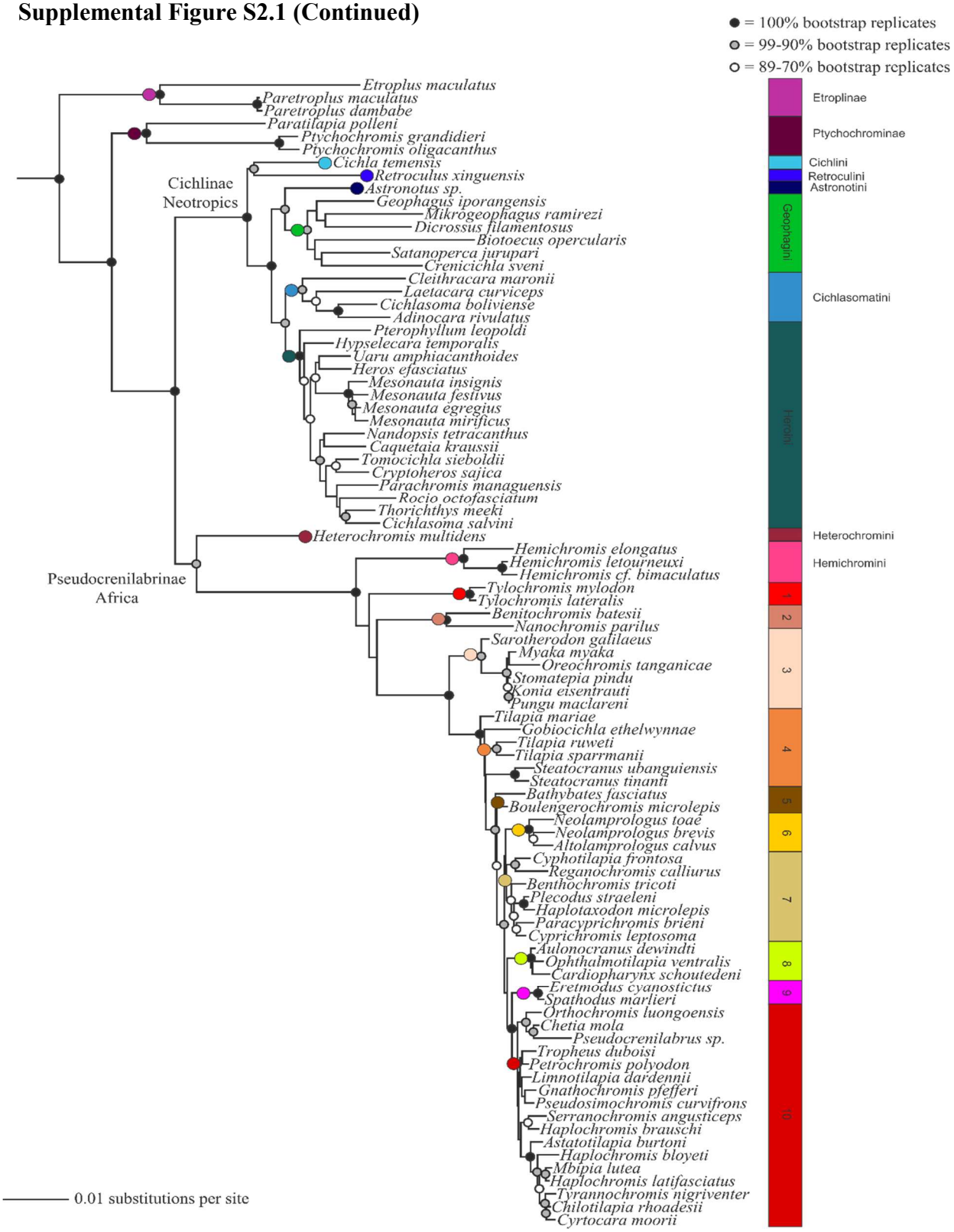

Supplemental Figure S2.2. Clade assignments based on McMahan et al 2013. Figure reproduced and modified with permission.

Supplemental Figure S2.2 (Continued)

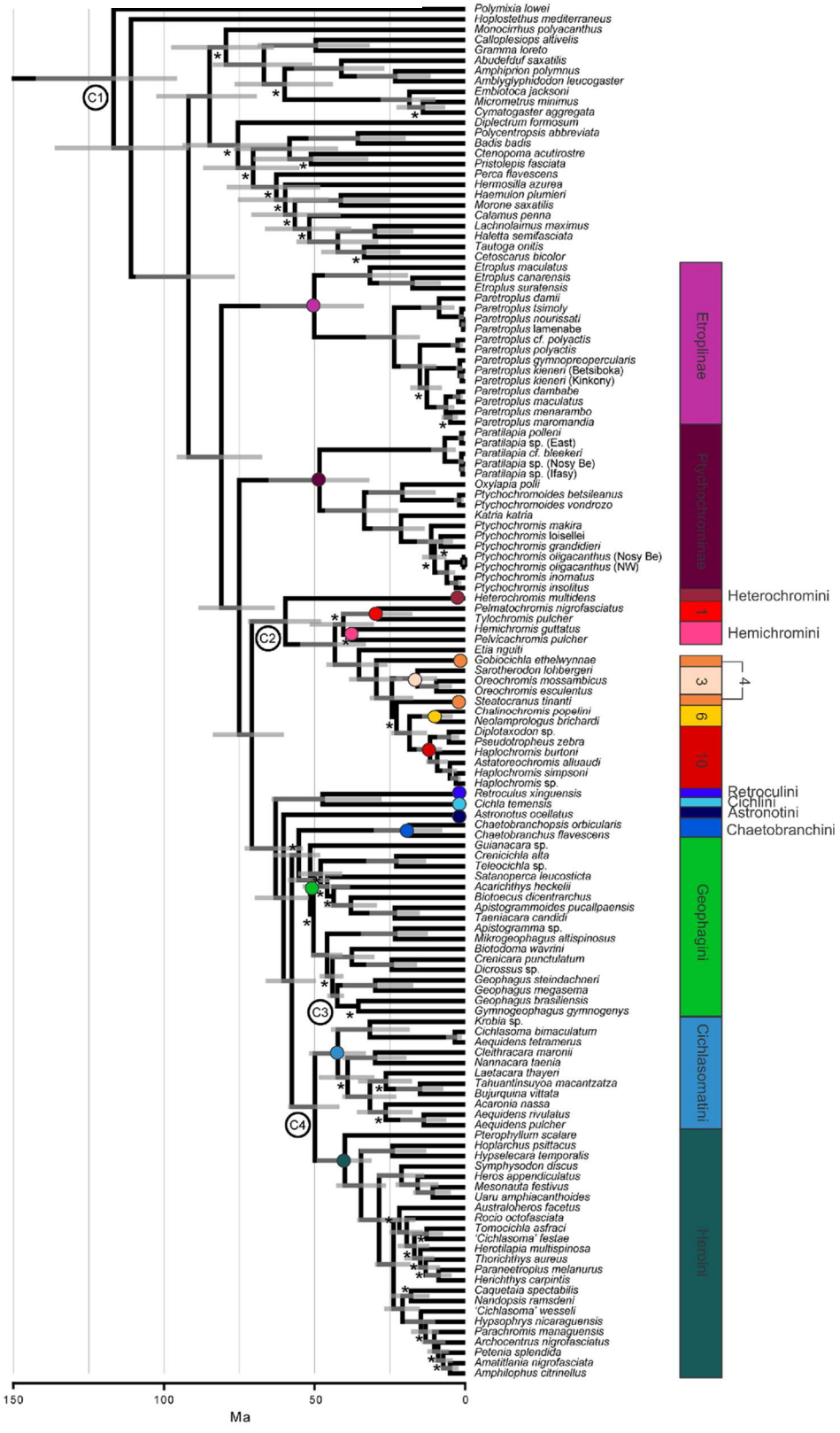

Supplemental Figure S2.3. Linear regressions of fin elements on body centroid size to calculate residuals which were then used in subsequent shape analyses.

Supplemental Figure S2.3 (Continued)

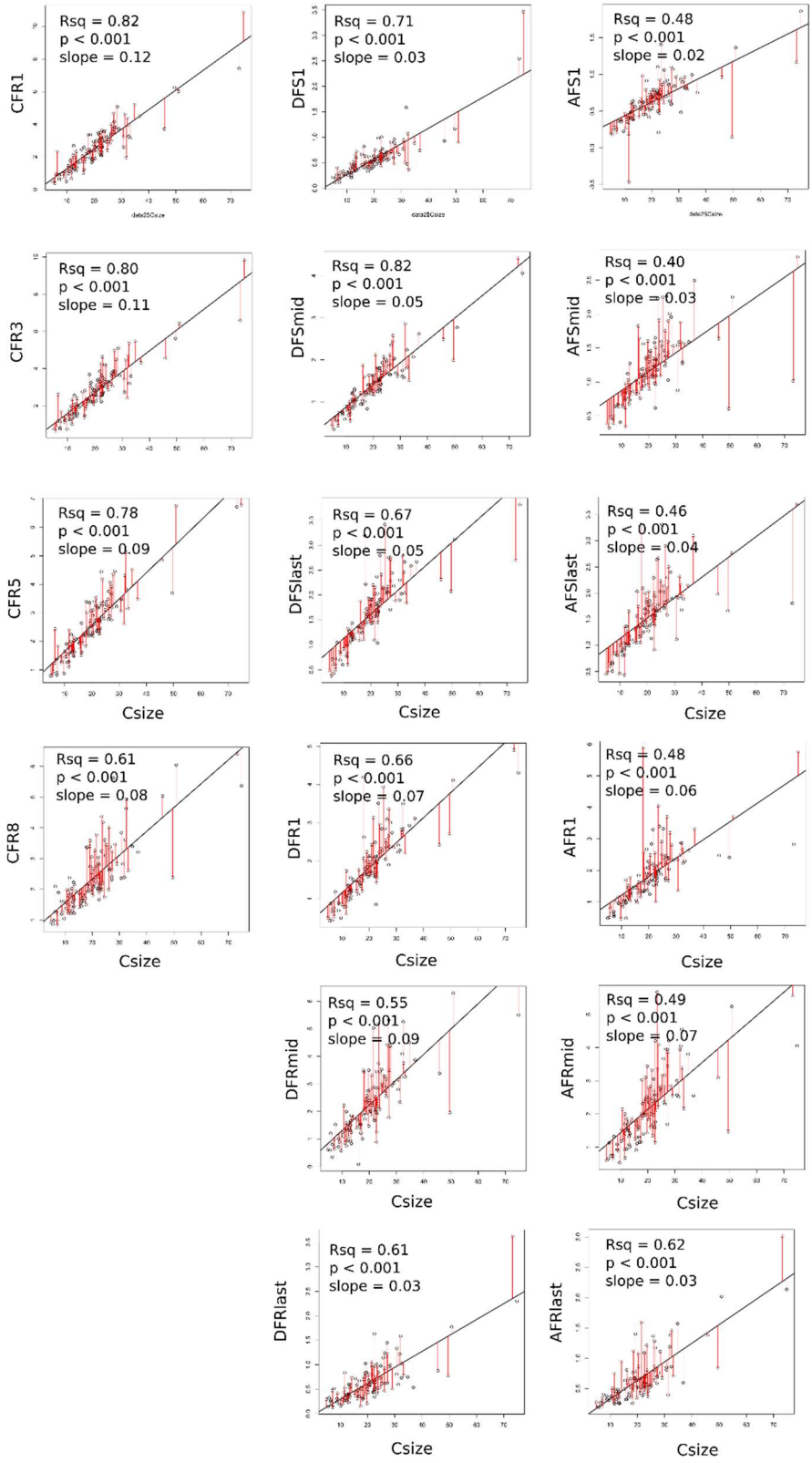

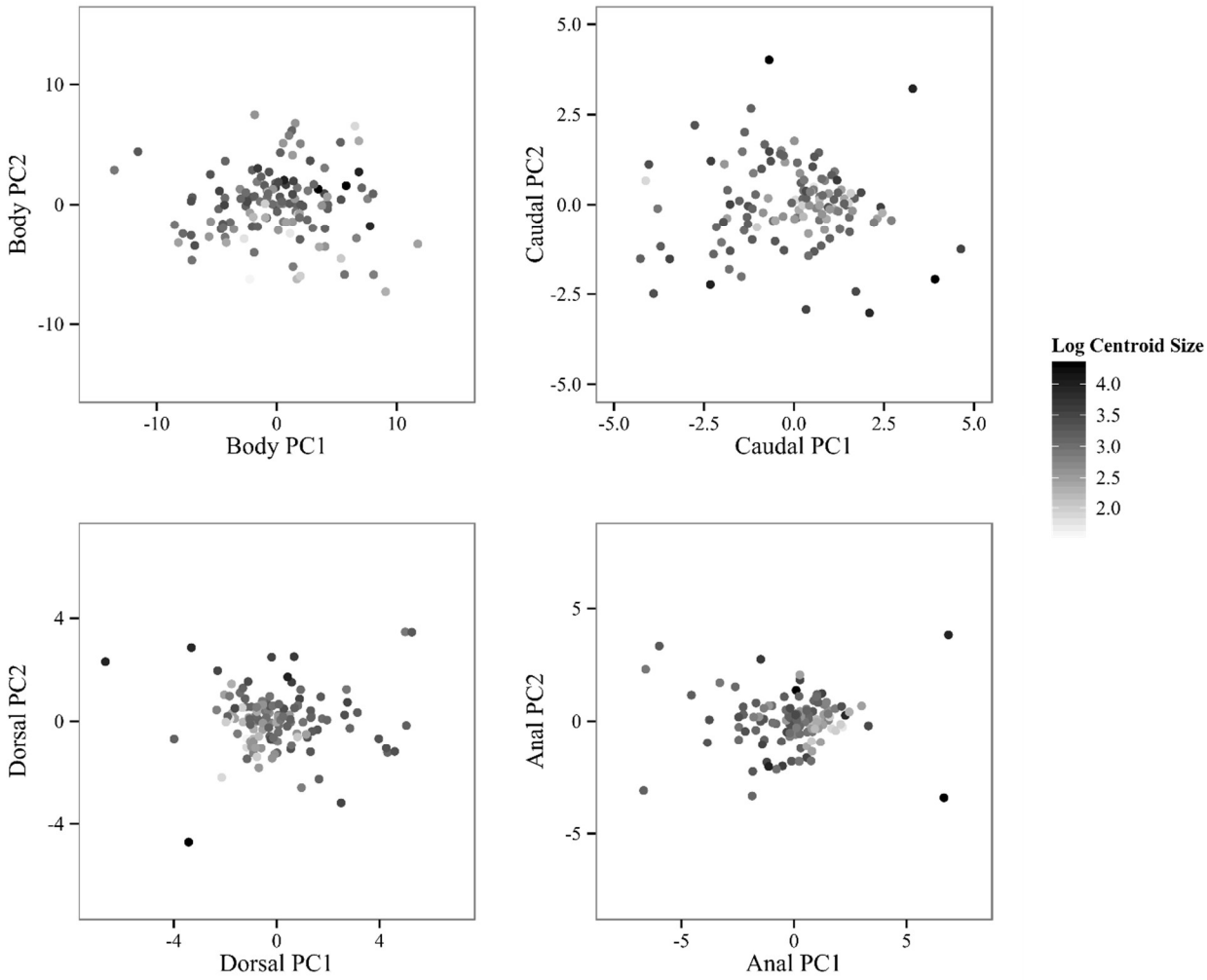

Supplemental Figure S2.4. Principal components of body and fin shapes colored by specimen size. From the lack of size clustering observed, it appears there are no dominant allometric patterns in body and fin shape among cichlids. Linear regressions of each PC1 and PC2 against body size revealed no allometric trends between shape and size (Supp. Table 2.3).

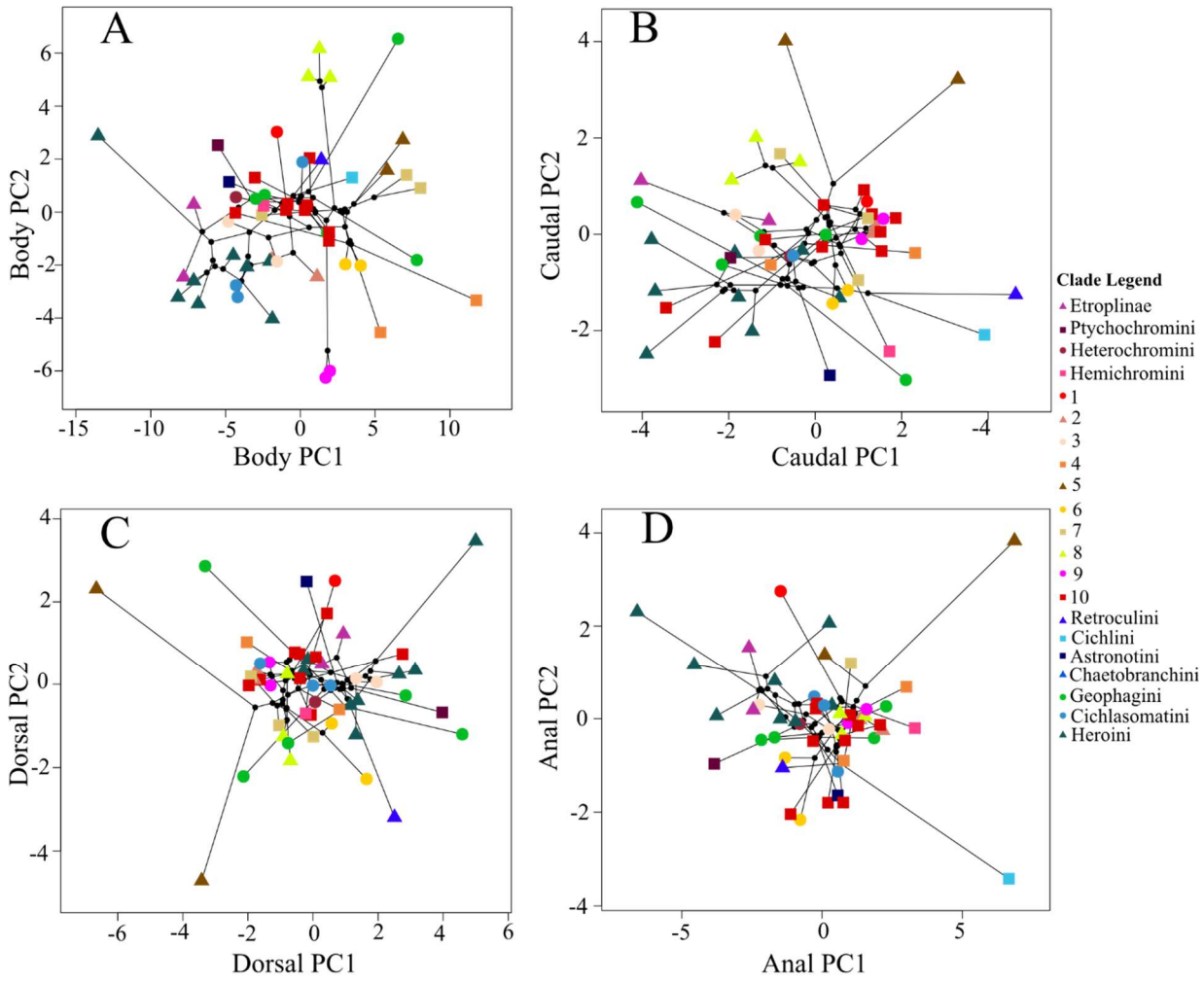

Supplemental Figure S2.5. Phylomorphospace of specimens represented in the Friedman et al 2013 tree, as calculated from the original PCA of all specimens.

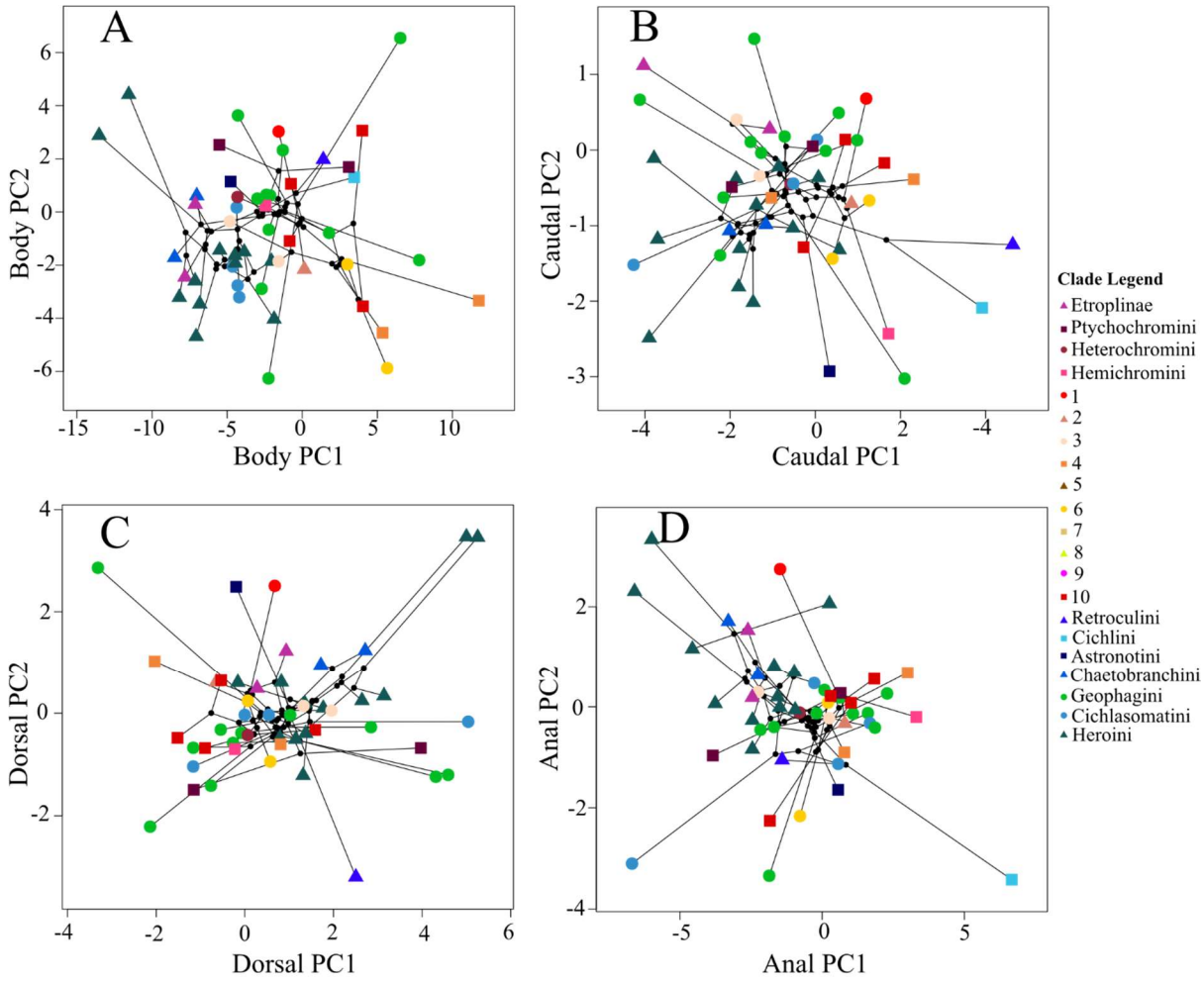

Supplemental Figure S2.6. Phylomorphospace of specimens represented in the McMahan et al 2013 tree, as calculated from the original PCA of all specimens.

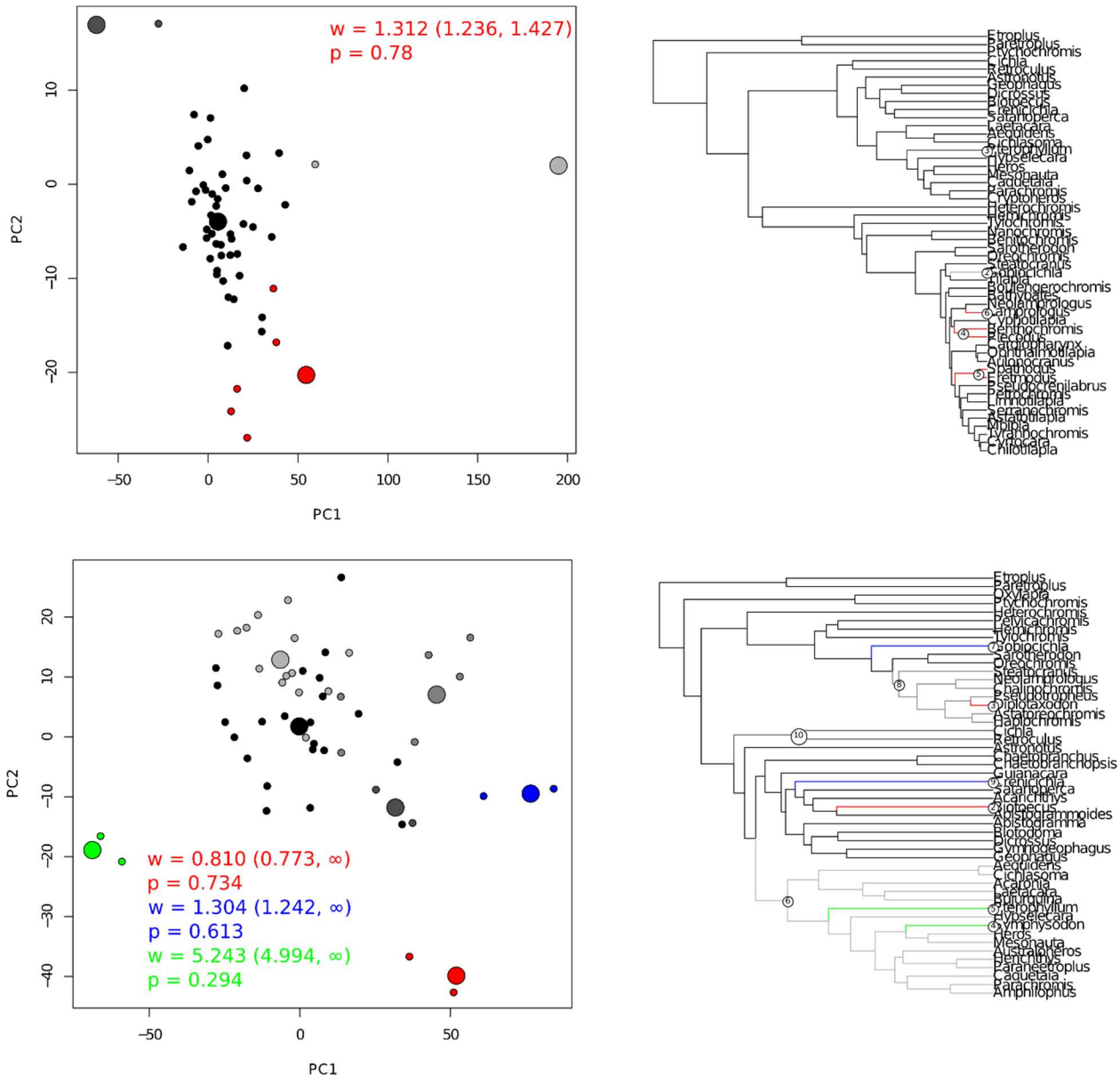

Supplemental Figure S2.7. SURFACE analysis and Wheatsheaf indices with 95% confidence intervals for body shape on the Friedman (top) and McMahan (bottom) trees.

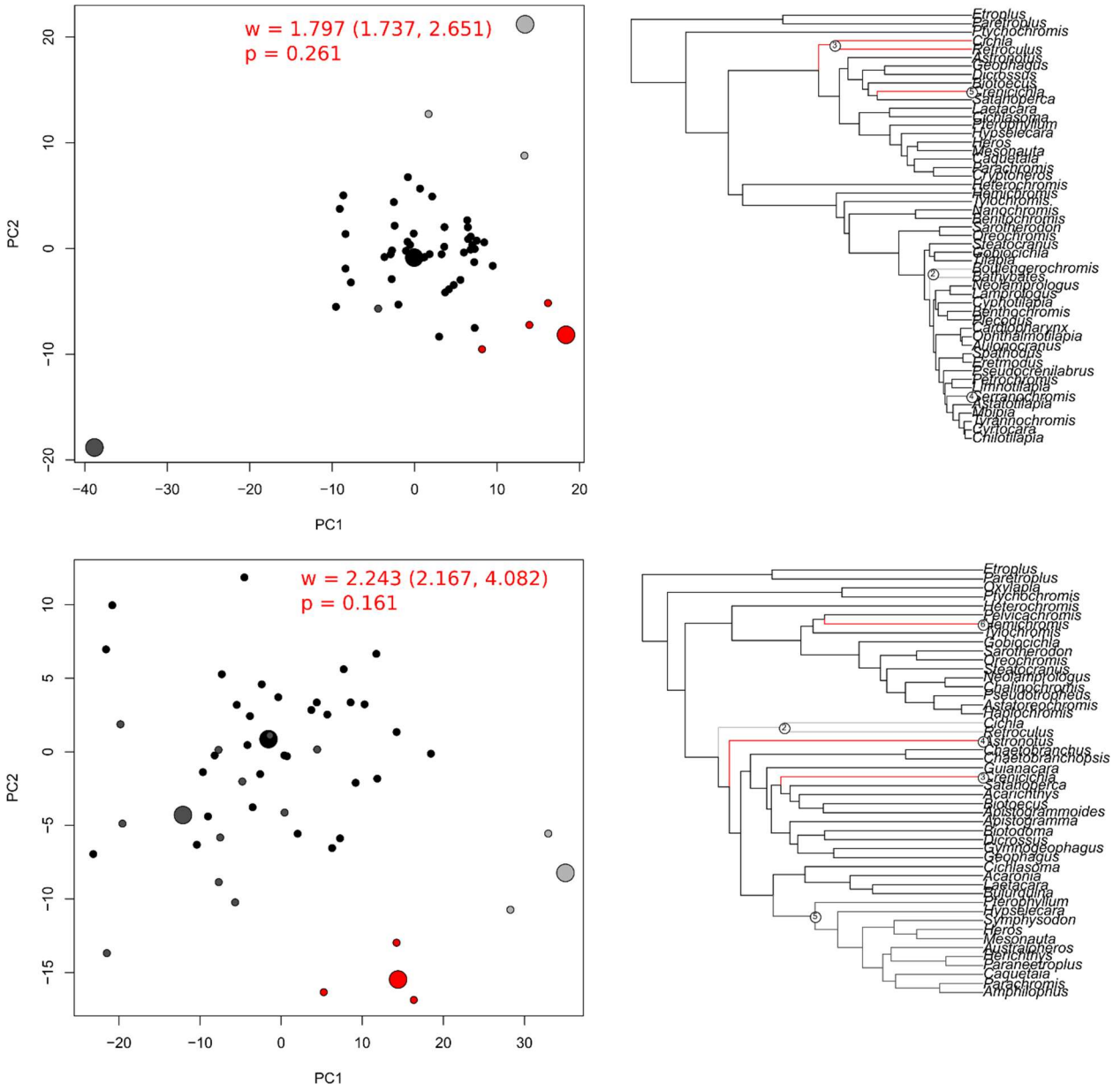

Supplemental Figure S2.8. SURFACE analysis and Wheatsheaf indices with 95% confidence intervals for caudal shape on the Friedman (top) and McMahan (bottom) trees.

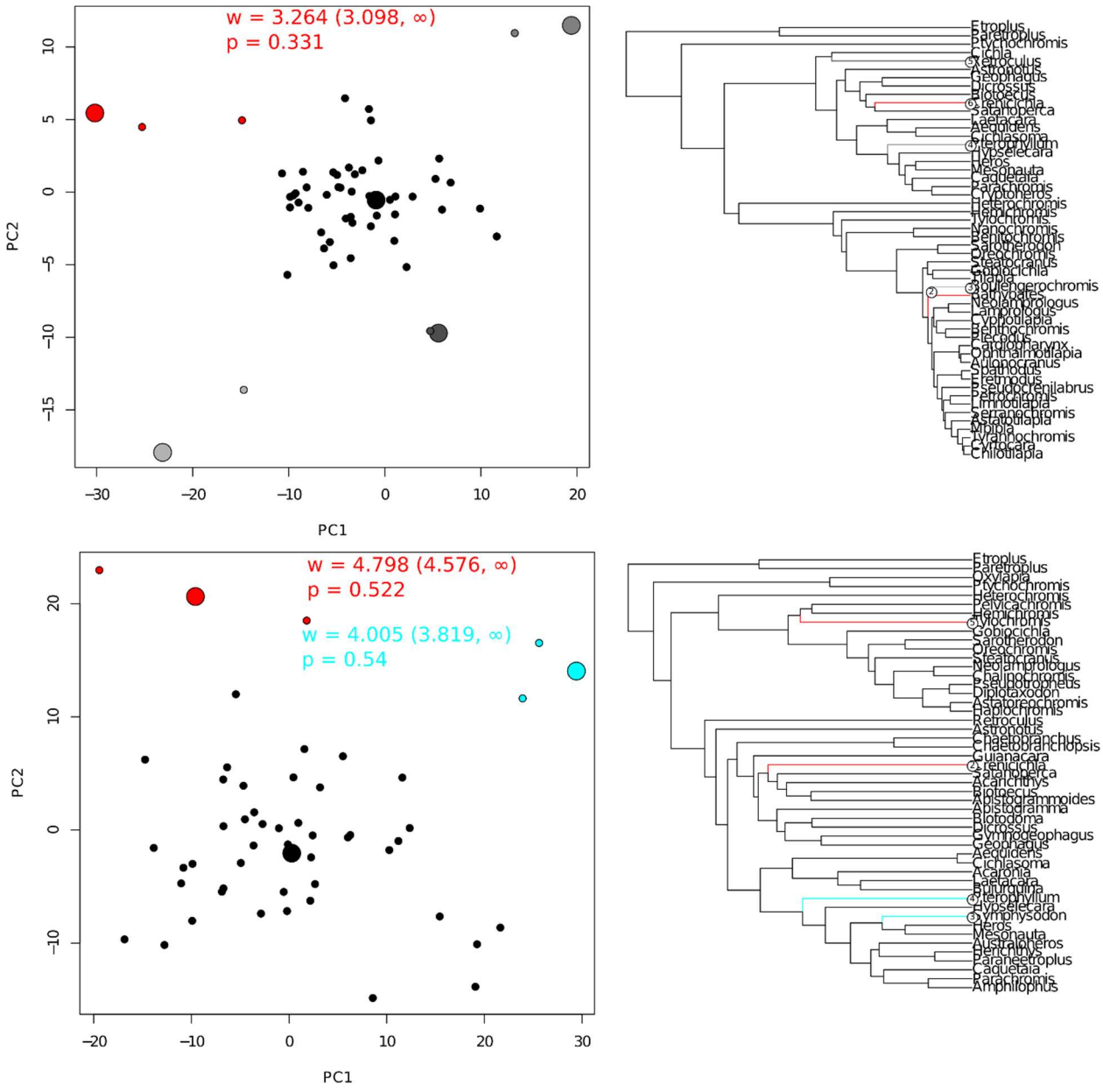

Supplemental Figure S2.9. SURFACE analysis and Wheatsheaf indices with 95% confidence intervals for dorsal fin shape on the Friedman (top) and McMahan (bottom) trees.

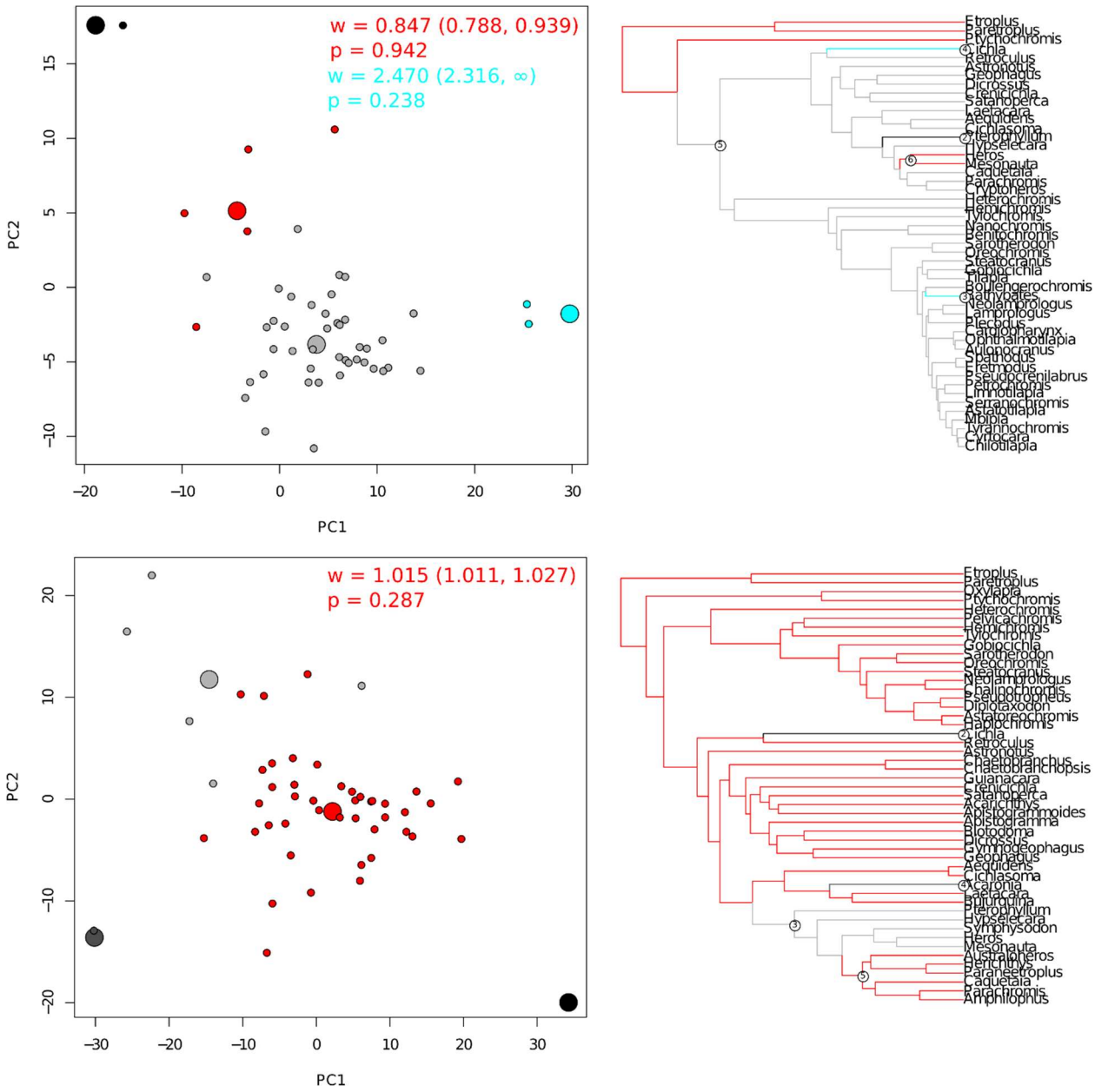

Supplemental Figure S2.10. SURFACE analysis and Wheatsheaf indices with 95% confidence intervals for anal fin shape on the Friedman (top) and McMahan (bottom) trees.

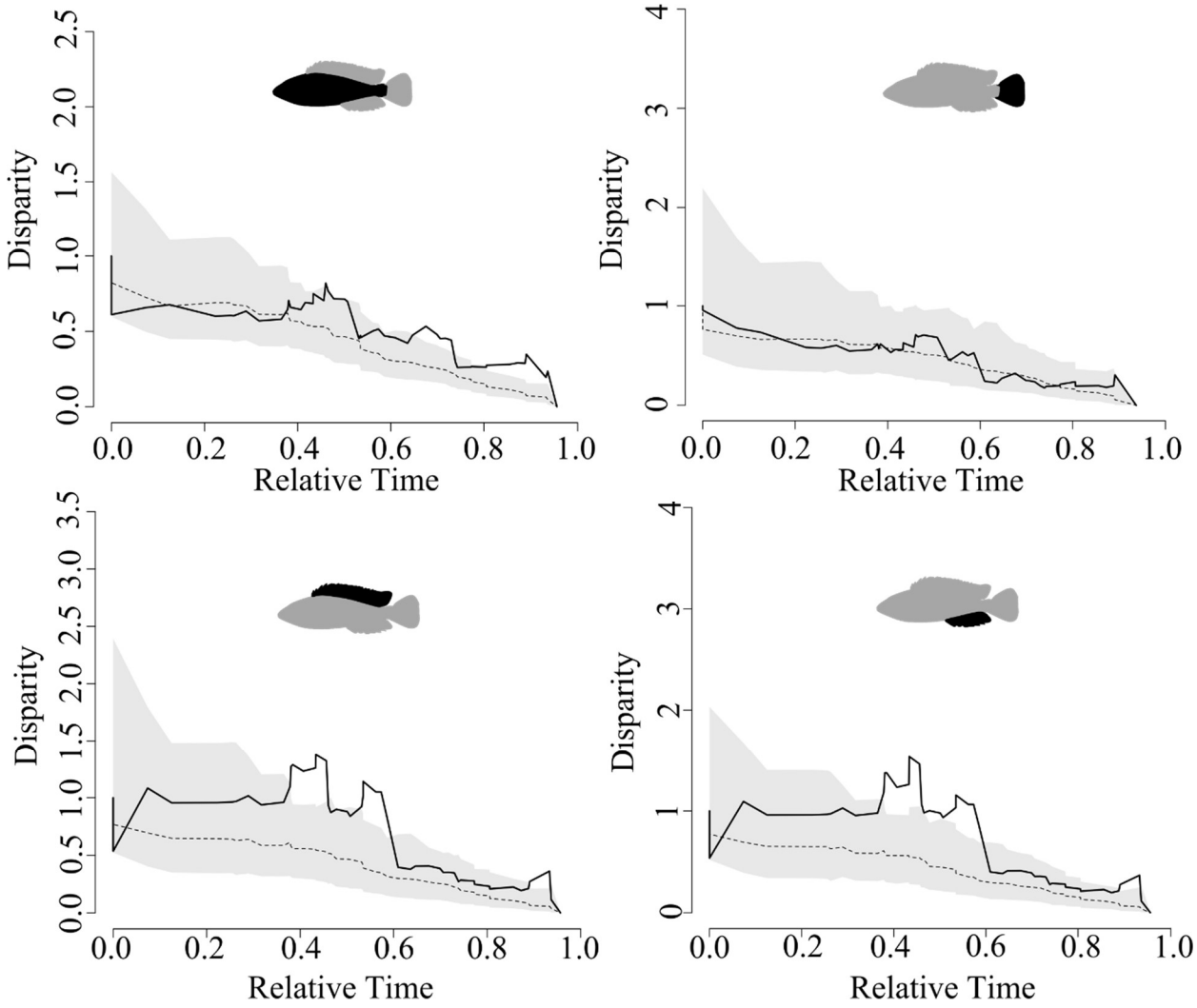

Supplemental Figure S2.11. Cichlid disparity through time calculated from the McMahan tree dataset (black line) with 95% confidence intervals following the method of Slater et al 2013. Mean expected disparity under the BM model is shown as the dotted line. Peaks above the grey confidence interval show higher disparity than expected under a BM model of trait evolution. Relative time is calculated from the tree length of the pruned subtrees specific to each morphological structure.

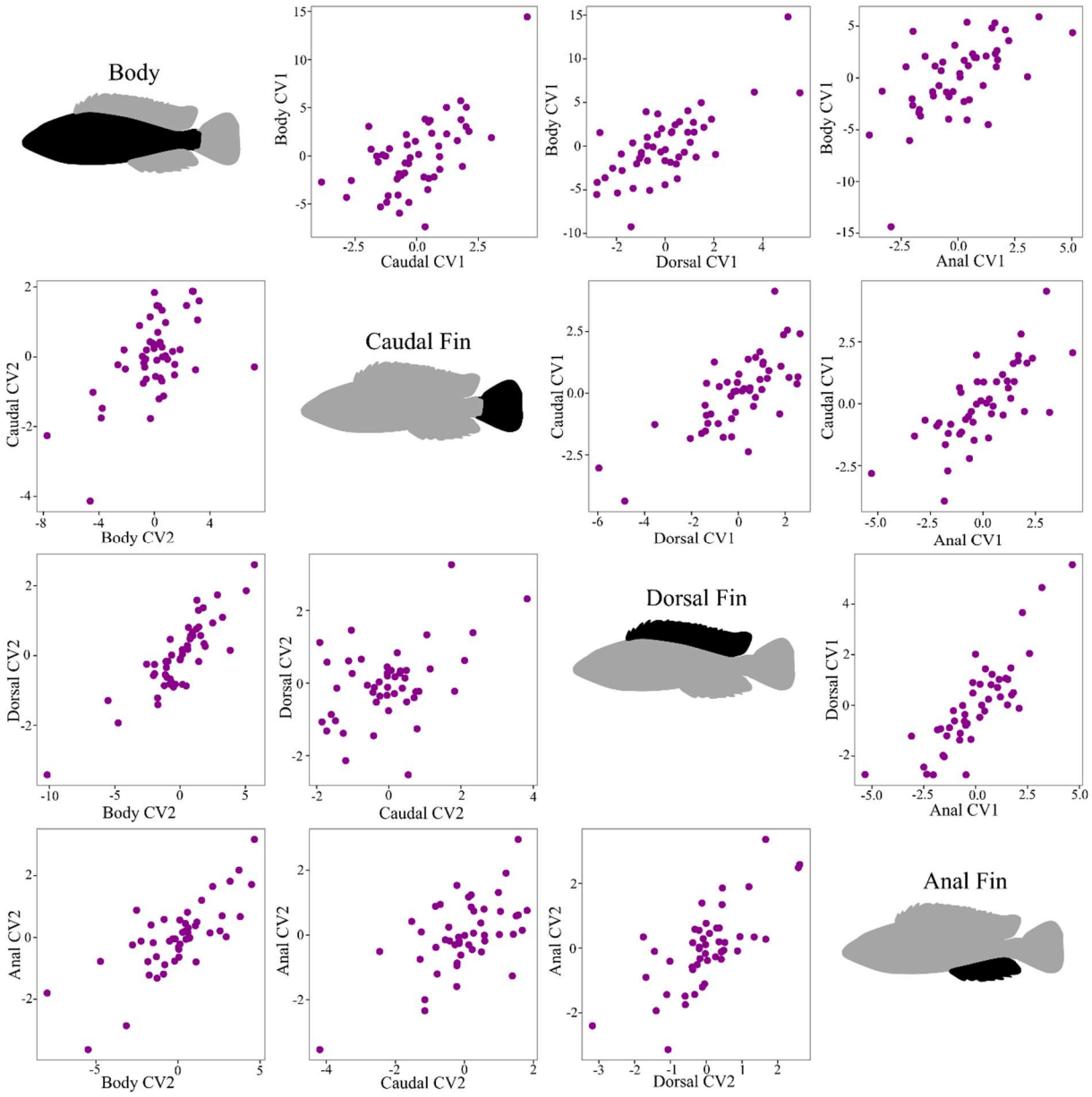

Supplemental Figure S2.12. Partial least squares canonical variates displaying covariation of independent contrasts of body and median fin shapes on the Friedman et al 2013 phylogeny.

Appendix to Chapter 3

Supplemental Table S3.1. Individuals and trials included in each analysis. All trials meeting the requirements for a given analysis were included. Species is indicated in the Fish code (Cicoce = *Cichla ocellaris*, Cresax = *Crenicichla saxatilis*, Symaeq = *Symphysodon aequifasciatus*). Numerical column entries are the number of trials for that individual included, with '-' when no trials were available. Avg. Gait Trajectory indicates whether (Y) or not (N) a given fish had sufficient data to be included in Figure 7. Species Gait Trajectory indicates whether the data for a given fish were included in the calculation of the species average trajectory.

Fish (Total Trials Attempted)	Trans. Speed	Max. Speed	Freq. and Amp.	Avg Gait Trajectory	Species Gait Trajectory
Cicoce1 (3)	3	3	1	Y	Y
Cicoce2 (3)	3	3	1	Y	Y
Cicoce3 (3)	3	3	2	Y	Y
Cicoce4 (4)	3	3	2	Y	Y
Cicoce5 (3)	3	3	-	N	N
Cresax1 (6)	2	2	2	Y	Y
Cresax2 (4)	1	1	1	Y	Y
Cresax3 (4)	1	-	-	N	N
Symaeq1 (3)	3	3	2	Y	Y
Symaeq2 (3)	3	3	2	Y	Y
Symaeq4 (3)	1	1	-	N	N
Symaeq5 (3)	3	3	2	Y	Y
Symaeq10 (2)	2	2	-	N	N

Appendix to Chapter 4

Supplemental Table S4.1. Packages used in custom code for this study. Download sources are available; the authors used packages included in the Anaconda distribution of Python 3.4 when available, and downloaded other packages using pip install.

Package	Version	Source URL	Function in Study
math	n/a	in base Python	mathematical constants
matplotlib	2.0.0	https://pypi.python.org/pypi/matplotlib/	plotting functions
NumPy	1.11.3	https://pypi.python.org/pypi/numpy	mathematical operations. Fourier transforms, finding maxima and minima for velocity and acceleration data
os	n/a	in base Python	filepath operations
pandas	0.19.2	https://pypi.python.org/pypi/pandas	data organiztion
PeakUtils	1.0.3	https://bitbucket.org/lucashnegri/peakutils	peak and trough finding, subtracting baselines from cyclical data
pickle	n/a	in base Python	storing data
SciPy	0.18.1	https://pypi.python.org/pypi/scipy	signal processing, least squares optimization
seaborn	0.7.1	https://github.com/mwaskom/seaborn	heatmaps
statsmodels	0.6.1	https://pypi.python.org/pypi/statsmodels	regression models

Supplemental Table S4.2. Maximum instantaneous speed related to caudal fin beat period and amplitude in a largemouth bass. β = regression coefficient, SEB = standard error of β. boot_n = number of bootstrap replicates. All p values are pseudo-p-values after bootstrapping.

Model 1:

Max_Spd ~ Period * Amplitude; F = 63.62; p = 0.002; df = 3, 65; n=69; boot_n: 2000

Model 2	**Correlations**		**β (boot 95% CI)**	**SEB**	**t**	**p (boot)**
Variable	**Period**	**Amplitude**				
Intercept	-	-	(34.8, 46.4)	2.949	13.74	0.000
Period (s)	-	-0.10	(-68.3, -50.3)	4.579	-12.93	0.000
Amplitude (cm)	-0.10	-	(0.9, 4.9)	1.029	2.813	0.004
Mean	0.34	2.22				
SD	0.12	0.55			**Adj. R^2**	0.728

Supplemental Table S4.3. Maximum instantaneous speed related to caudal fin beat period and amplitude for rainbow trout 1. β = regression coefficient, SEB = standard error of β. boot_n = number of bootstrap replicates. All p values are pseudo-p-values after bootstrapping.

Model 1:

Max_Spd ~ Period * Amplitude; F = 44.56; p = 0.004; df = 3, 76; n=80; boot_n = 2000

Model 2:

Max_Spd ~ Period + Amplitude; F = 67.48; p = 0.003; df = 2. 77; n=80; boot_n = 2000

Model 2	**Correlations**		**β (boot 95% CI)**	**SEB**	**t**	**p (boot)**
Variable	**Period**	**Amplitude**				
Intercept	-	-	(57.1, 67.3)	2.73	22.74	0.000
Period (s)	-	0.75	(-125.7, -63.4)	15.69	-6.00	0.000
Amplitude (cm)	0.75	-	(-37.8, 12.7)	3.10	-2.15	0.035
Mean	0.24	2.22				
SD	0.12	0.55			**Adj. R^2**	0.627

Supplemental Table S4.4. Maximum instantaneous speed related to caudal fin beat period and amplitude rainbow trout 2. β = regression coefficient, SEB = standard error of β. boot_n = number of bootstrap replicates. All p values are pseudo-p-values after bootstrapping.

Model 1:

Model 1	**Correlations**		**β**	**SEB**	**t**	**p**
Variable	**Period**	**Amplitude**	**(boot 95% CI)**			**(boot)**
Intercept	-	-	(22.01, 41.31)	5.10	6.47	0.000
Period (s)	-	0.37	(-73.72, 39.50)	30.57	-0.68	0.436
Amplitude (cm)	0.37	-	(6.46, 21.48)	3.98	3.36	0.002
Period:Amplitude	-	-	(-108.30, -25.81)	22.33	-2.86	0.011
Mean	0.24	1.32				
SD	0.08	0.46			**Adj. R^2**	0.709

Supplemental Table S4.5. Maximum instantaneous acceleration related to caudal fin beat period and amplitude in a largemouth bass. β = regression coefficient, SEB = standard error of β. boot_n = number of bootstrap replicates. All p values are pseudo-p-values after bootstrapping.

Model 1:

Max_Acc ~ Period * Amplitude; F = 32.77; p =0.009; df = 3, 65; n=69; boot_n: 2000

Model 1	**Correlations**		**β**	**SEB**	**t**	**P**
Variable	**Period**	**Amplitude**	**(boot 95% CI)**			**(boot)**
Intercept	-	-	$(-66.8, -34.3)*10^{-5}$	$8.4*10^{-5}$	-6.06	0.000
Period (s)	-	-0.10	$(85.4, 178.6)*10^{-5}$	0.000	5.50	0.000
Amplitude (cm)	-0.10	-	$(22.5, 36.5)*10^{-5}$	$3.6*10^{-5}$	8.21	0.000
Period:Amplitude	-	-	$(-94.0, -52.6)*10^{-5}$	0.000	-6.96	0.000
Mean	0.34	2.22				
SD	0.12	0.55			**Adj. R^2**	0.728

Supplemental Table S4.6. Maximum instantaneous acceleration related to caudal fin beat period and amplitude rainbow trout 1. β = regression coefficient, SEB = standard error of β. boot_n = number of bootstrap replicates. All p values are pseudo-p-values after bootstrapping.

Model 1:

Max_Acc ~ Period * Amplitude; F = 5.61; p = 0.100; df = 3, 76; n=80; boot_n= 2000

Model 2	**Correlations**		**β (boot 95% CI)**	**SEB**	**t**	**p (boot)**
Variable	**Period**	**Amplitude**				
Intercept	-	-	(-23.7, 4.34) * 10^{-5}	7.1*10^{-5}	-1.38	0.178
Period (s)	-	0.75	(38.4, 168.8) * 10^{-5}	0.000	2.96	0.006
Amplitude (cm)	0.75	-	(-8.1, 10.7) * 10^{-5}	4.62*10^{-5}	0.14	0.870
Period:Amplitude	-	-	(-81.8, -7.5) *10^{-5}	0.000	-2.25	0.030
Mean	0.24	2.22				
SD	0.12	0.55			Adj. R^2	0.149

Supplemental Table S4.7. Maximum instantaneous acceleration related to caudal fin beat period and amplitude rainbow trout 2. β = regression coefficient, SEB = standard error of β. boot_n = number of bootstrap replicates. All p values are pseudo-p-values after bootstrapping.

Model 1:

Max_Acc ~ Period * Amplitude; F =2.329; p = 0. 0.261; df = 3, 46; n = 50; boot_n: 2000

Model 1	**Correlations**		**β**	**SEB**	**t**	**p**
Variable	**Period**	**Amplitude**	**(boot 95% CI)**			**(boot)**
Intercept	-	-	(-46.1, 5.7) $*10^{-5}$	0.000	-1.05	0.198
Period (s)	-	0.37	(8.5, 322.1) $*10^{-5}$	0.001	1.94	0.059
Amplitude (cm)	0.37	-	(5.3, 45.6) $*10^{-5}$	0.000	2.25	0.047
Period:Amplitude	-	-	(-257.9, -34.5) $*10^{-5}$	0.001	-2.41	0.031
Mean	0.24	1.32				
SD	0.08	0.46			**Adj. R^2**	0.075